REFINEMENTS TO THE CURRENT UNDERSTANDING OF FUNCTIONAL MRI ACTIVATION IN WHITE MATTER

by

Erin L. Mazerolle

Submitted in partial fulfilment of the requirements
for the degree of Doctor of Philosophy

at

Dalhousie University
Halifax, Nova Scotia
June 2012

DALHOUSIE UNIVERSITY

DEPARTMENT OF PSYCHOLOGY

The undersigned hereby certify that they have read and recommend to the Faculty of Graduate Studies for acceptance a thesis entitled "Refinements to the Current Understanding of Functional MRI Activation in White Matter" by Erin L. Mazerolle in partial fulfilment of the requirements for the degree of Doctor of Philosophy.

Dated: June 1, 2012

External Examiner: _____

Research Supervisor: _____

Examining Committee: _____

_____

_____

Departmental Representative: _____

DALHOUSIE UNIVERSITY

DATE: June 1, 2012

AUTHOR: Erin L. Mazerolle

TITLE: Refinements to the Current Understanding of Functional MRI Activation in White Matter

DEPARTMENT OR SCHOOL: Department of Psychology

DEGREE: PhD CONVOCATION: October YEAR: 2012

_____

Signature of Author

To Mark

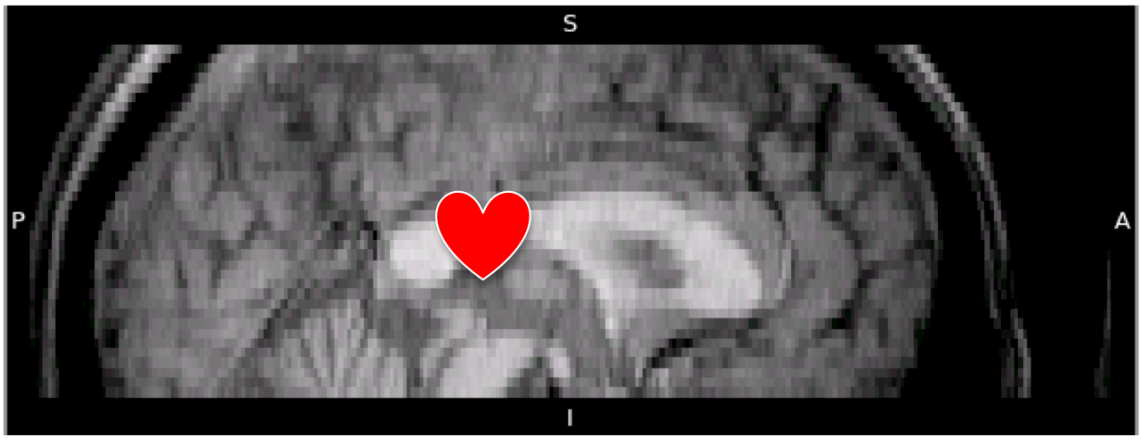

"That's not evidence of white matter activation,
that's just evidence of love." – MKZ

Table of Contents

List of Tables

List of Figures

Abstract

Functional magnetic resonance imaging (fMRI) is a widely used, noninvasive technique to map brain activation, and has provided considerable insight into human brain function over the past two decades. Until recently, fMRI studies have focused on gray matter; however, reports of fMRI activation in white matter are mounting. White matter fMRI activation has the potential to greatly expand the breadth of brain connectivity research, as well as improve the assessment and diagnosis of white matter and connectivity disorders. Despite these potential benefits, white matter fMRI activation remains controversial. The controversy is partially due to the existence of incompletely understood facets of fMRI signals in white matter. This thesis describes three experiments that aim to refine what is currently known about white matter fMRI activation. In the first experiment, one of the main concerns about fMRI activation in white matter was addressed; namely, whether white matter has sufficient cerebrovascular reactivity to support hemodynamic changes that can be measured with fMRI. It was demonstrated that white matter has the capacity to support detectable hemodynamic changes in the absence of partial volume effects. In the second experiment, the effect of static magnetic field strength on sensitivity to white matter fMRI activation was explored as a possible cause of the relative paucity of reports of white matter fMRI activation. The results showed greater sensitivity to white matter fMRI activation at 4 T relative to 1.5 T MRI. In the third experiment, the relationship between white matter activation and the activated network of gray matter regions was explored. This was accomplished using fMRI-guided tractography in which structural connections between activated clusters are evaluated. Structural connectivity between white matter fMRI activation and regions of gray matter activation was demonstrated, providing evidence of the functional significance of fMRI activation in white matter. These experiments provide important insights, which will allow for improved investigations of white matter fMRI activation in the future. In addition, it is posited that experimenter bias, via selective reporting of activation clusters, has contributed to the slow acceptance of fMRI activation in white matter.

List of Abbreviations and Symbols Used

%sc	percent signal change
^{14}C	carbon-14
^{18}F	fluorine-18
3D	three dimensional
Δ	change
σ	standard deviation
τ	spin echo time
ω	Larmor frequency
ADC	apparent diffusion coefficient
ASE	asymmetric spin echo
au	arbitrary units
B_0	static magnetic field
BET	brain extraction tool
BOLD	blood oxygen level dependent contrast
b-SSFP	balanced steady state free precession
Ca^{2+}	calcium ion
CBF	cerebral blood flow
CBV	cerebral blood volume
CC	corpus callosum
CO_2	carbon dioxide
CSF	cerebrospinal fluid
DOF	degrees of freedom
DTI	diffusion tensor imaging
DWI	diffusion weighted imaging
e.g.	*exempli gratia*
et al.	*et alia*
FA	fractional anisotropy
FAST	FMRIB's automated segmentation tool
FEAT	FMRI expert analysis tool

FILM	FMRIB’s improved linear model
FLAME	FMRIB’s local analysis of mixed effects
FLIRT	FMRIB's linear image registration tool
fMRI	functional magnetic resonance imaging
FMRIB	Functional MRI of the Brain
FNIRT	FMRIB's nonlinear image registration tool
FOV	field of view
FSL	FMRIB Software Library
FWHM	full width at half maximum
GABA	γ-aminobutyric acid
GLM	general linear model
GM	gray matter
GRASS	coherent gradient echo
HRF	hemodynamic response function
ICBM	International Consortium for Brain Mapping
i.e.	*id est*
Inc.	Incorporated
JHU	Johns Hopkins University
K^+	potassium ion
LFP	local field potential
Ltd.	Limited
MCFLIRT	motion correction FLIRT
min	minute
MIP	maximum intensity projection
MPFLASH	magnetization prepared fast low angle shot
MRI	magnetic resonance imaging
NMR	nuclear magnetic resonance
NMDA	N-methyl-D-aspartate
NO	nitric oxide
PLIC	posterior limb of the internal capsule
PSF	point spread function

R2*	relaxation rate (due to magnetic field inhomogeneities)
RETROICOR	retrospective image correction
RF	radiofrequency
ROI	region of interest
SD	standard deviation
SPIO	superparamagnetic iron oxide
SPM	Statistical Parametric Mapping
SNR	signal to noise ratio
T1	longitudinal relaxation time (due to spin-lattice interactions)
T2	transverse relaxation time (due to spin-spin interactions)
T2*	transverse relaxation time (due to magnetic field inhomogeneities)
TR	repetition time
TE	echo time
TE*	effective echo time
TEM	transverse electromagnetic
TI	inversion time
tSNR	temporal signal to noise ratio
WM	white matter

Acknowledgements

I would first like to acknowledge the mentorship and training received from my supervisor, Dr. Ryan C.N. D'Arcy, who, most importantly, shared his inspiring interest and enthusiasm for research. I am also grateful for the guidance of my committee members, Drs. Steven Beyea, Aaron Newman, and Kazue Semba. I would also like to acknowledge the helpful mentorship of my comprehensive project supervisor Drs. Chris Bowen, Yannick Marchand, and Aaron Newman, as well as my comprehensive chair Dr. Shelley Adamo. In addition, I have been fortunate to work with Dr. John Fisk while at Dalhousie.

Thanks are extended to Drew DeBay, Dr. Kirk Feindel, Jodie Gawryluk, Steve Patterson, Nicole Pelot, Dr. Dennis Phillips, and Dr. Tracy Taylor-Helmick for their significant support, advice, and motivation through difficulties. In addition, thanks to many individuals for helpful and insightful conversations. This long and hopefully complete list of people includes Dr. Tim Bardouille, Dr. Josh Bray, Dr. Kim Brewer, Therese Chevalier, Eva Gunde, Carl Helmick, Connie Jess, Dr. Lei Liew, Rahia Mashoodh, Sean McWhinney, Dr. Antonina Omisade, Dr. David Pitcher, James Rioux, Dr. Tyler Rolheiser, Dr. David Smith, Dr. Xiaowei Song, Tynan Stevens, Dr. Peggy St Jacques, Ryan Wilson, and Magdalena Wojtowicz. In addition, thanks for administrative and technical support are extended to Sujoy Ghosh-Hajra, Careesa Liu, David McAllindon, Janet Marshall, and Wendy Smith-D'Arcy. For their data collection efforts, I would like to thank Dr. Kim Brewer, Kim Dillen, and Jodie Gawryluk.

I would also like to acknowledge all the help and support I received on an earlier thesis plan involving rat fMRI. Thanks are extended to past committee members Drs. Chris Bowen and Douglas Rasmusson for their mentorship and guidance. In addition, thanks to Dr. Douglas Rasmusson for providing patient and generous training in rat electrophysiology. I would also like to acknowledge extensive technical support from Drew DeBay and Dr. Kirk Feindel, and additional help and support from Hannah Dahn, Steve Patterson, Nicole Pelot, and James Rioux.

Finally, for their patience throughout this process, thanks to my supportive family, Mark Zwicker, Dan Mazerolle, Kathy Mazerolle, and Kelly Mazerolle.

Chapter 1 Introduction

1.1. Overview

White matter, which contains the connections between brain regions, comprises approximately 50% of the human brain (Arai and Lo, 2009; Black, 2007; Harris and Attwell, 2012). The functional significance of white matter has been established by extensive lesion and anatomic studies, which have demonstrated the importance of intact white matter for normal brain function, and have implicated white matter damage and disconnections in numerous neurologic and psychiatric diseases (e.g., Catani & fftyche, 2005). Despite its importance, white matter is rarely considered in functional neuroimaging studies. A tool to non-invasively investigate the functional dynamics of white matter would substantially broaden current approaches to the study of brain connectivity, and be of considerable value to research into the assessment and progression of white matter diseases such as multiple sclerosis.

Recently, evidence has begun mounting that it is possible to study the functional dynamics of white matter with functional magnetic resonance imaging (fMRI). However, there are still a number of issues related to white matter fMRI that call its validity into question. This manuscript-based thesis will address some of these issues in order to refine the current understanding and enhance the interpretability of fMRI activation in white matter.

In this chapter, the relevant concepts in magnetic resonance imaging (MRI), fMRI, and diffusion tensor imaging (DTI) will be introduced (Section 1.2). Next, a rationale for how the study of brain connectivity could be improved by white matter fMRI techniques will be proposed, and the possible neurophysiologic explanations for fMRI activation in white matter will be outlined (Section 1.3). A review of the existing studies reporting white matter fMRI activation will follow (Section 1.4). The introduction will conclude with a description of the objectives of the experiments presented in this thesis (Section 1.5).

1.2. MRI Techniques

1.2.1. Principles of MRI

MRI is a non-invasive imaging technique with extensive applications in biomedical research and other fields. MRI is an application of nuclear magnetic resonance (NMR), which capitalizes on the magnetic properties of certain atomic nuclei. For MRI, the most commonly used atom is hydrogen, allowing the study of proton-dense body tissues with high water and fat content (Matthews, 2002).

Atomic nuclei have a number of fundamental physical properties (e.g., mass, charge). Of importance to NMR is another such property, called spin. The spin of hydrogen nuclei is such that they have a magnetic moment. When placed in a static magnetic field (called B_0), the spins tend to align either parallel or anti-parallel to B_0, with a slightly larger fraction of spins aligning parallel. A sample placed in a static magnetic field thus develops a bulk magnetization. This bulk magnetization displays resonance phenomena with a characteristic frequency (the Larmor frequency ω) that is directly proportional to B_0 and the properties of the atomic nucleus under investigation. By applying an oscillating electromagnetic field (also called a radiofrequency or RF pulse) at ω, the bulk magnetization is rotated into the transverse plane relative to B_0, and precesses around the axis of B_0 at ω. This results in an oscillating magnetic field, which will induce a voltage in a receive coil. This voltage is the basis for the NMR signal (Jezzard and Clare, 2002).

By varying the strength of the magnetic field experienced by the spins using gradient magnetic fields, ω will change as a function of the linear distance along the gradient. This property is the basis of spatial localization of NMR signals, which is required for imaging (Matthews, 2002). Slice selection can be achieved by applying a gradient along one axis such that the magnetic field varies between the slabs of tissue. The slabs will then have different ω, allowing independent excitation of the slices by applying an RF pulse at the appropriate frequency. Within a slice, localization can be achieved using phase and frequency encoding. For phase encoding, another gradient (orthogonal to the slice select gradient) is briefly applied. Because the spins are experiencing different magnetic fields, they have different resonance frequencies, which causes them to dephase. These phase differences can be used to localize signals along one

axis of a slice. In frequency encoding, another gradient is applied in the third orthogonal plane, again resulting in different ω along the gradient. This gradient remains on during signal acquisition, allowing the frequency differences to be used to localize signals along this axis.

Over time, the bulk magnetization (which had been flipped into the transverse plane by applying an RF pulse) becomes realigned to B_0. This return to equilibrium occurs due to interactions between the hydrogen nuclei and the surrounding environment (i.e., spin-lattice relaxation) and can be described by the longitudinal relaxation time constant (T1). T1 depends on an atom's efficiency in exchanging energy with its environment through motion of the molecules. For energy exchange to take place, the molecular motion must occur at specific frequencies. Therefore, T1 depends on factors such as molecule size, physical state, viscosity, and temperature (Jezzard and Clare, 2002; Matthews, 2002).

In addition to realigning with B_0, the transverse magnetization also decays. Each spin experiences a slightly different magnetic field, which results in slightly different precession frequencies. The frequency differences result in phase offsets between the spins, so that the vector sum of the spins' magnetization decreases. Local variations in the magnetic field are caused by two factors:

1) Molecular interactions that change the magnetic field experienced by the spins (i.e., spin-spin relaxation). The decay of transverse magnetization caused by molecular interactions can be described by the time constant T2.
2) Inhomogeneities in B_0. The decay due to inhomogeneity effects can be described by the time constant T2*.

Thus, processes contributing to both T2 and T2* are responsible for decay of the transverse magnetization (Jezzard and Clare, 2002; Matthews, 2002). In some pulse sequences, the dephasing of spins is refocused by applying a 180 degree RF pulse at some time (τ) after the initial RF pulse that flipped the spins into the transverse plane. This inverts the magnetization of the spins, such that they rephase and form a signal echo (called a spin echo) at time 2τ (Jezzard and Clare, 2002).

T1, T2, and T2* differences between tissue types can be used to generate image contrast by using imaging techniques (called pulse sequences) that are weighted for a

particular time constant. Figure 1.1 provides examples of T1-, T2-, and T2*-weighted images.

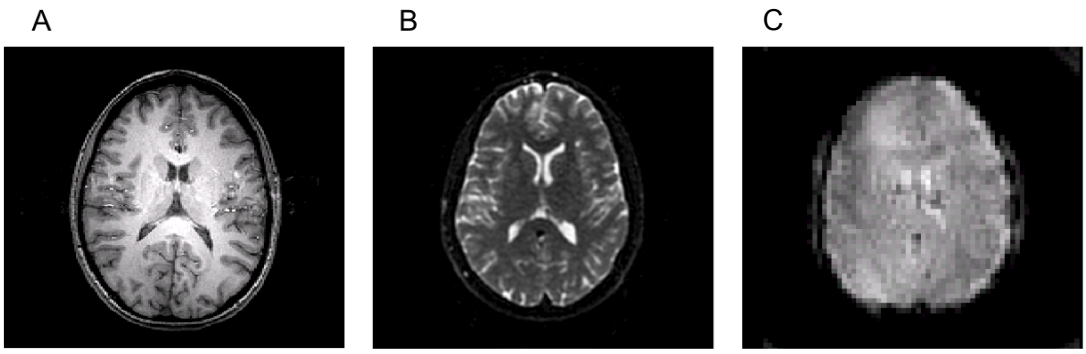

Figure 1.1. Examples of MRI images with different contrast. A: T1-weighted; B: T2-weighted; C: T2*-weighted (Mazerolle, unpublished results).

1.2.2. Principles of Functional MRI

1.2.2.1. Physics of Functional MRI. The most commonly used fMRI technique, blood oxygen level dependent (BOLD) contrast, capitalizes on the different magnetic properties of oxygenated and deoxygenated hemoglobin. While oxygenated hemoglobin is diamagnetic (i.e., will create a small magnetic field repelling an external magnetic field), deoxygenated hemoglobin is paramagnetic (i.e., will create a magnetic field attracting an external magnetic field). The magnetic field created by paramagnetic deoxygenated hemoglobin results in inhomogeneities in the static magnetic field. The field inhomogeneities result in faster signal decay due to shorter T2*. When using a T2*-weighted sequence, deoxygenated hemoglobin results in reduced image intensity (Matthews, 2002).

As discussed in detail in Section 1.2.2.2, neural activity leads to increased energy demands (Attwell and Laughlin, 2001). Via various complex and incompletely understood pathways, these increased energy demands are met by regional increases cerebral blood flow (CBF) and volume (CBV) to provide oxygenated blood to activated neurons (i.e., functional hyperemia). The increases in CBF and CBV overcompensate for the oxygen metabolized to support the demands of increased neural activity, such that neural activity is linked to an increase in oxygenated hemoglobin. Thus, regions with increased neural activity have relatively greater signal intensity on T2*-weighted images

(e.g., Kida and Hyder, 2005; Lauritzen and Gold, 2003; Logothetis, 2003; Matthews, 2002; Uğurbil et al., 2007).

1.2.2.2. Neurophysiological Basis of Functional MRI Signals. Seminal work by Logothetis and colleagues (2001) demonstrated that BOLD signal changes are strongly associated with the input activity to the region (i.e., post-synaptic activity or local field potentials; LFP). While Logothetis and colleagues (2001) also reported that BOLD signal changes were correlated with output activity (i.e., action potentials or spiking activity), they describe this correlation as fortuitous due to the inherent correlations between spiking and local field potentials. Rauch and colleagues (2008) went on to show that local field potentials are sufficient for BOLD signal changes, which can take place in the absence of spiking activity.

Recent evidence has revealed the multi-dimensional and context-dependent nature of this relationship. For example, regional differences in neurovascular coupling have been observed. Sloan and colleagues (2010) showed the relationship between LFP and BOLD activity differs between cortical and subcortical gray matter, with larger LFP responses and smaller BOLD responses in the striatum compared to the cortex. Furthermore, different experimental conditions have been shown to decouple the neural and hemodynamic response. Sirotin and Das (2009) showed that within V1, two distinct categories of hemodynamic responses could be observed. The first category of hemodynamic responses was stimulus-related and could be predicted by increased neural activity resulting from visual stimulation. Interestingly, the second category of hemodynamic responses could be measured in complete darkness in anticipation of an absent visual stimulus. This work demonstrates the existence of context-dependent dissociations between neural and hemodynamic responses.

In addition to the uncertainties in terms of the relationship between neural activity and the hemodynamic response, the metabolic pathways by which neural signals are transduced into hemodynamic changes are also incompletely understood. There is evidence that the increased glucose and oxygen metabolism (and the corresponding metabolites) associated with neural activity does not directly impact neurovascular coupling. Instead, other molecular events associated with neural activity are thought to be

the primary stimulus for the hemodynamic response (Lauritzen, 2005; Petzold and Murthy, 2011).

Neurovascular coupling pathways can be divided into two overlapping categories: neuron-mediated and astrocyte-mediated. Neuron-mediated pathways include the actions of inhibitory interneurons, which are known to act directly on smooth muscle by releasing vasodilators such as nitric oxide (NO) and vasoactive intestinal peptide, and vasoconstrictors such as somatostatin and neuropeptide Y (Cauli et al., 2004; Kleinfeld et al., 2011). In addition, γ-aminobutyric acid (GABA) may have a direct vasoactive effect, given that GABA interneurons have been found to project directly to cerebral vessels, which have been shown to express GABA receptors (Drake and Iadecoa, 2007; Vaucher et al., 2000; Kocharyan et al., 2008). In addition to the interneurons, projections from neurons located in subcortical regions such as the basal forebrain, raphe nucleus, ventral tegmental area, and locus coeruleus also contact blood vessels and exert vasodilatory or vasoconstrictive effects via neurotransmitters and neuropeptides (Drake and Iadacola, 2007). Finally, glutamatergic pyramidal cells are thought to release NO following activation of N-methyl-D-aspartate (NMDA)-type receptors and subsequent increase in intracellular calcium ion (Ca^{2+}) concentration (Lecrux and Hamel, 2011; Drake and Iadacola, 2007). The glutamate-evoked increase in intracellular Ca^{2+} concentration is also linked to increased production of the arachidonic acid metabolite prostaglandin E2, which induces vasodilation via an unidentified mediator (Petzold and Murthy, 2011). The effects of glutamate may be mediated by adenosine (Iliff et al., 2003), which is also produced by neural activity (Drake and Iadecola, 2007).

Astrocytes are ideally positioned to control neurovascular coupling, as they receive input from neurons and have processes (i.e., end feet) closely apposed to the smooth muscle cells that control the vascular tone of the corresponding arterioles. The morphological properties of astrocytes, combined with recent functional evidence (described below) have caused some to speculate that neurovascular coupling is mediated entirely by astrocytes (Petzold and Murthy, 2011) [1].

Glutamate has been implicated in astrocyte-mediated neurovascular coupling. In astrocytes, activation of metabotropic glutamate receptors is associated with intracellular

[1] One exception noted by Petzold and Murthy (2011) is gaseous vasoactive substances such as NO.

Ca^{2+} increases, which spread to distant regions of the astrocyte to form Ca^{2+} waves. The Ca^{2+} waves are associated with increased production of the arachidonic acid metabolites prostaglandin E2 and epoxyeicosatrienoic acids (Koehler et al., 2008; Petzold and Murthy, 2011). The vasoactive effects of these compounds can be either dilatory or constricting depending on factors such as NO concentration (Lecrux and Hamel, 2011; Drake and Iadecola, 2007).

Potassium has been implicated in both neuron- and astrocyte-mediated neurovascular coupling. Potassium ions (K^+) may mediate rapid vascular responses to neural activation (Lecrux and Hamel, 2011). K^+ is released during neuronal depolarization, and this increase in extracellular K^+ concentration (along with glutamate import) drives K^+ into astrocytes. The astrocytes then release K^+ perivascularly, which causes the arteriole smooth muscle cells to dilate (Petzold and Murthy, 2011). Interestingly, this astrocyte-mediated vasodilation is faster (66ms) than the vasodilation that results from freely diffusing extracellular K^+ (2.5s; Gjedde, 2002). The vasodilatory effects of increased extracellular K^+ concentration are partially mediated by NO (Drake and Iadecola, 2007; Lauritzen, 2005).

In addition to their effects on the smooth muscle cells of arterioles, neurons and astrocytes might also act on contractile cells found on capillary walls, called pericytes, to control neurovascular coupling. Pericytes have been shown to respond to many of the same vasoactive molecules as the arteriolar smooth muscle cells, including NO, adenosine, and arachidonic acid metabolites. However, conclusive *in vivo* evidence linking pericytes to neurovascular coupling is lacking (Hamilton et al., 2010).

1.2.3. Principles of Diffusion Imaging

Diffusion weighted imaging (DWI) and DTI applications primarily employ Stejskal-Tanner diffusion encoding. In this scheme, a pair of equal gradients is applied on either side of the spin echo. Spins that have changed position (i.e., diffused) between and during the application of the diffusion gradients result in reduced signal intensity (because they are not refocused by the spin echo). The amount of diffusion weighting (i.e., the loss of signal intensity due to diffusion) is dependent on the strength of the applied diffusion gradients, the duration of the diffusion gradients, and the time between the diffusion

gradients, and is typically expressed as a b-value, which has the unit s/mm^2. DWI can be used to evaluate the apparent diffusion coefficient (ADC) of tissue, which is important clinically for evaluating conditions such as stroke (Mukherjee et al., 2008; Basser and Özarslan, 2009).

Diffusion can be isotropic (i.e., occur equally in all directions). In the brain, isotropic diffusion occurs in the large cerebrospinal fluid (CSF) spaces where diffusion of water is not restricted. Diffusion is also considered isotropic in gray matter, where the complex microstructure restricts diffusion approximately equally in all directions at the spatial scale that can be measured with diffusion MRI. In regions where many fibres are aligned (e.g., white matter tracts), water tends to diffuse along the axis of the tract because diffusion is restricted in directions perpendicular to the tract. This phenomenon is known as anisotropic diffusion (Jones et al., 1999).

Anisotropic diffusion can be characterized by applying diffusion gradients along different spatial axes. By acquiring at least six images with noncollinear diffusion gradients, plus an image with no diffusion weighting, the diffusion tensor (an ellipsoid model of the anisotropic diffusion) can be calculated. This information can be used to calculate the fractional anisotropy (FA) at each voxel. High FA indicates a preferred direction of diffusion (Mukherjee et al., 2008; Nucifora et al., 2007). An example FA map is presented in Figure 1.2.

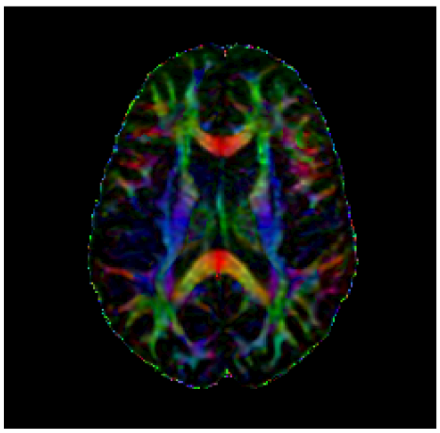

Figure 1.2. Example of a colour FA map, calculated from diffusion tensor images. The intensity (brightness) represents the amount of fractional anisotropy. The colours represent the preferred direction of diffusion (red: left-right; green: anterior-posterior; blue: inferior-superior; Mazerolle, unpublished results).

Fibre tracking algorithms map the white matter pathways of the brain by following the direction of diffusion from voxel to voxel. These algorithms are typically constrained by a minimum FA value and a maximum fibre turning angle to exclude brain regions that are not likely white matter and improbable fibres, respectively (Mukherjee et al., 2008). Fibre tracking is a major advance in neuroscience research as it allows the structural connectivity of the brain to be mapped non-invasively *in vivo* (Nucifora et al., 2007; Jones et al., 1999).

1.3. Rationale for Studying Functional MRI Activation in White Matter

1.3.1. Impetus

There is a growing interest in brain imaging to describe the entire network of connections in the human brain (i.e., map the human connectome). Brain connectivity is a fundamental concept in neuroscience and is especially important in cognitive neuroscience, as it is from distributed networks of brain regions that complex functions emerge. Intact brain connectivity is necessary for normal function, and disconnections are implicated in many neurologic and psychiatric conditions, including multiple sclerosis (Charil et al., 2006) and schizophrenia (White et al., 2008).

MRI studies of connectivity have mainly used DTI tractography to map structural connections and functional connectivity analyses (e.g., correlations among the fMRI timecourses of gray matter regions) to understand functional connections. While DTI tractography has permitted significant advances in the current understanding of brain connectivity, the technique is limited to evaluating structure, and does not provide information about the functional dynamics of the identified networks. Information from DTI tractography can be augmented with functional connectivity analyses, which typically infers connectivity based on correlations between the time series of different gray matter regions.

DTI tractography and functional connectivity approaches (and combinations thereof) are fundamentally limited by the fact that neither directly evaluates the functional dynamics within the white matter pathways. Studying the activation patterns of the white matter pathways is crucial for understanding the interactions among different nodes in a brain network, as well as evaluating whether structural white matter changes are

associated with functional changes. This approach may also clarify whether observed correlations between gray matter regions (a typical approach to studying functional connectivity using fMRI) result from direct connections, or indirect connections mediated by other gray matter areas.

In addition to the potential applications for brain connectivity research, white matter fMRI could also be applied to the diagnosis and assessment of white matter disorders. This is of particular interest in conditions such as multiple sclerosis, in which a clinical-radiological paradox has been observed. That is, the functional deficits experienced by multiple sclerosis patients (especially deficits in the cognitive domain) do not always correlate well with imaging and pathology findings (Calabrese et al., 2011; Pelletier et al., 2009). Furthermore, the dynamic progression of multiple sclerosis may be characterized inadequately by structural measures. However, it is possible that the functional deficits experienced by multiple sclerosis patients are related to changes in the tissue function (e.g., decreased functional efficiency) that could be detected by studying a functional metric of white matter.

1.3.2. Neurophysiological Explanations

Despite growing evidence for white matter fMRI activation (see Section 1.4), it remains a contentious issue, in part because the neurophysiological mechanism is not understood. It is worth repeating that, as stated by Tettamanti and colleagues (2002), Mazerolle and colleagues (2008), and Yarkoni and colleagues (2009), the primary argument against white matter fMRI activation is the historical lack of reports, rather than any fundamental property that would preclude its existence. The following section will review what is known about white matter energy demands and neurovascular coupling, and posit that there is sufficient existing evidence to warrant further study into white matter fMRI activation and its neurophysiological mechanisms.

1.3.2.1. White Matter Hemodynamics. As white matter has three to six times less CBF and CBV relative to gray matter, it was previously thought that fMRI was sensitive exclusively to gray matter (Logothetis and Wandell, 2004). However, hemodynamic changes can be detected in white matter during vascular challenges, such as breath-holding tasks or hypercapnia (Driver et al., 2010; Helenius et al., 2003; Macey

et al., 2003; Mandell et al., 2008; Preibisch and Haase, 2001; Rostrup et al., 2000; van der Zande et al., 2005). Thus, there is evidence that white matter has the vascular capacity to support hemodynamic changes that are detectable with fMRI. However, as will be discussed in Chapter 2, the methodology used to define white matter regions of interest (ROIs) is somewhat lacking in most of these studies, leaving open the possibility that the signal changes observed in white matter are the result of contamination from nearby gray matter (i.e., partial volume effects).

1.3.2.2. Neurovascular Coupling in White Matter. Despite evidence that the hemodynamics of white matter are sufficient to support measureable changes with fMRI, a crucial question that remains is whether activity-dependent hemodynamic changes take place. Activity-dependent hemodynamic changes are a necessary feature for any neural activity to be detectable with fMRI.

As described in Section 1.2.2.2, the neurophysiologic source of fMRI signals has been linked to post-synaptic potentials, which are mainly localized to gray matter. Although there are some synapses and even some cell bodies in white matter (Harris and Attwell, 2012), post-synaptic potentials account for less than 1% of the energy demands in white matter (Harris and Attwell, 2012), making them an unlikely source for fMRI signal changes.

In white matter, the primary type of neural activity is spiking. As noted above, Logothetis' group showed that BOLD signal changes require only LFPs and can take place in the absence of spiking activity (Rauch et al., 2008). While Rauch and colleagues (2008) provide strong evidence that LFPs are sufficient for BOLD signal changes, their results do not rule out the possibility that action potentials are also sufficient for inducing a hemodynamic response (i.e., by finding a method to block LFP activity and then measuring spiking and BOLD signal changes). It is important to note that the relationship between neural activity and hemodynamic changes has only been studied for gray matter, where post-synaptic potentials do require the majority of energy (Attwell and Laughlin, 2001; Harris and Attwell, 2012). Furthermore, even within gray matter, a relationship between spiking and fMRI activation has not been ruled out (e.g., Smith et al., 2002).

In white matter, it is possible that metabolic demands associated with action potentials (i.e., increased activity at energy-dependent ion pumps; Aiello and Bach-y-

Rita, 2000; Erecińska and Dagani, 1990) are met with a measurable hemodynamic response. The brain does not have any major energy or oxygen reserves, relying on blood perfusion to meet its metabolic demands (Lecrux and Hamel, 2011). Thus, any spiking related energy demands might result in a hemodynamic response. Before such a conclusion can be reached, it is crucial to first consider the magnitude of activity dependent metabolic demands in white matter to evaluate whether they might reasonably be expected to produce changes that could be detected with fMRI. Harris and Attwell (2012) have proposed an energy budget for white matter, in which they estimate that the energy associated with action potentials in white matter comprises only 0.4-7% of the total energy demand in white matter (depending on myelination status). The vast majority of white matter energy demands are thought to arise from maintaining the resting potential (independent of restoring the ionic gradients due to action potentials) and housekeeping processes such as macromolecule turnover and axoplasmic transport.

A feature not included in Harris and Attwell's (2012) energy budget for action potentials is the potential involvement of non-neuronal cell types. Astrocytes exist in white matter (Harris and Attwell, 2012; Waxman and Ritchie, 1993; Rash, 2010), and may perform similar functional roles as gray matter astrocytes. One example is K^+ siphoning, in which the increase in extracellular K^+ concentration associated with spiking activity results in increased K^+ uptake into astrocytes. It has been proposed that K^+ is first transported across layers of myelin via gap junctions before being taken up by astrocytes (Rash, 2010). Astrocytes then release K^+ perivascularly, which relaxes the smooth muscle cells of the arterioles surrounded by the astrocyte's end feet. Thus, K^+ siphoning is associated with hemodynamic changes, and has been speculated to contribute to neurovascular coupling in gray matter (Petzold and Murthy, 2011).

The presence of K^+ channels in the astrocytes and oligodendrocytes of white matter have been confirmed for the rat optic nerve (Rash, 2010). Kalsi and colleagues (2004) found that astrocyte expression of K^+ channels is localized to perivascular endfeet and on processes located within myelinated axon bundles, consistent with a K^+ siphon function. Oligodendrocytes, which make up myelin, are often considered to be passive insulators, serving to promote saltatory conduction by preventing ion flux at locations other than nodes of Ranvier. In contrast, it has recently been proposed that myelin might

also act as a K^+ siphon for spiking axons via gap junctions between the axons and innermost myelin layer, between successive myelin layers, and between the outermost myelin layer and astrocytes (Rash, 2010). While diffusion of K^+ through gap junctions is not an energy-demanding process, as it is driven by an electrochemical gradient, this may be an important pathway linking action potentials and a hemodynamic response.

In addition to the neurovascular mechanisms speculated above, experimental evidence of activity dependent metabolic changes in white matter has been established. Weber and colleagues (2002) investigated activity-dependent glucose uptake changes in a rodent model using [^{18}F]fluorodeoxyglucose autoradiography. They reported increased glucose uptake in the corpus callosum associated with electrical stimulation of a cortical region with callosal projections. Furthermore, the increase in glucose uptake was greater for higher frequency stimulation. However, it has not yet been experimentally demonstrated that activity-dependent increases in glucose uptake in white matter are coupled to a hemodynamic response that could be measured with fMRI. In addition, the lack of temporal information available from the autoradiography technique means that the observed increased in metabolic demands associated with spiking rate may occur over too slow a time scale (i.e., many minutes or hours) for this effect to be relevant for typical fMRI experiments. For these reasons, it will be important for future studies to experimentally verify whether the metabolic increases observed by Weber and colleagues (2002) are accompanied by BOLD signal changes.

While there are still some unanswered questions, it is impossible to rule out BOLD signal changes associated with white matter activation. Indeed, given the extent of reports of white matter fMRI activation (described in Section 1.4), there is a strong impetus for further refining the understanding of BOLD signal changes in white matter.

1.4. White Matter Functional MRI Activation: A Chronology

The earliest reports of fMRI activation in white matter came from Mosier and colleagues, who reported individual level activation in the corpus callosum and internal capsule associated with swallowing (1999a,b). However, this work relied on uncorrected statistical thresholds ($p < 0.03$). Mosier and Bereznaya (2001) later confirmed corpus

callosum activation could be observed during swallowing at corrected statistical thresholds.

Brandt and colleagues (2000) reported negative signal change in the occipital white matter containing the optic radiations contralateral to the visually stimulated hemisphere (uncorrected $p < 0.001$). However, this is the only report of task-related negative signal changes in white matter, making it difficult to interpret.

Chiu and colleagues (2001) reported signal changes in the white matter adjacent to the activated cortical gray matter during a finger tapping task. However, very few voxels in white matter were activated. Furthermore, the activated white matter voxels tended to be contiguous with larger, more strongly activated gray matter clusters, suggesting that the white matter activation may have been the result of blurring or partial volume effects.

Tettamanti and colleagues (2002) published a key report of white matter fMRI activation, in which activation in the genu of the corpus callosum associated with a visuo-motor interhemispheric transfer task (the Poffenberger paradigm) was observed. Most importantly, the authors speculated about the possible neurophysiological underpinnings of task-related hemodynamic changes in white matter. Tettamanti and colleagues' (2002) findings were confirmed by Omura and colleagues (2004), and expanded upon by Weber and colleagues (2005), in which the relationship between interhemispheric transfer and attention was explored. Weber and colleagues (2005) confirmed previous findings of genu activation associated with the interhemispheric transfer task; however, effects of attention were localized to areas such as the parietal lobe and the superior colliculi. In addition to the studies using the Poffenberger paradigm, Aramaki and colleagues (2006) reported corpus callosum activation associated with interhemispheric interactions during bimanual coordination.

D'Arcy and colleagues (2006) used visual hemifield presentation of functionally lateralized stimuli to elicit interhemispheric transfer. By using an exploratory data analysis approach, activation in the splenium of the corpus callosum activation could be observed, providing the first fMRI evidence of posterior callosal activation associated with an interhemispheric transfer task.

In Mazerolle and colleagues (2008), the group expanded and refined their earlier approach, employing whole brain coverage, acquiring data at high field (4 T), and using a

general linear model-based analysis technique. Splenium activation was observed in approximately 20% of individuals, as well as at the group level when liberal thresholds were applied ($p < 0.005$ uncorrected). Gawryluk and colleagues (2009) went on to provide insight to the physics of detecting white matter fMRI activation, showing that sensitivity to white matter clusters could be improved when T2-weighting was increased, although this effect appears to be due to a general increase in sensitivity from combining T2*- and T2-weighting, rather than a white matter specific effect (McWhinney et al., unpublished observations). The group went on to functionally map the corpus callosum, showing distinct areas of activation for two different interhemispheric transfer tasks (Gawryluk et al., 2011a). Fabri and colleagues (2011) recently expanded this work, demonstrating that different tactile, gustatory, visual, and motor tasks could be mapped to distinct callosal regions.

Gawryluk and colleagues (2011b) also confirmed that activation could be detected in the internal capsule during a motor task. In addition, recent work has demonstrated that white matter fMRI activation is elicited by the symbol digit modalities test, a neuropsychological test of information processing that is sensitive to impairments associated with multiple sclerosis (Gawryluk et al., unpublished observations).

Other conditions under which white matter fMRI activation has been observed include a study of native signers viewing American Sign Language sentences with inflectional morphology (genu of the corpus callosum; Newman et al., 2010). In addition, white matter fMRI activation was observed for both healthy controls and Alzheimer's patients during a memory task (various white matter regions; Weis et al., 2011). In a multi-study analysis, Yarkoni and colleagues (2009) reported fMRI signal changes associated with reaction time in the right lateral genu of the corpus callosum, as well as in parts of the posterior corona radiata bilaterally (among gray matter regions).

1.5. Current Objectives

The overall objective of this thesis is to refine the understanding of observations of fMRI activation in white matter. The experiments presented in this manuscript-based thesis will introduce and address three research questions:

1) Can white matter support hemodynamic changes that can be detected with fMRI in the absence of partial volume effects?
2) What is the relationship between sensitivity to white matter fMRI activation and field strength?
3) What is the relationship between white matter fMRI activation and the activated network in gray matter?

Chapter 2 describes research investigating the first question, in which the potential contribution of partial volume effects to white matter fMRI activation are evaluated. As discussed in Section 1.3.2.1, hemodynamic changes in white matter associated with vascular challenges are well established; however, such studies have employed problematic methodologies for defining white matter ROIs. It is possible that the signal changes in white matter reported by these studies were the result of gray matter contamination of the white matter ROIs. In order to confirm that task related white matter fMRI activation might have a hemodynamic origin, it is crucial to verify that white matter can support vascular changes when controlling for partial volume effects. Whole brain hemodynamic changes will be elicited using a vascular challenge (i.e., a breath-holding fMRI task). White matter ROIs will be defined conservatively to determine whether hemodynamic changes can be detected in white matter in the absence of partial volume effects. The effect of spatial smoothing will also be evaluated to determine whether white matter signal changes can be explained by smoothing related signal contamination.

Chapter 2 Hemodynamic Changes in White Matter during a Breath-Holding Task Do Not Result Solely from Partial Volume Effects: Implications for White Matter Functional MRI

2.1. Publication Status

Mazerolle EL, Brewer KD, Beyea SD, Gawryluk JR, Bowen CV, D'Arcy RCN (in preparation) Hemodynamic changes in white matter during a breath-holding task do not result solely from partial volume effects: implications for white matter fMRI.

2.2. Student Contributions to Manuscript

Framing the research question, devising the data analysis approach, data analysis, interpretation of the results, and writing the manuscript.

2.3. Abstract

The ability to detect functional magnetic resonance imaging (fMRI) activation in white matter remains contentious. Although cerebral blood flow and volume are lower in white matter than in gray matter, there is evidence that white matter is capable of supporting hemodynamic changes that are measureable with fMRI. We sought to evaluate the contribution of partial volume effects on the fMRI signal changes that are measured in white matter. For this study, participants completed a vascular challenge (breath-holding task) while fMRI data were acquired at 4T. Region of interest (ROI) analyses were performed to compare the signal changes in conservatively defined gray and white matter ROIs. The impact of spatial smoothing was also evaluated to determine whether white matter signal changes result from smoothing-related signal contamination. We found significant signal changes associated with the breath-holding task in both gray and white matter ROIs, even when smoothing was not applied. The findings suggest that hemodynamic signals can originate in white matter (as opposed to resulting from partial volume effects), and provide insight into the possible source of white matter fMRI activation.

2.4. Introduction

Reports of white matter functional magnetic resonance imaging (fMRI) activation are becoming more common (D'Arcy et al., 2006; Fabri et al., 2011; Gawryluk et al., 2009, 2011a,b; Mazerolle et al., 2008, 2010; Mosier and Bereznaya, 2001; Newman et al., 2010; Omura et al., 2004; Tettamanti et al., 2002; Weber et al., 2005; Weis et al., 2011; Yarkoni et al., 2009). White matter fMRI could be applied to investigate the functional dynamics of brain connectivity noninvasively, and thus broaden the current studies of brain connectivity, which focus mainly on structural connectivity or indirect examinations of functional connectivity via correlations among gray matter regions. White matter fMRI might also be applied to the assessment of white matter disorders and disconnection syndromes in order to better evaluate dynamic changes in disease state.

Despite the potential clinical and research value of studying white matter fMRI activation, the technique remains controversial due to two issues: 1) The source of fMRI signal changes has been linked to post-synaptic potentials, which mainly take place in gray matter (e.g., Logothetis et al., 2001). 2) Functional MRI is a hemodynamic technique that relies on the coupling between neural activity and blood oxygenation changes, but cerebral blood flow (CBF) and volume (CBV) are lower in white matter compared to gray matter (Logothetis and Wandell, 2004; Weis et al., 2011). The current study will focus on the latter issue.

Notwithstanding lower CBF and CBV in white matter, the ability to detect hemodynamic changes in white matter is well established by studies of vascular challenges such as breath-holding or hypercapnia tasks (Driver et al., 2010; Helenius et al., 2003; Macey et al., 2003; Mandell et al., 2008; Preibisch and Haase, 2001; Rostrup et al., 2000; van der Zande et al., 2005). Hypercapnia and breath-holding studies rely on the vasodilatory properties of carbon dioxide. Increasing the amount of carbon dioxide in the blood (either by inspiring increased concentrations of carbon dioxide or by holding one's breath) and measuring the resulting signal changes with fMRI can thus be used to evaluate the cerebrovascular reactivity of brain regions (Driver et al., 2010).

However, many of the existing reports of hemodynamic signal changes in white matter associated with vascular challenges have employed potentially problematic methods for defining their regions of interest (ROIs) that might lead to gray matter signal

contamination of the white matter ROIs (i.e., partial volume effects). For example, Rostrup and colleagues (2001) and Helenius and colleagues (2003) defined ROIs manually, a subjective process which might result in misclassification of gray and white matter voxels. Macey and colleagues (2003) applied a somewhat liberal probability threshold of 50% to partial volume estimates output by an automated tissue segmentation routine. Some studies have not adequately reported their ROI generation methods, preventing an evaluation of the level of rigor applied (Mandell et al., 2008; Preibisch and Haase, 2001; van der Zande et al., 2005).

To our knowledge, only one study defined their gray and white matter ROIs using a conservative approach designed to minimize partial volume effects. Driver and colleagues (2010) performed tissue type segmentation on anatomic images acquired at the same spatial resolution as functional images (2 x 2 x 3 mm^3). In addition, the authors applied a 99% probability threshold to the partial volume estimates of white matter (output by FMRIB's Automated Segmentation Tool; FAST; Zhang et al., 2001). With these methods, the authors reported hemodynamic changes in white matter, confirming the results of the studies noted above in which ROI generation techniques may have resulted in misclassification of voxels and/or partial volume effects.

However, studies reporting task-related white matter fMRI activation have typically used lower resolution fMRI acquisitions (e.g., 3.75 x 3.75 x 5 mm^3) than the resolution employed by Driver and colleagues (2010) The lower spatial resolution typically employed in white matter fMRI activation studies may make the definition of white matter ROIs that are not contaminated by partial volume effects from gray matter more difficult. In the current study, we evaluated whether hemodynamic changes in white matter associated with a vascular challenge could be detected with standard resolution fMRI and conservatively defined white matter ROIs. To do this, we used a breath-holding task to elicit whole brain signal changes. Functional MRI data were acquired with 3.75 x 3.75 x 5 mm^3 spatial resolution. Gray and white matter signal changes were evaluated using ROIs derived from partial volume estimate maps created by FAST and thresholded at 99% probability. We also evaluated the impact of spatial smoothing on signal changes in white matter ROIs. We hypothesized that even when applying conservative metrics to define white matter ROIs, signal changes associated with the vascular challenge would

still be detected. Based on previous reports, we predicted smaller signal changes in white matter compared to gray matter (Driver et al., 2010; Helenius et al., 2003; Macey et al., 2003; Preibisch and Haase, 2001; Rostrup et al., 2000; van der Zande et al., 2005). We further hypothesized that white matter signal changes would still be detected even when spatial smoothing was not applied.

2.5. Methods

2.5.1. Task and Participants

Data from a previous study (Brewer et al., 2009) were reanalyzed for the current study. Healthy participants performed a visually-cued breath-holding task, in which 30 s of regular breathing was alternated with 30 s of breath-holding (repeated four times). Eight participants completed the task; however, one participant was excluded due to poor task compliance. In addition, three subjects were excluded due to poor registration results (see below). Similar studies have previously used four or five participants (e.g., Brewer et al., 2009; Driver et al., 2010; Jochimsen et al., 2010).

2.5.2. MRI Acquisition

The data were collected using a 4T Oxford magnet with a Varian INOVA console. A body coil provided gradients (Tesla Engineering Ltd.) and a transverse electromagnetic head coil was used for transmit/receive (Bioengineering Inc.). The fMRI acquisition used an asymmetric spin echo (ASE) spiral sequence (two shots, TR = 1.5 s, spin echo centre = 70 ms, effective echo time = 25 ms, 64 x 64 matrix, 240 x 240 mm^2 field of view [FOV], 13 5 mm axial slices). A high resolution, whole brain spiral image was collected for registration purposes (four shots, 128 x 128 matrix, 240 x 240 mm^2 FOV; 22 5 mm axial slices). For anatomic reference, registration, and tissue segmentation, a structural image was collected using a 3D magnetization prepared fast low angle shot sequence (TR/TI/TE = 10/500/5 ms, 11 degree flip angle, 256 x 256 x 64 matrix, 240 x 240 x 192 mm^3 FOV).

2.5.3. Data Analysis

2.5.3.1. Pre-Processing. Analyses were performed with the fMRI expert analysis tool (FEAT) version 5.98 in FMRIB Software Library (FSL; Smith et al., 2004). Pre-

statistics processing included the following steps: motion correction using MCFLIRT (Jenkinson et al., 2002), non-brain removal using BET (Smith, 2002), mean-based intensity normalisation, and highpass temporal filtering (Gaussian weighted least-squares straight line fitting, with $\sigma = 60$ s). Additionally, we evaluated the effect of spatial smoothing by repeating the analyses both on smoothed data (Gaussian kernel, 6 mm full width at half maximum) and unsmoothed data.

2.5.3.2. Statistical Analysis. Time series statistical analyses were carried out using FMRIB's Improved Linear Model (FILM) with local autocorrelation correction (Woolrich et al., 2001). The breath-holding task was modelled as a sinusoid with a period of 60 s (Brewer et al., 2009). This model fit the signal changes observed in the data more closely than the standard hemodynamic response function, likely due to the different physiological source (i.e., neural activation versus vascular challenge). Motion parameters output from the motion correction were included in the model as regressors of no interest. *Z* (Gaussianised *t*) statistic images were reported using a threshold for clusters determined by $z > 2.3$ and a (corrected) cluster significance threshold of $p < 0.05$ (Worsley et al., 1992).

2.5.3.3. Tissue Segmentation and ROI Generation. Partial volume estimate maps of gray and white matter were calculated from each participant's structural image using FAST (Zhang et al., 2001). *A priori* tissue probability maps were used to initialize the segmentation. The partial volume estimate maps output by FAST were thresholded at 99% probability to ensure conservatively defined ROIs (Driver et al., 2010). The resulting gray and white matter ROIs were registered to fMRI space using the registration parameters described below (nearest neighbour interpolation). The masks were also eroded with a kernel of 3 x 3 x 3 voxels to exclude any voxels on the border of the ROIs. The erosion transformation resulted in empty gray matter ROIs due to the their sparse spatial pattern. However, a small white matter ROI including only deep white matter structures was created for each participant via the erosion transformation. The JHU ICBM-DTI White Matter Labels atlas (Oishi et al., 2005) was used to determine which white matter regions where included in the eroded white matter ROI. Parts of the corpus callosum, internal and external capsules, corona radiata, and superior longitudinal fasciculus were included in the eroded white matter ROIs of all four subjects. Voxels

from other regions (posterior thalamic radiation, sagittal stratum, superior fronto-occipital fasciculus) also belonged to the eroded white matter ROI for some subjects.

Despite the application of a conservative threshold to the probability maps output by FAST, tissue segmentation can be problematic in subcortical regions. We performed three steps to ameliorate this issue: 1) We manually removed any voxels on the CSF-white matter borders that were misclassified as gray matter. 2) Voxels belonging to the cerebellum and midbrain were excluded from the ROIs. Cerebellum and midbrain exclusion ROIs were derived from the MNI structural atlas (Collins et al., 1995; Mazziotta et al., 2001) and the Talairach atlas (Talairach and Tournoux, 1988; Lancaster et al., 2000, 2007), respectively. 3) To investigate the possible contribution of misclassified gray and white matter voxels in subcortical regions that were not corrected in steps 1 or 2, results were also evaluated for ROIs restricted to slices superior to the lateral ventricles (superior ROIs). Signal changes associated with the breath-holding task were evaluated for resulting ROIs (gray matter, superior gray matter, white matter, superior white matter, and eroded white matter) using featquery.

2.5.3.4. Registration. FMRIB's Linear Image Registration Tool (FLIRT; Jenkinson and Smith, 2001; Jenkinson et al., 2002) was used to coregister the structural images and the high resolution spiral image (six degrees of freedom, normal search). The high resolution spiral image was then registered to functional space (six degrees of freedom, normal search). The registrations were inspected visually to ensure quality (see Figure 2.1 for an example registration report). Using the parameters above, the data from five participants did not register well from structural space to functional space, likely due to the image distortions caused by susceptibility induced field gradients (see Figure 2.2 for an example of misregistration). For two of the remaining participants, excluding the intermediate registration step and using seven degrees of freedom and no search produced satisfactory registration results (based on visual inspection). However, we were not able to achieve satisfactory registration for the three remaining participants. These data were excluded from the analyses to avoid registration-related misclassification of gray or white matter voxels. Thus, data from four participants were included in the analysis.

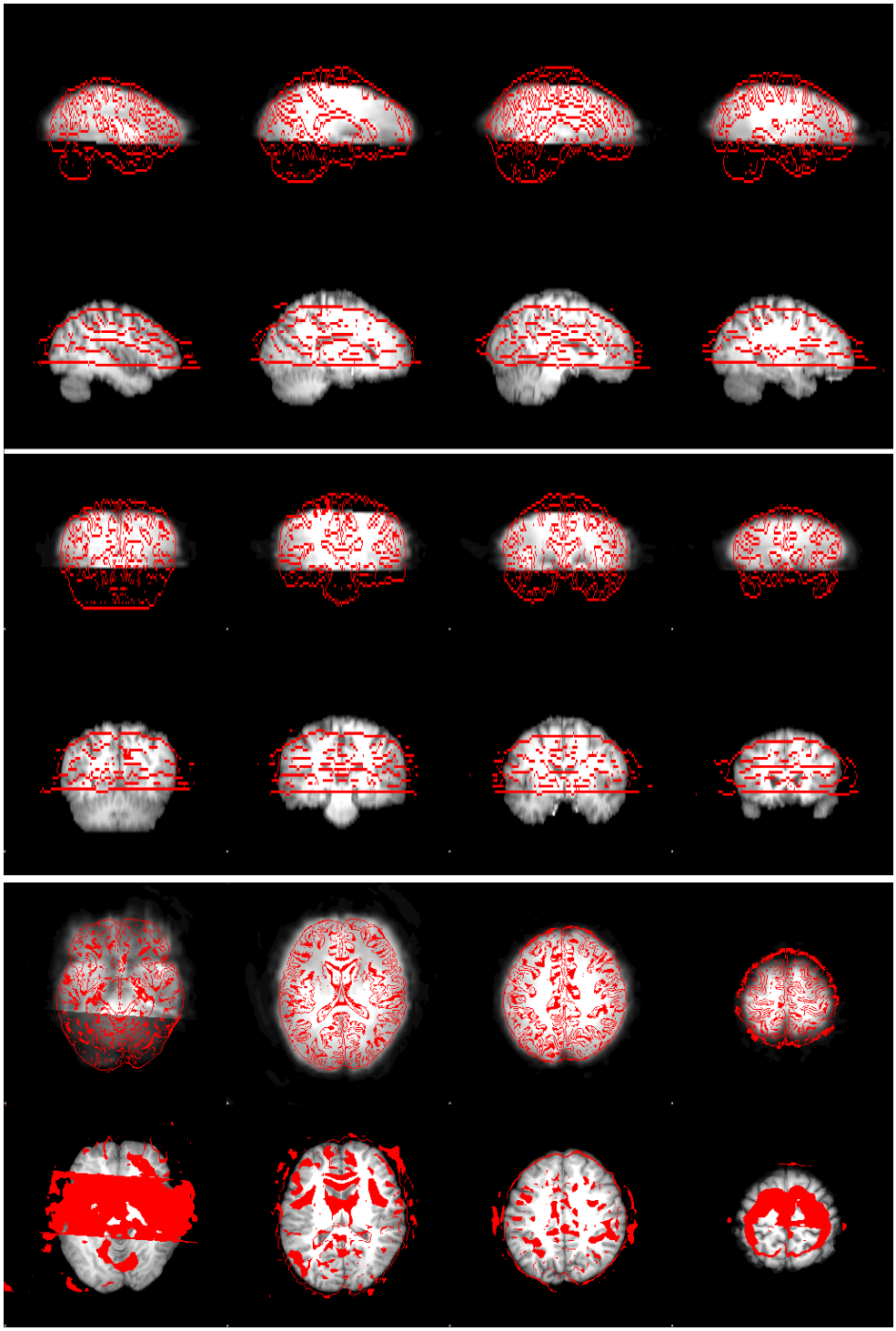

Figure 2.1. Summary of the registration results from a representative participant with good registration. Top panel: sagittal views; middle panel: coronal views; bottom panel: axial views. In each panel, the upper row depicts slices from the functional image, with the edges of the registered structural image overlaid in red; the lower row depicts slices from the structural image, with the edges of the registered functional image overlaid in red.

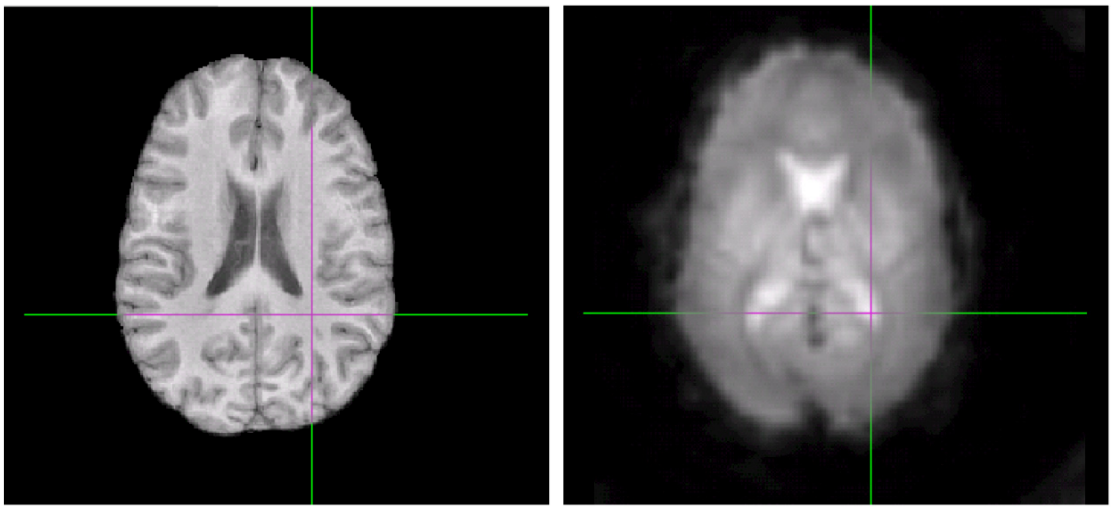

Figure 2.2. An example participant with poor registration results. The crosshairs are in the same location in both images. Note that the white matter of the anatomic image (left) is registered to a region of the lateral ventricles in the functional image (right).

2.6. Results

Whole brain signal changes were elicited by the breath-holding task. Figure 2.3 shows maps of significant signal changes for an example participant, for both smoothed and unsmoothed data. Maps for the remaining subjects can be found in Supplementary Figure 2.1. Figure 2.4 depicts an example participant's ROIs overlaid on a map of significant signal changes (smoothed data). The extent of significant signal changes, maximum percent signal change and *z*-score, and mean percent signal change and z-score (including only voxels with significant signal changes) are presented in Tables 2.1 and 2.2 for smoothed and unsmoothed data, respectively.

In all participants analyzed (N = 4), significant signal changes were observed in both gray and white matter ROIs (Figure 2.4). Furthermore, white matter signal changes were evident in both smoothed and unsmoothed data (Figure 2.3, Tables 2.1 and 2.2). The grand average mean signal change in white matter was 1.79 and 2.45% for smoothed and unsmoothed data, respectively, suggesting that smoothing-related signal contamination from gray matter is not responsible for the observed hemodynamic signal changes in white matter. In gray matter, grand average mean signal change was 2.59 and 3.32% for smoothed and unsmoothed data, respectively. White matter signal changes were also observed in the superior ROIs (i.e., slices not affected by poor tissue segmentation in

subcortical regions), with grand average mean signal changes of 1.65 and 2.22% for smoothed and unsmoothed data, respectively. In gray matter, grand average mean signal change in the superior ROIs was 2.39 and 2.97% for smoothed and unsmoothed data, respectively. The mean percent signal change and mean *z*-score values were similar between the superior ROIs and the whole brain ROIs (see Tables 2.1 and 2.2). Finally, significant signal changes were also detected in the eroded white matter ROIs (i.e., the most conservatively defined ROIs), with grand average mean signal changes of 1.01 and 1.47% for smoothed and unsmoothed data, respectively.

As expected, mean signal changes in white matter were smaller than those in gray matter (range of grand average mean signal change: 1.01-2.45% for white matter; 2.39-3.32% for gray matter). In addition, the percentage of voxels with significant signal changes was smaller in white matter, but still represented a substantial proportion of voxels (47-74% in the non-eroded white matter ROIs versus 67-85% in the gray matter ROIs). Even when no spatial smoothing was applied and the eroded white matter ROIs were used, approximately 20% of voxels had significant signal changes associated with the breath-holding task.

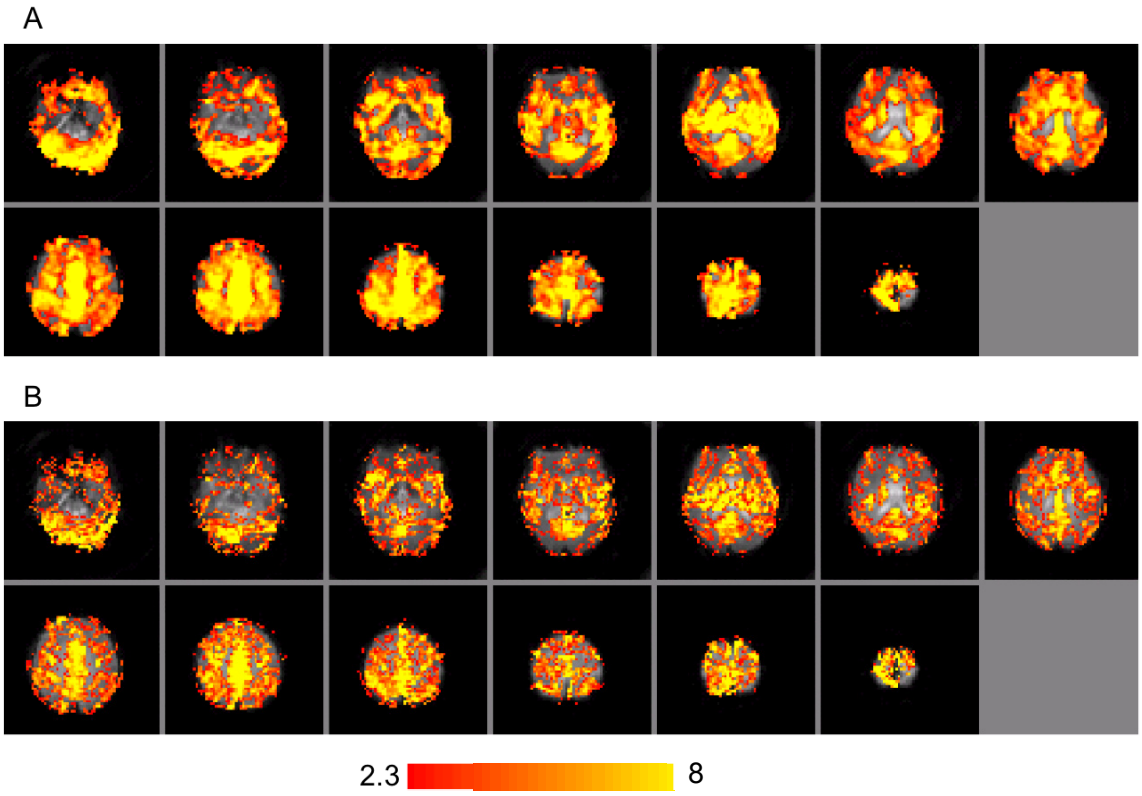

Figure 2.3. Significant signal changes associated with the breath-hold task for an example participant for both smoothed (A) and unsmoothed (B) data. The scale bar represents *z*-scores. Data from the remaining participants are in Supplementary Figure 2.1.

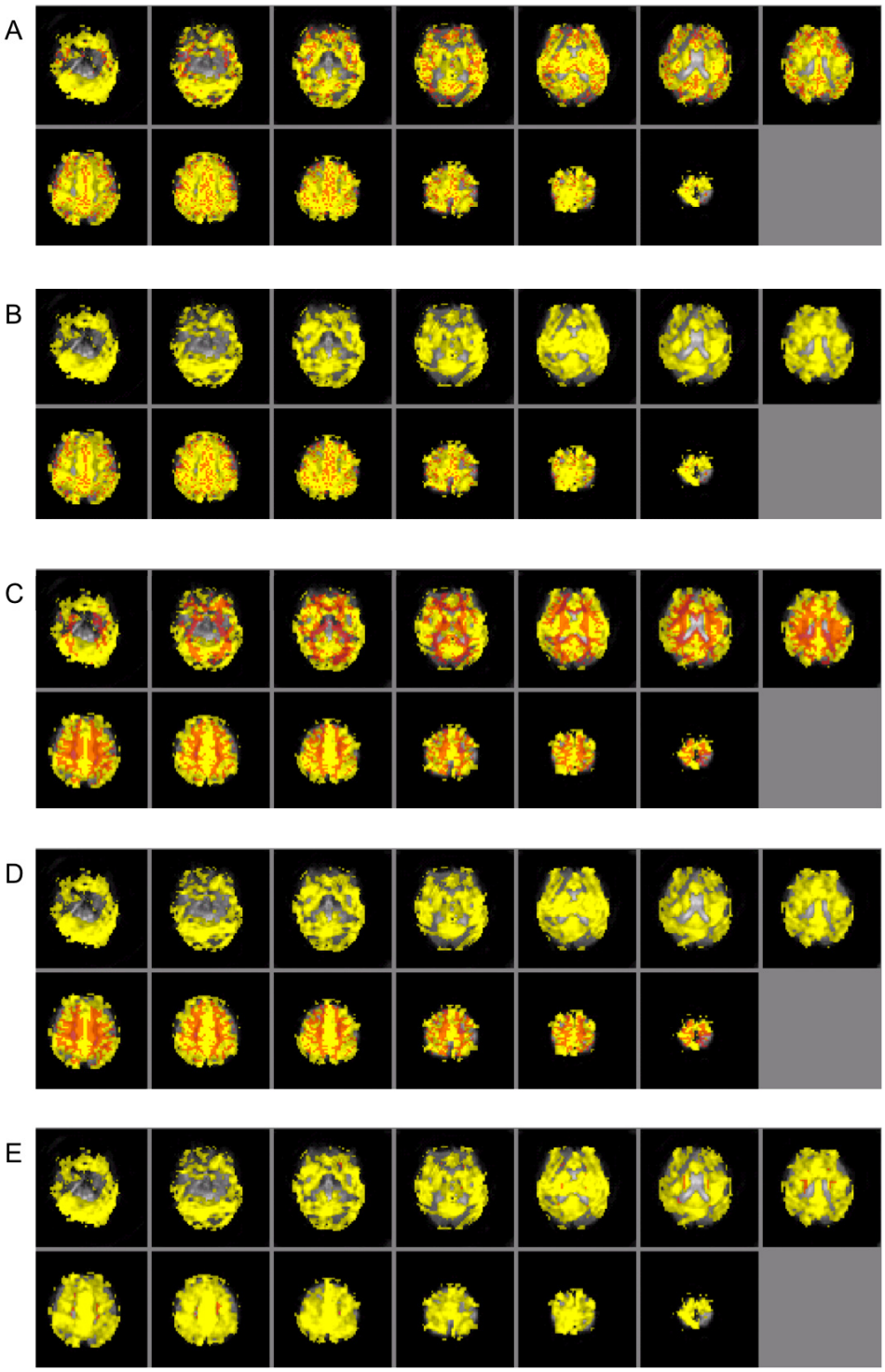

Figure 2.4. ROIs (red) overlaid on a map of significant signal changes (yellow) for an example participant. A: all gray matter, B: superior gray matter, C: all white matter, D: superior white matter, E: eroded white matter.

Table 2.1. Results from smoothed data.

A. Signal changes associated with the breath-holding task (grand average results).

	ROI	% of ROI with significant signal changes	Max %sc	Max *z*-score	Mean %sc	Mean *z*-score
Grand average	GM (all)	80.95	11.28	11.35	2.59	5.54
	GM (superior ROI)	84.52	9.94	10.65	2.39	5.87
	WM (all)	64.85	12.39	10.88	1.79	5.11
	WM (superior ROI)	74.12	11.76	10.55	1.65	5.27
	WM (eroded ROI)	34.16	2.56	7.48	1.03	4.29

GM: gray matter; WM: white matter; %sc: percent signal change.

Table 2.1. Results from smoothed data.

B. Signal changes associated with the breath-holding task (individual results).

Participant	ROI	ROI size (# of voxels)	# of voxels with significant signal changes	% of ROI with significant signal changes	Max %sc	Max *z*-score	Mean %sc	Mean *z*-score
1	GM (all)	1903	1186	62.32	6.35	9.32	1.70	4.06
	GM (superior ROI)	767	495	64.54	4.99	7.84	1.53	4.04
	WM (all)	4635	1886	40.69	6.29	9.41	1.36	3.97
	WM (superior ROI)	1741	799	45.89	6.29	8.48	1.26	3.90
	WM (eroded ROI)	188	14	7.45	3.66	5.07	1.52	3.73
2	GM (all)	2142	1758	82.07	12.14	13.83	2.78	6.40
	GM (superior ROI)	760	658	86.58	10.33	13.83	2.70	7.17
	WM (all)	4403	3422	77.72	14.11	12.68	1.87	5.79
	WM (superior ROI)	1519	1392	91.64	14.11	12.68	1.79	6.17
	WM (eroded ROI)	92	71	77.17	2.67	9.13	0.88	4.59
3	GM (all)	2205	1997	90.57	13.04	10.18	2.72	5.47
	GM (superior ROI)	817	777	95.10	10.85	8.88	2.38	5.67
	WM (all)	4602	2976	64.67	13.93	10.02	1.86	5.10
	WM (superior ROI)	1577	1184	75.08	11.42	9.62	1.54	5.03
	WM (eroded ROI)	167	32	19.16	1.64	7.88	0.83	4.36
4	GM (all)	1932	1716	88.82	13.59	12.05	3.15	6.23
	GM (superior ROI)	726	667	91.87	13.59	12.05	2.95	6.60
	WM (all)	4745	3622	76.33	15.23	11.43	2.08	5.58
	WM (superior ROI)	1811	1519	83.88	15.23	11.43	2.01	5.97
	WM (eroded ROI)	146	48	32.88	2.28	7.85	0.88	4.47

GM: gray matter; WM: white matter; %sc: percent signal change.

Table 2.2. Results from unsmoothed data.

A. Signal changes associated with the breath-holding task (grand average results).

	ROI	% of ROI with significant signal changes	Max %sc	Max *z*-score	Mean %sc	Mean *z*-score
Grand average	GM (all)	67.08	18.25	10.79	3.32	5.01
	GM (superior ROI)	71.79	14.83	10.13	2.97	5.21
	WM (all)	47.09	21.28	10.83	2.45	4.62
	WM (superior ROI)	53.92	20.53	9.86	2.22	4.73
	WM (eroded ROI)	20.01	3.53	7.39	1.47	3.98

GM: gray matter; WM: white matter; %sc: percent signal change.

Table 2.2. Results from unsmoothed data.

B. Signal changes associated with the breath-holding task (individual results).

Participant	ROI	ROI size (# of voxels)	# of voxels with significant signal changes	% of ROI with significant signal changes	Max %sc	Max *z*-score	Mean %sc	Mean *z*-score
1	GM (all)	1903	897	47.14	11.69	9.03	2.43	3.95
	GM (superior ROI)	767	379	49.41	7.91	7.77	2.14	3.93
	WM (all)	4635	1380	29.77	11.00	10.30	2.03	3.89
	WM (superior ROI)	1741	578	33.20	9.55	7.40	1.85	3.84
	WM (eroded ROI)	201	15	7.46	5.23	5.17	2.02	3.40
2	GM (all)	2142	1461	68.21	16.78	12.43	3.60	5.63
	GM (superior ROI)	760	574	75.53	15.79	12.43	3.39	6.23
	WM (all)	4403	2399	54.49	24.86	11.54	2.52	4.94
	WM (superior ROI)	1519	979	64.45	24.86	11.54	2.43	5.28
	WM (eroded ROI)	92	40	43.48	2.99	8.03	1.20	3.97
3	GM (all)	2205	1707	77.41	22.13	10.35	3.33	5.00
	GM (superior ROI)	817	668	81.76	13.22	8.99	2.78	4.99
	WM (all)	4602	2246	48.80	20.55	10.48	2.50	4.80
	WM (superior ROI)	1577	868	55.04	19.01	9.53	2.02	4.63
	WM (eroded ROI)	167	20	11.98	2.53	7.59	1.24	4.23
4	GM (all)	1932	1460	75.57	22.40	11.34	3.92	5.45
	GM (superior ROI)	726	584	80.44	22.40	11.34	3.58	5.71
	WM (all)	4745	2623	55.28	28.69	10.98	2.74	4.88
	WM (superior ROI)	1811	1141	63.00	28.69	10.98	2.57	5.18
	WM (eroded ROI)	146	25	17.12	3.37	8.77	1.44	4.33

GM: gray matter; WM: white matter; %sc: percent signal change.

2.7. Discussion

2.7.1. Summary and Interpretation of Findings

The results provide evidence that hemodynamic changes associated with a vascular challenge can be detected in white matter, even when stringent analysis techniques are employed to control for partial volume effects. This is an important finding in terms of understanding the source of fMRI activation in white matter, as it confirms that there is sufficient CBF and CBV in white matter to detect hemodynamic changes, in contrast to previous assertions (Logothetis and Wandell, 2004; Weis et al., 2011). This finding is consistent with previous studies that demonstrated hemodynamic changes associated with vascular challenges in white matter ROIs. However, many of the previous studies used problematic approaches to define white matter ROIs, which might have resulted in non-white matter signal contamination (Helenius et al., 2003; Macey et al., 2003; Mandell et al., 2008; Preibisch and Haase, 2001; Rostrup et al., 2000; van der Zande et al., 2005).

Our results are also consistent with the study reported by Driver and colleagues (2010), in which ROIs were defined conservatively. However, the fMRI data acquired by Driver and colleagues (2010) had higher spatial resolution than is typical of the fMRI studies that have previously reported activation in white matter (D'Arcy et al., 2006; Fabri et al., 2011; Gawryluk et al., 2009, 2011a,b; Mazerolle et al., 2008, 2010; Mosier and Bereznaya, 2001; Newman et al., 2010; Omura et al., 2004; Tettamanti et al., 2002; Weber et al., 2005; Weis et al., 2011; Yarkoni et al., 2009). Furthermore, Driver and colleagues (2010) reported $\Delta R2^*$ values instead of percent signal change, making it difficult to relate the findings to white matter fMRI activation studies, which tend to report results in terms of percent signal change and/or *z*-score. In the current study, we demonstrated for the first time that, even when using standard resolution fMRI, very conservative white matter ROIs can be defined (by applying stringent probability thresholds to partial volume estimate maps and by removing boundary voxels via ROI erosion), and that these conservative white matter ROIs still exhibit significant signal changes associated with a vascular challenge.

Consistent with previous results (Driver et al., 2010; Helenius et al., 2003; Macey et al., 2003; Preibisch and Haase, 2001; Rostrup et al., 2000; van der Zande et al., 2005),

mean signal changes were smaller in white matter compared to gray matter. Differences in cerebrovascular reactivity of gray matter and white matter are consistent with the known vasculature differences between the two tissue types (Duvernoy et al., 1981) and may explain why some fMRI activation studies have shown smaller magnitude responses in white matter than gray matter (Fraser et al., submitted; Gawryluk et al., 2009; Mazerolle et al., 2010; Tettamanti et al., 2002; Yarkoni et al., 2009).

Our methodology included steps designed to minimize partial volume effects. First, we analyzed the data both with and without spatial smoothing. Spatial smoothing is routinely applied in fMRI data analysis to increase signal to noise, as well as ensure the data comply with the random field theory assumptions important for the statistical analysis (Worsley and Friston, 1995). In our data, significant signal changes could be observed in white matter ROIs even with spatial smoothing disabled (Table 2.2), providing evidence that white matter signal changes do not result solely from contamination due to spatial smoothing.

Second, we defined the ROIs conservatively. To do this, we restricted the probability threshold of the partial volume estimate maps to 99%, we reported the results with problematic inferior slices excluded, and we reported the results for an eroded white matter ROI. The presence of significant signal changes in these conservative ROIs (particularly in the eroded white matter ROI) provides strong evidence that white matter is capable of supporting hemodynamic changes measurable with fMRI and that the signal changes observed in white matter cannot be explained solely on the basis of partial volume effects.

2.7.2. Caveats

2.7.2.1. Other Potential Sources of Partial Volume Effects. Despite our careful registration procedure, resampling during the registration process might result in partial volume effects. For example, neighbouring gray and white matter voxels might be combined into a single voxel when transformed from high resolution structural space to lower resolution functional space. Importantly, the eroded white matter ROIs did not contain any boundary voxels that would have been susceptible to this potential source of

partial volume effects, yet still exhibited significant signal changes associated with the vascular challenge.

Furthermore, the point spread function (PSF) inherent to the fMRI data acquisition (i.e., spatial overlap between nearby voxels) may have contributed to gray matter signal contamination of the white matter ROI. The extent of the PSF is difficult to estimate (Robson et al., 1997), but the eroded white matter ROIs were multiple voxels away from gray matter, which likely minimized gray matter contamination of this ROI via the PSF. We note that the PSF affects all voxels, and thus also confounds the interpretation of gray matter fMRI activation.

2.7.2.2. Interpreting White Matter Functional MRI Activation. While the finding of significant signal changes in the eroded white matter ROI provides strong evidence for white matter hemodynamic changes in the absence of partial volume effects, the volume of the eroded ROI was very restricted. Thus, it is possible that the findings do not generalize to other regions of white matter. Indeed, regional differences in white matter vasculature may lead to corresponding differences in sensitivity to white matter fMRI activation. This may partially explain, for example, why the majority of white matter fMRI findings are reported so far in the corpus callosum (D'Arcy et al., 2006; Fabri et al., 2011; Gawryluk et al., 2009, 2011a; Mazerolle et al., 2008, 2010; Mosier and Bereznaya, 2001; Newman et al., 2010; Omura et al., 2004; Tettamanti et al., 2002; Weber et al., 2005; Yarkoni et al., 2009), with relatively few reports of white matter activation outside this region (but see Gawryluk et al., 2011b; Weis et al., 2011; Yarkoni et al., 2009). More work is needed to evaluate the cerebrovascular reactivity of white matter across different brain regions and compare it systematically to reports of fMRI activation in corresponding regions. This may require higher resolution acquisitions, as some regions of white matter are small compared to the voxel resolution of the current study.

It is also important to consider the physiological differences in the source of the signals measured in the current study (vascular challenge) versus those signals measured in typical fMRI activation studies (hemodynamic changes that result from neural activity; i.e., neurovascular coupling). While it is established that hemodynamic changes can take place in white matter during vascular challenges, it remains to be shown whether neural

activity in white matter is linked to hemodynamic changes. The majority of investigations of neurovascular coupling have focused exclusively on gray matter (e.g., Attwell and Iadecola, 2002; Carmignoto and Gómez-Gonzalo, 2010; Logothetis and Wandell, 2004), even in studies specifically aimed at evaluating regional differences in neurovascular coupling (e.g., Devonshire et al., 2012; Sloan et al., 2010). One exception is an autoradiography study in a rodent model, in which glucose metabolism increases associated with electrical stimulation of the corpus callosum were demonstrated (Weber et al., 2002). Given that the brain has limited energy stores and thus tight metabolic-hemodynamic coupling (Huppert et al., 2009; Lecrux and Hamel, 2011; but see Brown et al., 2004), it is likely that the observed glucose uptake increases are met by corresponding hemodynamic increases, which could potentially be measured using fMRI. However, more research is needed to confirm the existence of neural activity dependent hemodynamic changes in white matter.

2.7.3. Conclusion

In contrast to the assertion that CBF and CBV in white matter is too low to detect activation with fMRI (Logothetis & Wandell, 2004; Weis et al., 2011), our finding provides evidence that white matter has the cerebrovascular reactivity to support measurable hemodynamic changes. This finding represents a key step in establishing whether existing reports of white matter fMRI activation might have a hemodynamic origin. However, studies investigating neurovascular coupling in white matter are still required to confirm that neural activity is associated with hemodynamic changes.

2.8. Acknowledgements

This work was supported by the National Research Council of Canada and the Natural Sciences and Engineering Research Council of Canada. Thanks are extended to D.R. DeBay, K.W. Feindel, J.A. Rioux, S.A. Patterson, and N.A. Pelot for helpful conversations and editorial support.

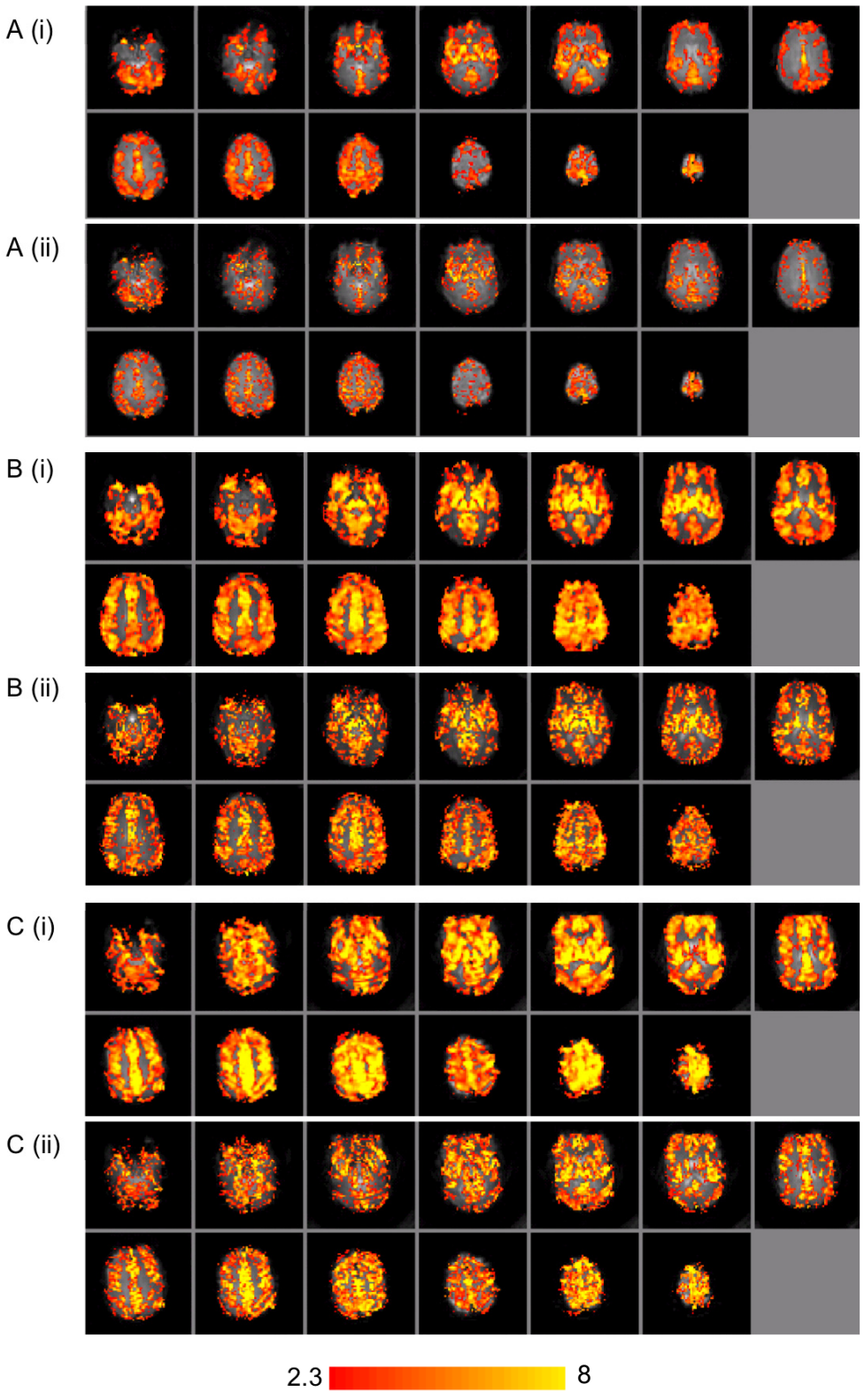

Supplementary Figure 2.1. Significant signal changes associated with the breath-hold task for three participants (A-C) for both smoothed (i) and unsmoothed (ii) data. The fourth participant is depicted in Figure 2.3. The scale bar represents *z*-scores.

2.9. Summary of Chapter 2 and Transition to Chapter 3

In Chapter 2, it was demonstrated that hemodynamic changes could be detected in white matter even when controlling for partial volume effects. This finding confirms that it is possible that white matter fMRI activation is hemodynamic in nature. Importantly, the results of Chapter 2 provide evidence that is directly relevant to one of the main issues evoking controversy surrounding white matter fMRI activation; that is, in contrast to previous assertions (Logothetis and Wandell, 2004; Weis et al., 2011), white matter CBF and CBV are sufficient for a detectable hemodynamic response.

However, the fMRI signals detected in white matter may still be smaller than those in gray matter. While white matter CBF and CBV may be sufficient for fMRI, these hemodynamic parameters are lower in white matter relative to gray matter (discussed in Section 1.2.3.1). Previous research has suggested that white matter fMRI activation is smaller in magnitude than that in gray matter (Fraser et al., submitted; Mazerolle et al., 2010; Tettamanti et al., 2002; Yarkoni et al., 2009). Given the small magnitude of white matter fMRI activation, it is important to consider the influence of factors that might improve sensitivity.

High field MRI confers greater sensitivity to BOLD fMRI (e.g., Gati et al., 1997) and thus might improve detection of small signal changes in white matter. Indirect experimental evidence supporting the importance of high field MRI can be derived by comparing D'Arcy and colleagues 1.5 T study (2006) and Mazerolle and colleagues 4 T study (2008). These studies used similar experimental designs and both reported callosal activation. However, D'Arcy and colleagues' (2006) study at 1.5 T required more sensitive data-driven analysis techniques to detect fMRI activation in white matter, whereas Mazerolle and colleagues' (2008) study at 4 T detected white matter fMRI activation using a more conservative general linear model (GLM)-based analysis technique.

In Chapter 3, the relationship between sensitivity to white matter fMRI activation and field strength will be evaluated. A task that has been previously shown to elicit white matter fMRI activation at 4 T (finger tapping; Gawryluk et al., 2011b) will be employed for the same group of participants at both 1.5 T and 4 T to determine whether high field fMRI is particularly important for detecting activation in white matter.

Chapter 3 Understanding Why White Matter Functional MRI Activation Is Scarcely Reported: Sensitivity to White Matter Activation Increases with Field Strength

3.1. Publication Status

Mazerolle EL, Gawryluk JR, Dillen KNH, Beyea SD, Stevens TMR, Bowen CV, Newman AJ, Schmidt MH, Clarke DB, D'Arcy RCN (in preparation) Understanding why white matter fMRI is scarcely reported: sensitivity to white matter activation increases with field strength.

3.2. Student Contributions to Manuscript

Framing the research question, data analysis, interpretation of the results, and writing the manuscript.

3.3. Abstract

Functional magnetic resonance imaging (fMRI) activation in white matter is controversial. Given that many of the studies that report fMRI activation in white matter used high field MRI systems, we investigated the field strength dependence of sensitivity to white matter fMRI activation. Data were acquired during a motor task (finger tapping) at 1.5 T and 4 T. Group and individual level activation results were considered in both the motor cortex and the posterior limb of the internal capsule. In addition, we evaluated the temporal signal to noise (tSNR) of the different tissue types as a function of field strength. We found that field strength dependent sensitivity increases were greater for white matter than gray matter. A similar pattern of results was observed for tSNR. The analysis of tSNR and an examination of the frequency spectra suggest that field strength related increases in physiological noise might be less problematic for white matter. We therefore conclude that high field MRI may be critical for fMRI studies aimed at investigating activation in both gray and white matter.

3.4. Introduction

3.4.1. Functional Magnetic Resonance Imaging in White Matter

Despite recent reports of white matter functional magnetic resonance imaging (fMRI) activation (Aramaki et al., 2006; D'Arcy et al., 2006; Fabri et al., 2011; Gawryluk et al., 2009, 2011a,b; Mazerolle et al., 2008, 2010; Mosier and Bereznaya, 2001; Newman et al., 2010; Omura et al., 2004; Tettamanti et al., 2002; Weber et al., 2005; Weis et al., 2011; Yarkoni et al., 2009), the ability to detect fMRI signal changes in white matter remains controversial (Logothetis and Wandell, 2004; Weis et al., 2011). White matter fMRI activation may be smaller in magnitude than gray matter activation (Fraser et al., submitted; Mazerolle et al., 2010; Tettamanti et al., 2002; Yarkoni et al., 2009), which could make detection of fMRI activation in white matter more difficult. In fact, many of the studies reporting white matter fMRI activation have used 3 T or 4 T magnets (Aramaki et al., 2006; Gawryluk et al., 2009, 2011a,b; Mazerolle et al., 2008, 2010; Weber et al., 2005; Yarkoni et al., 2009). For gray matter, high field MRI offers inherently increased sensitivity to fMRI activation relative to 1.5 T systems (Di Salle et al., 2003; Duong et al., 2003; Gati et al., 1997, 2000; Fera et al., 2004; Hoenig et al., 2005; Krasnow et al., 2003; Krüger et al., 2001; Meindl et al., 2008; Triantafyllou et al., 2005; Turner et al., 1993; Uğurbil et al., 1993, 1999; van der Zwaag et al., 2009; Yang et al., 1999). Due to the widespread availability of clinical MRI systems, a large proportion of fMRI studies have historically been performed at 1.5 T (Krasnow et al., 2003; Meindl et al., 2008; Hoenig et al., 2005), which may contribute to the overall scarcity of reports of white matter fMRI activation. To test this hypothesis, we compared internal capsule activation during a motor task at 1.5 T and 4 T. A similar task has previously been used to elicit white matter fMRI activation in the internal capsule at 4 T (Gawryluk et al., 2011b).

3.4.2. Field Strength and Sensitivity to Functional MRI Activation

Increased field strength improves sensitivity to fMRI activation in two ways. First, the signal to noise ratio (SNR) is proportional to field strength (Hu and Norris, 2004; Vaughan et al., 2001). Second, the effect of magnetic susceptibility on the resulting magnetic field is known to scale with the strength of the applied magnetic field. In this way, blood oxygen level dependent (BOLD) contrast (which depends on susceptibility

differences caused by the relative concentration of diamagnetic oxygenated hemoglobin and paramagnetic deoxygenated hemoglobin) is improved at higher magnetic fields (Di Salle et al., 2003; Hu and Norris, 2004). Increased fMRI contrast allows for improved sensitivity to brain activity (i.e., higher *z*-scores). There is considerable experimental evidence of field strength dependent sensitivity increases in gray matter (Duong et al., 2003; Gati et al., 1997; Fera et al., 2004; Hoenig et al., 2005; Krasnow et al., 2003; Krüger et al., 2001; Meindl et al., 2008; Triantafyllou et al., 2005; Turner et al., 1993; van der Zwaag et al., 2009; Yacoub et al., 2001; Yang et al., 1999).

3.4.3. The Current Study

In the current study, a finger tapping task is employed to elicit activation in the posterior limb of the internal capsule (Gawryluk et al., 2011b). We hypothesized that sensitivity to white matter fMRI activation will increase with field strength, which may partially explain the overall scarcity of fMRI studies reporting activation in white matter. In addition to activation results, we also examined temporal signal to noise (tSNR) as a function of tissue type and field strength, as this metric has been linked to successful detection of fMRI activation (e.g., Bodurka et al., 2007). Temporal SNR provides important information because it can be evaluated and compared between tissue types and field strengths even in the absence of significant activation.

3.5. Methods

3.5.1. Participants

Data from seven healthy participants (four females) were analyzed. The mean age of the participants was 24.5 ± 3.5 years. All participants were right handed as assessed by the Edinburgh Handedness Inventory (Oldfield, 1971), and had normal or corrected-to-normal vision. The study was approved by local research ethics boards. Each participant provided written informed consent prior to participation and received compensation for participating.

3.5.2. Task

The task was based on a previous study in which internal capsule activation was observed at 4 T (Gawryluk et al., 2011b). Participants performed eight blocks of visually cued sequential finger tapping (four blocks of each hand, pseudo randomly presented). Each tapping block was 20 s in duration, interleaved with 20 s rest blocks. Subjects performed the finger tapping at 2 Hz. E-Prime (Psychology Software Tools, Inc.) was used to present stimuli, which were back-projected onto a screen mounted inside the magnet bore, and viewed through a mirror mounted on the head coil.

3.5.3. MRI Acquisition

All participants were scanned at both 1.5 T and 4 T. The 1.5 T MRI was a General Electric system with an eight channel head coil. The 4 T MRI used an Oxford magnet, with gradients provided by a body coil (Tesla Engineering Ltd.), a Varian INOVA console, and a transverse electromagnetic (TEM) head coil for transmit/receive (Bioengineering Inc.).

Scan order was counterbalanced across participants. Imaging parameters were matched approximately on the two systems. Whole-brain functional images were collected with a T2*-weighted, single-shot spiral out sequence with the following parameters: TR = 2 s, flip angle = 90°, field of view = 240 x 240 mm^2, 64 x 64 matrix, 22 5 mm slices, and 0.5 mm slice gap. An echo time of 40 ms was used at 1.5 T, and an echo time of 15 ms was used at 4 T to compensate for the shorter T2* at higher fields. A high resolution T1-weighted anatomic image was collected at each session for registration purposes (TR/TE = 25/5 ms, flip angle = 40°, field of view = 240 x 240 mm^2, 256 x 256 matrix, 64 3 mm slices, no gap) using a magnetization prepared fast low angle shot (MPFLASH) sequence at 4 T and a spoiled-GRASS (SPGR) sequence at 1.5 T.

3.5.4. Data Analysis

3.5.4.1. Pre-Processing and Statistical Analyses. Pre-processing and statistical analyses were performed with the fMRI expert analysis tool (FEAT) version 5.98 in FMRIB Software Library (FSL; Smith et al., 2004). Pre-statistics processing included the following steps: motion correction using MCFLIRT (Jenkinson et al., 2002), non-brain

removal using BET (Smith, 2002), spatial smoothing using a Gaussian kernel (5 mm full width at half maximum), mean-based intensity normalisation, and highpass temporal filtering (Gaussian weighted least-squares straight line fitting, with $\sigma = 50$ s).

For the first-level analyses, time series statistical analyses were carried out using FMRIB's Improved Linear Model (FILM) with local autocorrelation correction (Woolrich et al., 2001). Motion parameters (output from the motion correction) were included in the model as regressors of no interest. Activation was modelled by convolving a boxcar function representing the task with the double gamma hemodynamic response function in FEAT. *Z* (Gaussianised *t*) statistic images were reported using a threshold for clusters determined by $z > 2.3$ and a (corrected) cluster significance threshold of $p < 0.05$ (Worsley et al., 1992). *T*-contrasts were calculated to evaluate activation for task > rest. FLIRT was used to register the functional images to the anatomic images (seven degrees of freedom [DOF]), and to register the anatomic images to the Montreal Neurological Institute template (12 DOF; Jenkinson and Smith, 2001; Jenkinson et al., 2002). Registration to standard space was then further refined using FNIRT nonlinear registration (Andersson 2007a,b). Group level activation results for 1.5 T, 4 T, 1.5 T > 4 T, and 4 T > 1.5 T were examined using FMRIB's Local Analysis of Mixed Effects stage 1 (FLAME 1; Beckmann et al., 2003; Woolrich et al., 2004; Woolrich, 2008).

3.5.4.2. Region of Interest Analysis. At both the individual and group levels, FSL's featquery tool was used to evaluate activation in the posterior limb of the internal capsule (PLIC). We focused on the PLIC because it contains corticospinal fibres connecting the primary motor and sensory cortices with the spinal cord, and has been previously shown using combined fMRI and diffusion tensor imaging (DTI) to house the structural connections associated with finger tapping activation (Guye et al., 2003). The region of interest (ROI) was selected from the JHU ICBM-DTI White Matter Labels Atlas (Oishi et al., 2005). The PLIC ROIs for a representative participant, for both field strengths, are shown in Figure 3.1. Note that although the region of orbitofrontal susceptibility artifact signal dropout is larger for the 4 T images, the PLIC ROI does not overlap with any low signal voxels. The PLIC ROIs are shown for each participant in Supplementary Figure 3.1.

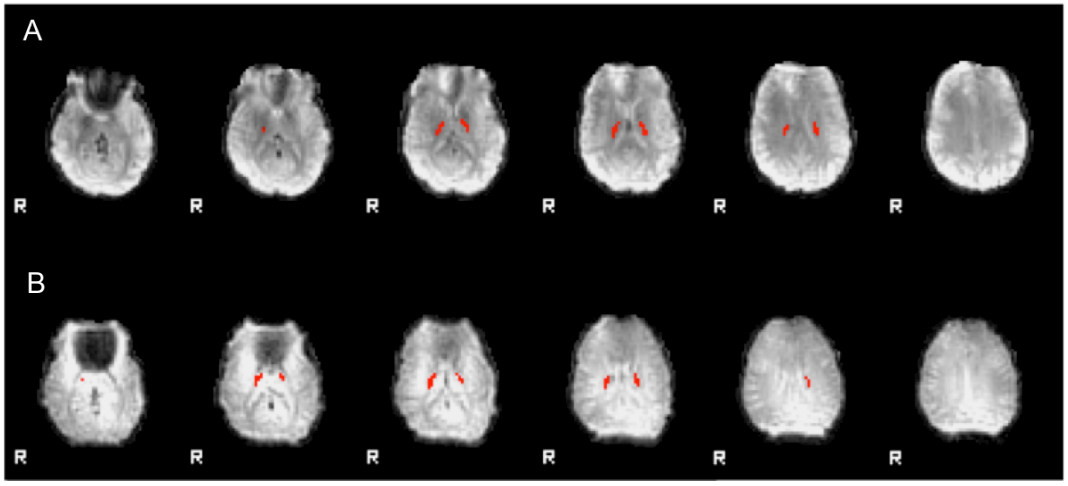

Figure 3.1. PLIC ROI overlaid on a functional volume for a representative participant, for A: 1.5 T and B: 4 T.

To determine whether activation on the white matter ROI likely originated from the PLIC (rather than, for example, resulting from gray matter signal contamination of the ROI during spatial smoothing and/or other causes of partial volume effects), we also evaluated whether the activation on the PLIC ROI included local maxima (identified using FSL's cluster tool). To be considered a local maximum, the *z*-score of the voxel had to be the largest within an 8 mm radius.

In addition to investigating the PLIC ROI, we also evaluated activation in sensorimotor cortex. Sensorimotor cortex also is activated by the finger tapping task and thus serves as a region of gray matter that can be compared to the white matter activation results. The sensorimotor cortex ROI was defined as the precentral gyrus, postcentral gyrus, and the supplementary motor cortex using the Harvard-Oxford Cortical Atlas in FSL. The sensorimotor cortex ROI was further refined to ensure only gray matter was included. Gray matter masks were defined for each participant using FMRIB's Automated Segmentation Tool (FAST; Zhang et al., 2001). *A priori* tissue probability maps were used to initialize the segmentation. A 99% probability threshold was applied to the resulting partial volume estimate maps. For both the PLIC and sensorimotor cortex ROIs, activation extent (number of significantly activated voxels), maximum *z*-score, and the mean *z*-score and mean percent signal change of significantly activated voxels was calculated.

3.5.4.3. Temporal SNR Analysis. Temporal SNR was calculated for fMRI data that had not been pre-processed, except for motion correction. The time series were also detrended using fsl_regfilt to remove activation-related variance. Thus, the tSNR values reflect factors such as temporal drift and autocorrelation, which can impact activation sensitivity if the corrections applied in the fMRI analysis do not fully compensate for their effects. Voxel-wise tSNR was calculated as the mean of the time series divided by the standard deviation of the time series. Mean tSNR values were derived for the whole brain (conservatively masked using the 80^{th} percentile voxel intensity to remove areas of susceptibility artifact related signal dropout), and for white matter and gray matter separately. Gray and white matter masks were created by thresholding the partial volume estimates output by FAST at 99% probability and registering the masks to functional space (nearest neighbor interpolation). The cerebellum was excluded by registering the cerebellum mask from the Montreal Neurological Institute Structural Atlas (Collins et al., 1995; Mazziotta et al., 2001) to each participant. We also calculated the mean tSNR for the PLIC and sensorimotor cortex ROIs.

3.5.4.4. Power Spectra Analysis. To evaluate the potential sources of variance contributing to tissue type differences in activation and tSNR results, the power spectra of the time series data were evaluated. Pre-processed fMRI data were detrended using fsl_regfilt to remove variance associated with the model. Thus, the remaining signal variance is assumed to be noise. Voxel-wise power spectra of the noise were calculated using the fslpspec function, and averaged across participants for the gray and white matter ROIs (described above). Power differences between the ROIs were then calculated for both 1.5 T and 4 T.

3.6. Results

3.6.1. Functional MRI Activation

The group level analysis revealed activation in sensorimotor cortex, the supplementary motor area, and the cerebellum for both 1.5 T and 4 T. Activation was observed in the PLIC ROI for 4 T, but not 1.5 T (see Figure 3.2). When compared statistically using a *t*-contrast, no activation was observed in the 1.5 T > 4 T contrast. For the 4 T > 1.5 T contrast, significant activation was observed, including in the PLIC and

motor cortex ROIs (Table 3.1). However, no local maxima were co-localized with the PLIC ROI, for either the 4 T or 4 T > 1.5 T contrasts.

Table 3.1. Group level ROI results.

ROI	Contrast	Max *z*-score	Extent (activated voxels/total ROI voxels)	% of ROI activated
PLIC	1.5 T	0.00	0/566	0.00
	4 T	3.82	226/566	39.93
	4 T > 1.5 T	2.62	13/566	2.30
Sensorimotor cortex	1.5 T	4.57	5272/25013	21.08
	4 T	5.00	9819/26609	36.90
	4 T > 1.5 T	3.96	785/25007	3.14

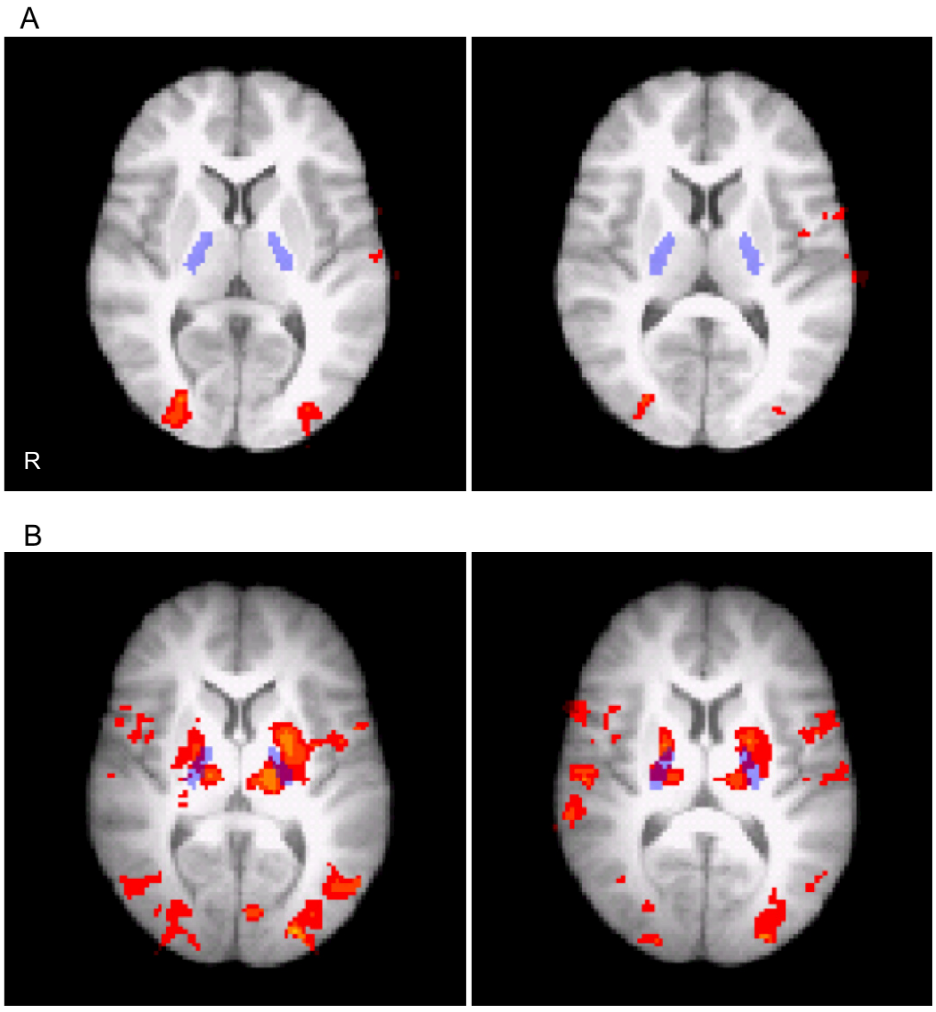

Figure 3.2. Group level activation (red) in a finger tapping task (z > 2.3, p < 0.05) at A: 1.5 T and B: 4 T. Two slices through the PLIC are shown. The PLIC ROI is overlaid in transparent blue.

Activation results for a representative participant are presented in Figures 3.3 and 3.4 for the PLIC and sensorimotor cortex ROIs, respectively. Individual level PLIC ROI results are summarized in Table 3.2, and were consistent with the group level findings. While only five of the seven participants showed PLIC activation at 1.5 T, PLIC activation was detected in all seven participants at 4 T. Furthermore, six of the seven participants had a higher maximum z-score and larger extent of activation in the PLIC for 4 T relative to 1.5 T. The maximum z-score was significantly greater for 4 T than 1.5 T ($t(6) = 2.40$, $p < 0.05$, one-tailed). The extent of activation was also significantly greater for 4 T than 1.5 T ($t(6) = 2.18$, $p < 0.05$, one-tailed). In addition, the mean z-score across

significantly activated voxels was significantly greater for 4 T than 1.5 T ($t(6) = 2.06$, $p < 0.05$, one-tailed); however, this finding should be interpreted with caution due to the large proportion of participants with very few activated voxels in the PLIC ROI at 1.5 T. Only one participant had a local maximum located on the PLIC ROI for 1.5 T, whereas four of the seven participants had local maxima on the PLIC ROI for 4 T.

The individual level sensorimotor cortex ROI results are presented in Table 3.3. While there was no difference in maximum *z*-score between 1.5 T and 4 T ($t(6) = 0.85$, p = n.s., one-tailed), the mean *z*-score across significantly activated voxels was significantly greater for 4 T than 1.5 T ($t(6) = 2.65$, $p < 0.05$, one-tailed). A larger extent of sensorimotor cortex activation was observed at 4 T versus 1.5 T (47.02 ± 11.61% and 33.44 ± 10.90% for 4 T and 1.5 T, respectively); this effect was statistically significant ($t(6) = 2.43$, $p < 0.05$, one-tailed).

For completeness, we have included mean percent signal change for the ROIs and field strengths in Supplementary Table 3.1. Note that due to the choice of TE at each field strength (40 ms for 1.5 T, 15 ms for 4 T), percent signal change would be expected to be similar for 1.5 T and 4 T results.

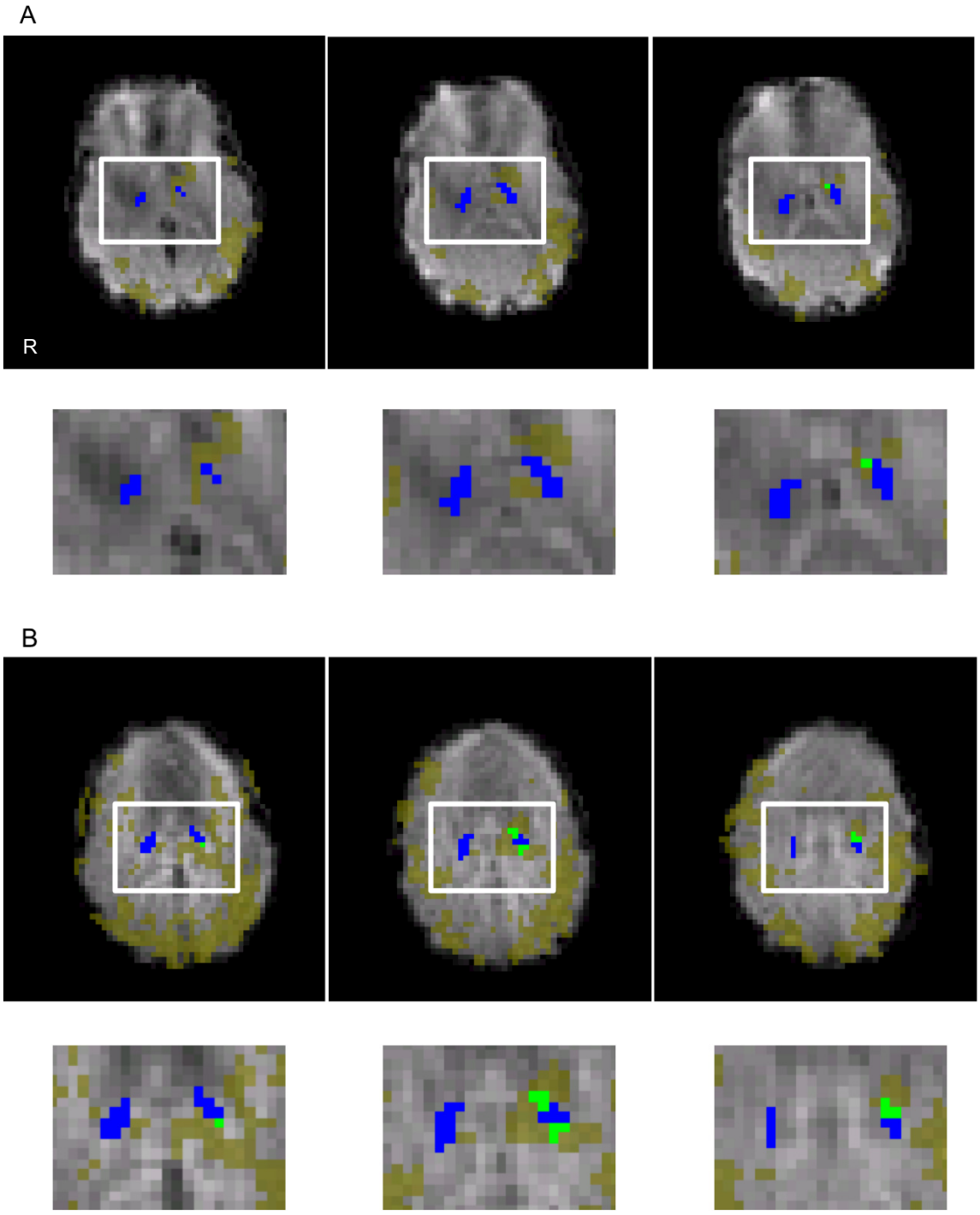

Figure 3.3. Individual level activation in the PLIC for a representative participant. A subset of relevant slices is shown. A) 1.5 T. B) 4 T. For each panel, the top row depicts the whole slice and the bottom row depicts a zoomed-in region around the internal capsule (outlined in white on the top row slices). Yellow: activation; green: activated voxels in the PLIC ROI; blue: other voxels in the PLIC ROI.

Table 3.2. Summary statistics for the PLIC ROI (individual level analysis).

A. 1.5 T.

Participant	Max *z*-score	Extent (activated voxels/total ROI voxels)	% of ROI activated	Mean *z*-score (activated voxels only)	Local max in ROI?
1	2.40	0/44	0.00	0.00	no
2	5.31	13/40	32.50	3.16	no
3	2.57	0/42	0.00	0.00	no
4	3.13	2/40	5.00	2.77	no
5	3.44	1/42	2.38	3.44	yes
6	2.48	1/48	2.08	2.48	no
7	3.26	5/36	13.89	2.99	no
Average	**3.23**	**-**	**7.98**	**2.12**	**1/7**
SD	1.01	-	11.82	1.48	-

B. 4 T.

Participant	Max *z*-score	Extent (activated voxels/total ROI voxels)	% of ROI activated	Mean *z*-score (activated voxels only)	Local max in ROI?
1	4.08	9/46	19.57	3.03	no
2	3.64	6/49	12.24	2.77	no
3	4.05	5/46	10.87	3.25	no
4	5.18	8/38	21.05	3.39	yes
5	5.10	11/47	23.40	3.60	yes
6	3.91	9/49	18.37	2.90	yes
7	4.65	21/40	52.50	3.71	yes
Average	**4.37**	**-**	**22.57**	**3.23**	**4/7**
SD	0.60	-	13.96	0.36	-

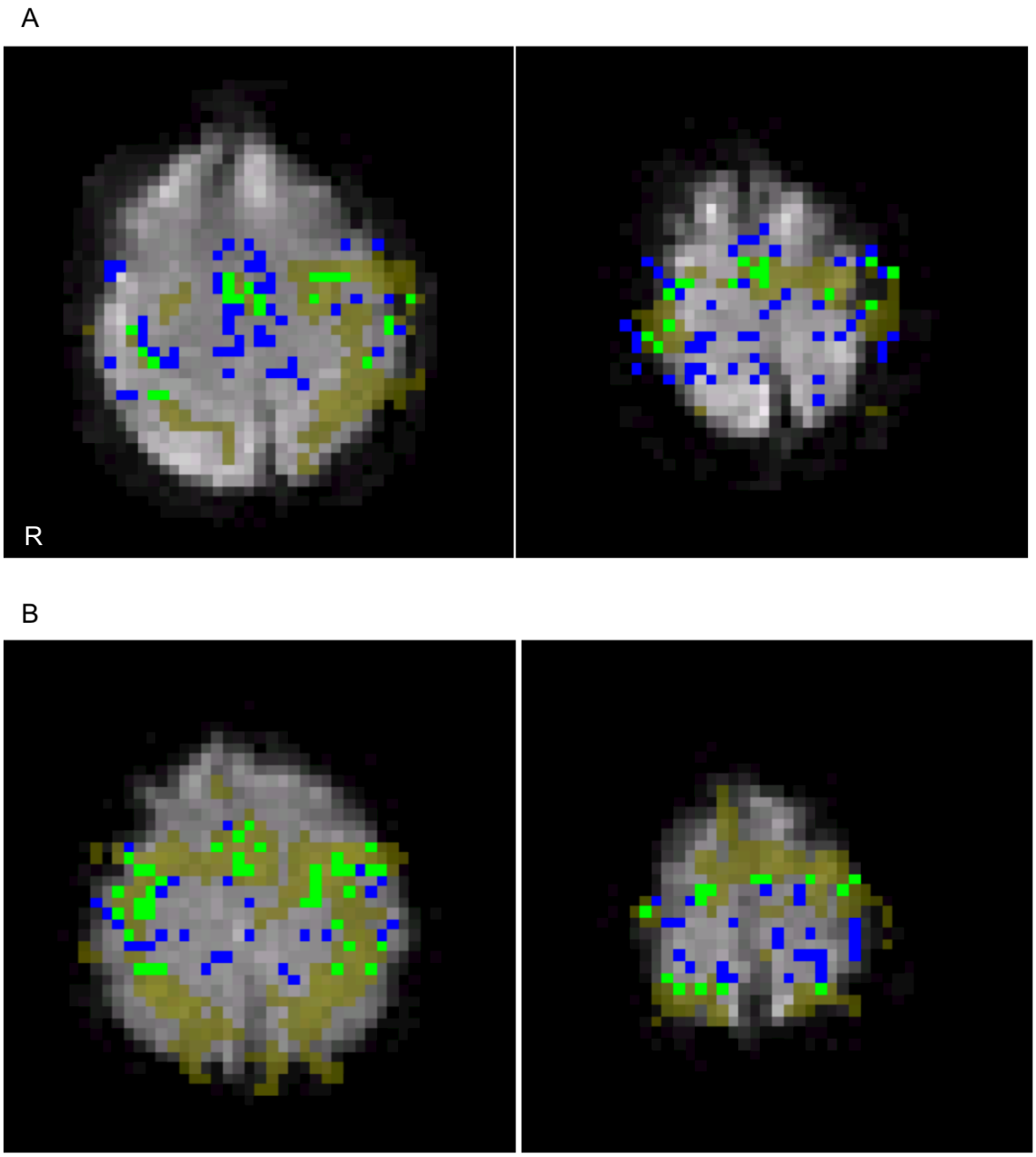

Figure 3.4. Individual level sensorimotor cortex ROI activation for a representative participant. Two relevant slices are shown. A) 1.5 T. B) 4 T. Yellow: activation; green: activated voxels in the sensorimotor cortex ROI; blue: other voxels in the sensorimotor cortex ROI.

Table 3.3. Summary statistics for the sensorimotor cortex ROI (individual level analysis).

A. 1.5 T.

Participant	Max *z*-score	Extent (activated voxels/total ROI voxels)	% of ROI activated	Mean *z*-score (activated voxels only)
1	12.11	105/480	21.88	4.61
2	12.58	189/379	49.87	5.32
3	9.56	115/493	23.33	4.05
4	9.57	217/622	34.89	4.80
5	9.45	106/457	23.19	4.17
6	10.42	204/509	40.08	4.62
7	11.53	159/389	40.87	4.63
Average	10.74	**-**	33.44	4.60
SD	1.32	-	10.90	0.42

B. 4 T.

Participant	Max *z*-score	Extent (activated voxels/total ROI voxels)	% of ROI activated	Mean *z*-score (activated voxels only)
1	11.69	285/547	52.10	5.33
2	12.23	193/427	45.20	5.64
3	9.94	193/536	36.01	4.35
4	9.68	174/586	29.69	4.47
5	12.39	255/503	50.70	5.18
6	10.30	307/470	65.32	4.97
7	11.60	187/373	50.13	5.20
Average	11.12	**-**	47.02	5.02
SD	1.12	-	11.61	0.46

3.6.2. Temporal SNR

Temporal SNR results are presented in Figure 3.5. The mean tSNR for the whole brain was 82.4 for 1.5 T and 100.6 for 4 T (i.e., an increase of 22.1% for 4 T). Whole brain tSNR was significantly greater 4 T relative to 1.5 T ($t(6)=3.52$, $p < 0.01$, one-tailed). The gray matter tSNR was 83.5 and 96.0 for 1.5 T and 4 T, respectively (i.e., an increase of 15.0% for 4 T), whereas the white matter tSNR was 97.8 and 144.0 for 1.5 T and 4 T, respectively (i.e., an increase of 47.2% for 4 T). The tSNR difference between white matter and gray matter was significantly greater at 4 T than 1.5 T ($t(6)=5.69$, $p < 0.001$, one-tailed). The relatively larger field strength dependent tSNR increase for white matter

was also observed when comparing the PLIC and sensorimotor cortex ROIs. For the sensorimotor cortex ROI, tSNR was 82.8 and 119.7 for 1.5 T and 4 T, respectively (i.e., an increase of 44.6% for 4 T). For the PLIC ROI, tSNR was 99.5 and 186.3 7 for 1.5 T and 4 T, respectively (i.e., an increase of 87.2% for 4 T). The tSNR difference between the PLIC and sensorimotor cortex ROIs was significantly greater at 4 T than 1.5 T ($t(6) = 2.83$, $p < 0.05$, one-tailed).

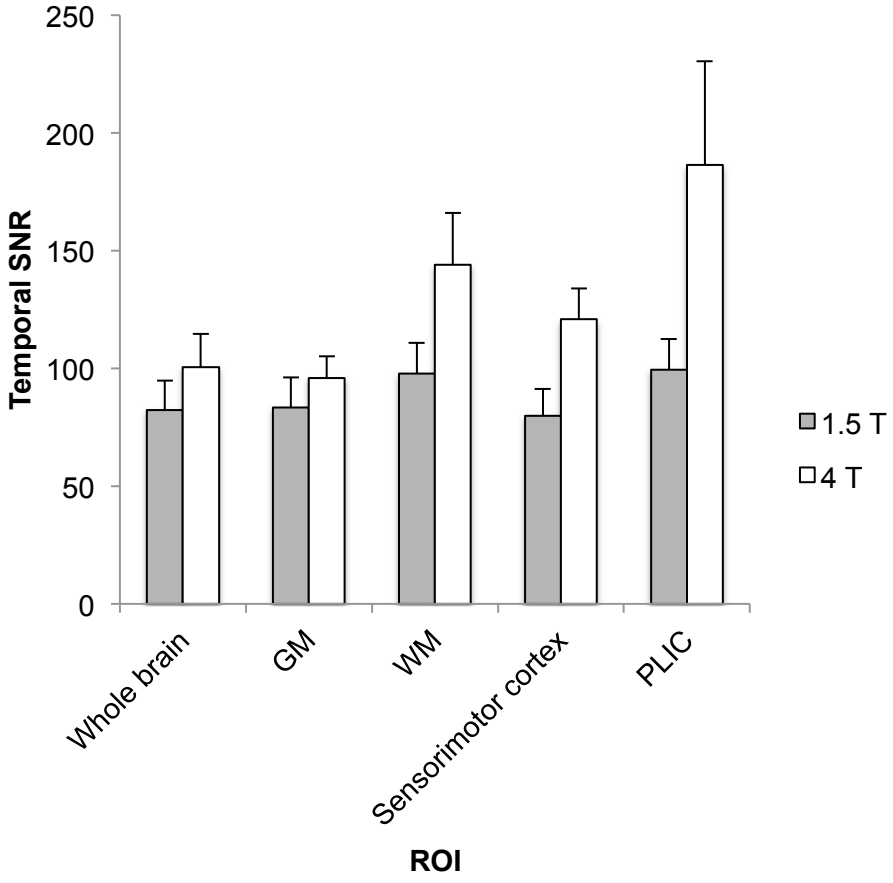

Figure 3.5. ROI analysis of grand average (n = 7) tSNR results for 1.5 T and 4 T data. Error bars represent standard deviations.

3.6.3. Power Spectra

To evaluate the potential sources of tissue type differences in terms of activation and tSNR results, the power spectra of the noise in the gray and white matter ROIs were evaluated for both 1.5 T and 4 T. The difference spectra (gray matter minus white matter)

are depicted in Figure 3.6. At 1.5 T, the tissue type differences are relatively uniform across frequencies. In contrast, a large peak difference at approximately 0.05 Hz is apparent at 4 T, as well as a number of smaller peak differences at higher frequencies.

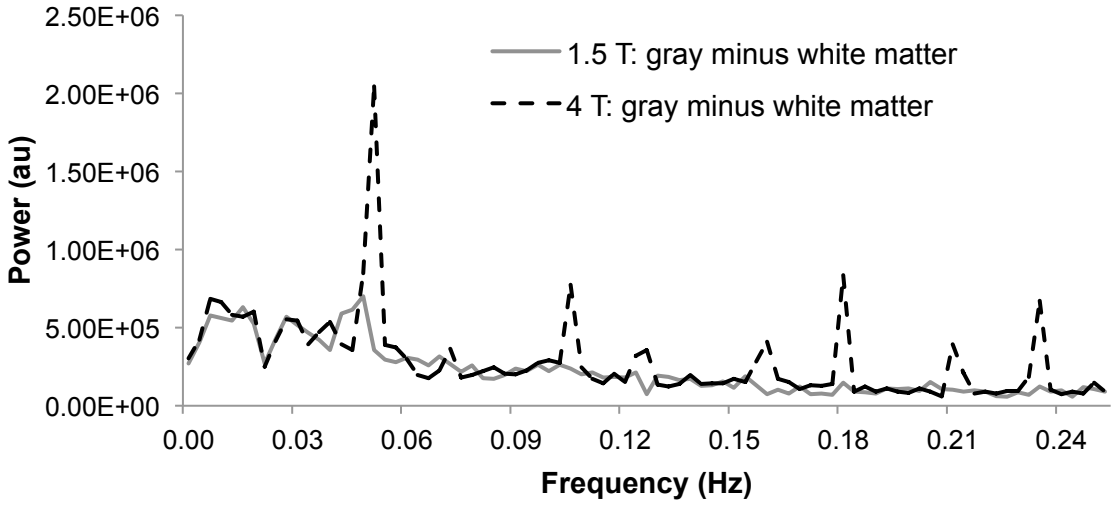

Figure 3.6. Grand average (n = 7) power spectra difference between the gray and white matter ROIs for 1.5 T and 4 T data. Note that the signals have been detrended to remove activation-related variance; thus the power spectra are assumed to represent the frequency components of the noise.

3.7. Discussion

3.7.1. Summary of Findings

Consistent with previous results, PLIC activation was detected at 4 T for a finger tapping task (Gawryluk et al., 2011b). As predicted, group level sensitivity to PLIC activation was increased at 4 T relative to 1.5 T. In addition, PLIC activation was detected in more individuals at 4 T than 1.5 T. At conventional thresholds, 1.5 T may not be sensitive enough to detect fMRI signal changes in white matter. Furthermore, we found relatively greater field strength dependent tSNR gains for white matter relative to gray matter, suggesting that high field may be particularly advantageous for white matter fMRI. Below, we speculate on the possible mechanisms of this phenomenon.

We also determined whether local activation maxima were observed on the PLIC ROI, in order to evaluate if the activation on the white matter ROI likely originated from the PLIC rather than from gray matter signal contamination (see below for a discussion of

partial volume effects). The individual level analysis revealed local maxima on the PLIC ROI for the majority of participants at 4 T. However, no local maxima were observed on the PLIC ROI for the group analysis. Individual differences in the functional organization of the PLIC may have contributed variance resulting in the absence of a PLIC local maximum on the group activation maps.

At the group level, statistical contrasts revealed that 4 T fMRI was significantly more sensitive to motor cortex activation (Table 3.1). At the individual level, greater activation extent and greater mean *z*-scores were observed for 4 T relative to 1.5 T in gray matter (Table 3.3), which is consistent with previous studies of the field strength dependence of BOLD fMRI (Di Salle et al., 2003; Duong et al., 2003; Gati et al., 1997; Gati et al., 2000; Fera et al., 2004; Hoenig et al., 2005; Krasnow et al., 2003; Krüger et al., 2001; Meindl et al., 2008; Triantafyllou et al., 2005; Turner et al., 1993; Uğurbil et al., 1999; van der Zwaag et al., 2009; Yang et al., 1999).

Consistent with previous findings, we observed greater tSNR for white matter than gray matter (Figure 3.5; Bodurka et al., 2007; Gonzalez-Castillo et al., 2011). Importantly, field strength related increases in tSNR were significantly greater for white matter than gray matter. This finding is consistent with the notion that high field fMRI is particularly important for detecting activation in white matter.

3.7.2. Effect of Physiological Noise

In general, physiological noise is more prominent at higher fields due to the relationship between physiological noise and image SNR (Fera et al., 2004; Triantafyllou et al., 2005). Consistent with previous research demonstrating that physiological noise comprises a smaller proportion of the total noise in white matter compared to gray matter (Greve et al., 2011; Krüger and Glover, 2001), the spectral analysis of the noise revealed a large power difference between the tissue types in the low frequency range to which physiological artifacts are often aliased (Figure 3.6; Biswal et al., 1996). Given that white matter signals are less contaminated by physiological noise, white matter may be relatively more robust to field strength related increases in physiological noise than gray matter. Physiological noise differences between gray and white matter might be attributed differences in vasculature between the tissue types (Dagli et al., 1999; Duvernoy et al.,

1981). However, other sources of noise differences between gray and white matter cannot yet be ruled out. Future studies should employ physiological noise removal procedures to evaluate whether sensitivity at 4 T could be enhanced, particularly for gray matter activation.

3.7.3. Caveats

3.7.3.1. Susceptibility Induced Field Gradients at 4 T. In the 4 T data, the close proximity of the inferior parts of the PLIC ROI to the regions of orbitofrontal susceptibility artifact signal dropout may have affected the activation results. For example, the image distortions at the boundaries of the dropout region may have contaminated the PLIC ROI. If so, task correlated signal intensity changes in the distorted regions (i.e., task correlated motion) may have been erroneously characterized as activation. However, we included the estimated motion parameters (output from the motion correction) as regressors of no interest in our activation model, which limits the potential contribution of movement-related signal changes that survive the motion correction (Johnstone et al., 2006).

3.7.3.2. Spatial Resolution and Partial Volume Effects. At the current fMRI spatial resolution (3.75 x 3.75 x 5 mm^3), the dimensions of the PLIC (less than 10 mm in the left-right dimension on most slices; Oishi et al., 2005) are such that partial volume effects likely contributed to some voxels in the PLIC ROI. In this study, we were able to evaluate whether the fMRI activation likely originated in the PLIC ROI (as opposed to neighbouring gray matter regions) by determining whether an activation local maximum was localized to the white matter region. At 4 T, the majority of participants had local maxima co-localized to the PLIC ROI, providing evidence that the activated voxels in the PLIC were not merely the result of partial volume effects. In the future, higher resolution fMRI scans will be crucial to disentangling the signal changes associated with the different tissue types. However, as we have demonstrated in the current study, white matter fMRI activation may be difficult to detect at lower SNR, which could limit the spatial resolution for white matter fMRI research.

3.7.4. Conclusions

We have shown that high field fMRI may be particularly important for detecting activation in white matter. Furthermore, field strength dependent increases in fMRI sensitivity may be greater for white matter than for gray matter. The scarcity of reports of white matter fMRI activation (relative to gray matter) may be due in part to the prevalence of 1.5 T MRI systems. High field MRI may be critical for fMRI studies aimed at investigating activation in both gray and white matter.

3.8. Acknowledgements

This work was supported by the National Research Council of Canada Genomics and Health Initiative and the Natural Sciences and Engineering Research Council of Canada.

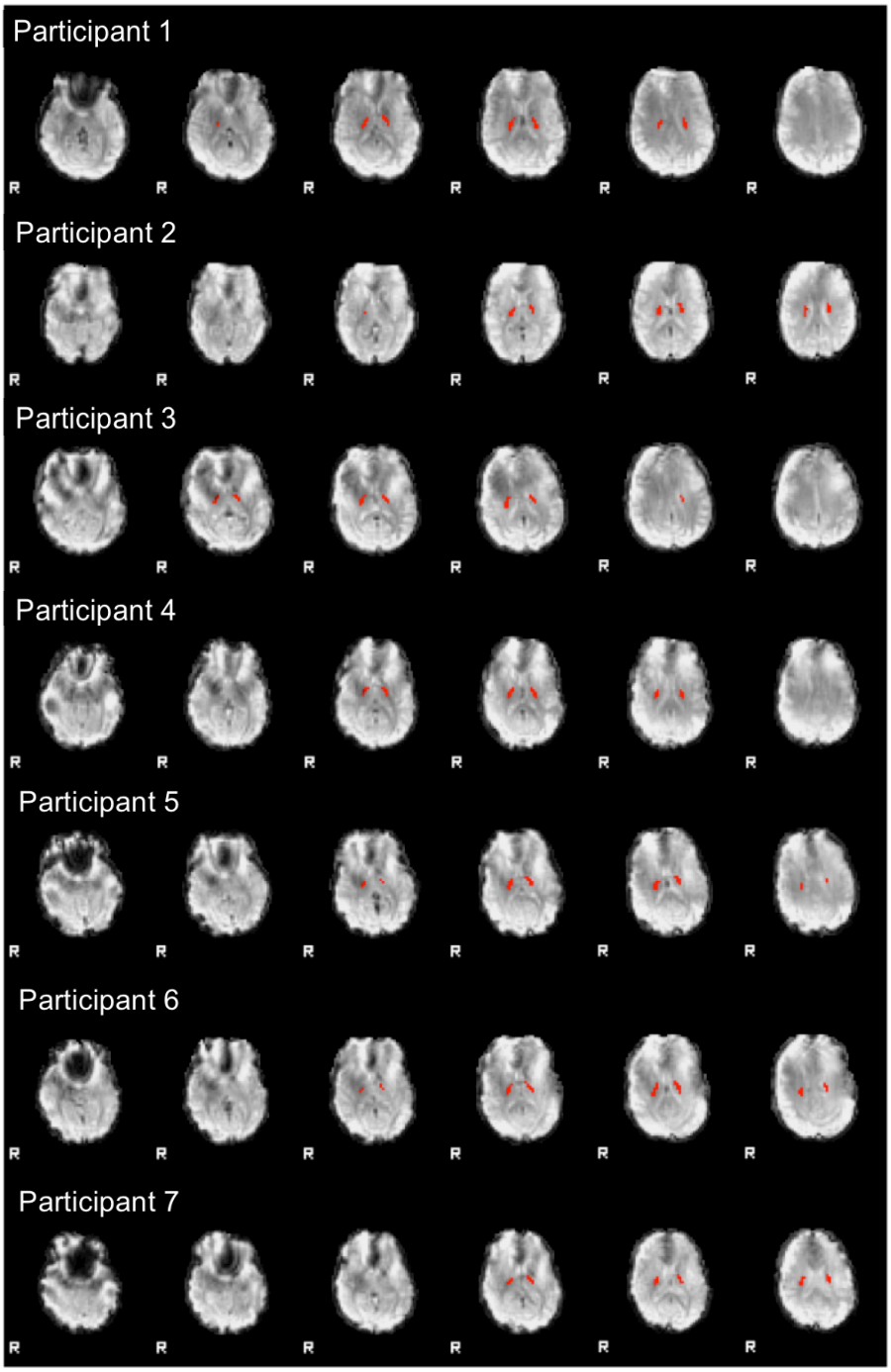

Supplementary Figure 3.1A. PLIC ROI overlaid on a functional volume from each participant (1.5 T data).

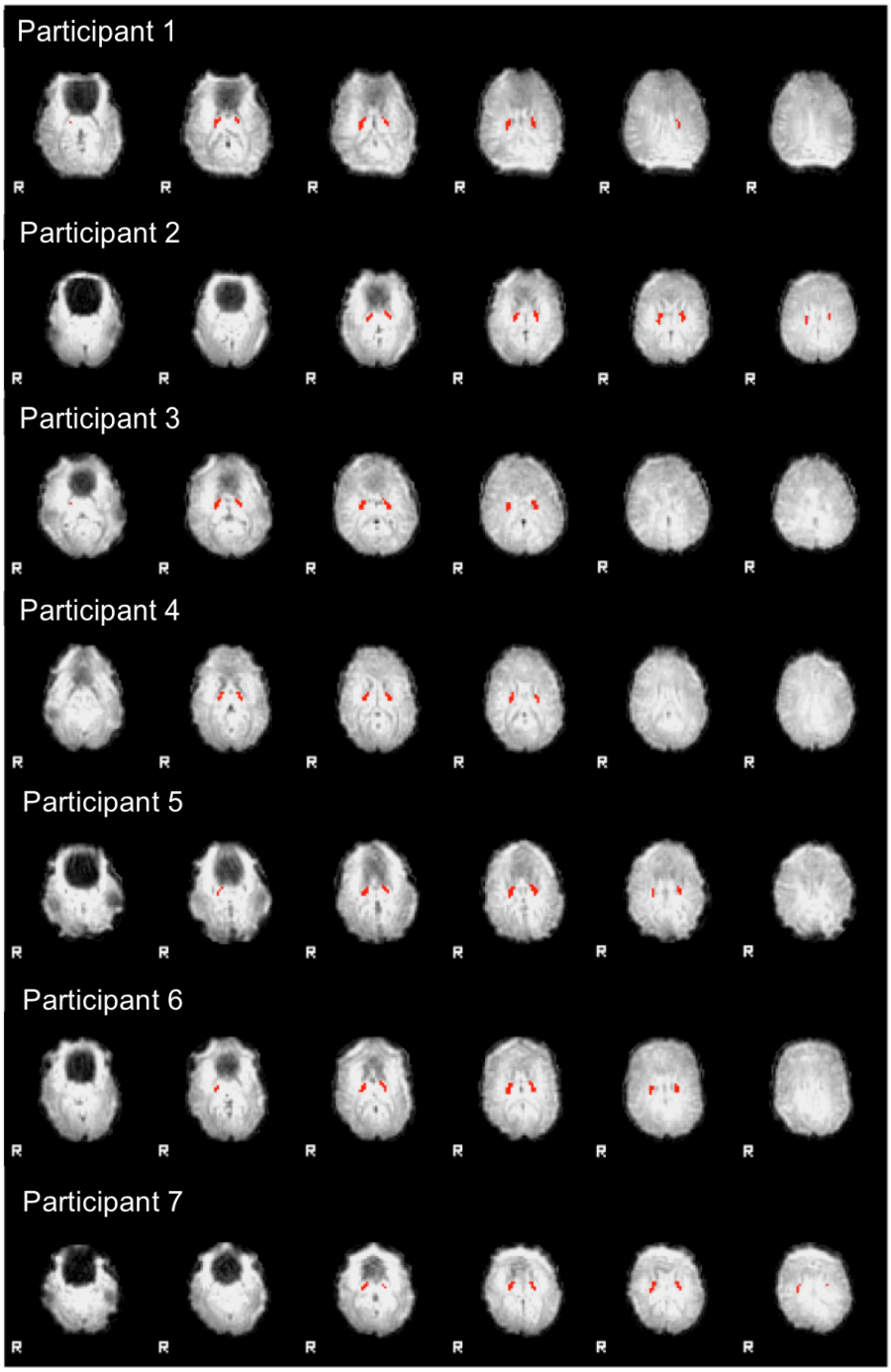

Supplementary Figure 3.1B. PLIC ROI overlaid on a functional volume from each participant (4 T data).

Supplementary Table 3.1. Mean percent signal change for significantly activated voxels.

	Sensorimotor cortex ROI		PLIC ROI	
Participant	1.5 T	4 T	1.5 T	4 T
1	1.60	1.25	0.00	0.33
2	1.58	0.91	0.51	0.18
3	1.42	0.99	0.00	0.42
4	1.17	0.71	0.41	0.22
5	1.31	1.38	0.59	0.42
6	1.32	1.13	0.51	0.24
7	1.68	1.43	0.47	0.54
Average	**1.44**	**1.11**	**0.36**	**0.34**
SD	0.19	0.26	0.25	0.13

3.9. Summary of Chapter 3 and Transition to Chapter 4

The results of Chapter 3 confirmed that sensitivity to white matter fMRI activation is dependent on field strength, and that high field MRI may be key for studies aimed at evaluating activation in both gray and white matter regions. The results also showed that the field strength dependent sensitivity gains are larger in white matter than gray matter, suggesting that the paucity of studies reporting white matter fMRI activation may be partially due to the prevalence of 1.5 T MRI systems.

Having presented evidence in support of the hemodynamic nature of white matter fMRI activation (Chapter 2) and a possible explanation for the relatively limited number of reports of white matter fMRI activation (Chapter 3), the focus of this thesis will now shift towards refining the functional explanation of white matter activation clusters. Chapter 4 presents research aimed at improving the interpretation of the functional significance of white matter fMRI activation by investigating the relationship between white matter fMRI activation and the activated network in gray matter. Specifically, whether regions of white matter fMRI activation are structurally connected to regions of gray matter activation will be determined. In Chapter 4, fMRI data from an interhemispheric transfer task will be evaluated. A functionally guided tractography approach will be employed to determine if activated clusters in the corpus callosum are structurally connected to activated regions of gray matter.

Chapter 4 Confirming White Matter Functional MRI Activation in the Corpus Callosum: Co-Localization with DTI Tractography

4.1. Publication Status

Mazerolle EL, Beyea SD, Gawryluk JR, Brewer KD, Bowen CV, D'Arcy RCN (2010) Confirming white matter fMRI activation in the corpus callosum: co-localization with DTI tractography. NeuroImage 50:616-621.

4.2. Student Contributions to Manuscript

Implementing diffusion imaging, helping to design the experiment, helping to recruit participants and collect data, devising the analysis approach, data analysis, intepretation of the results, and writing the manuscript.

4.3. Abstract

Recently, functional magnetic resonance imaging (fMRI) activation has been detected in white matter, despite the widely-held belief that fMRI activation is restricted to gray matter. The objective of the current study was to determine whether the regions of white matter fMRI activation were structurally connected to the functional network in gray matter. To do this, we used fMRI-guided tractography to evaluate whether tracts connecting regions of gray matter fMRI activation were co-localized with white matter fMRI activation. An established interhemispheric transfer task was employed to elicit activation in the corpus callosum. Diffusion tensor imaging (DTI) tractography was used to determine the existence of tracts that connected regions of gray matter fMRI activation to regions of activation in the corpus callosum. Corpus callosum activation was detected in the majority of participants. While there was individual variability in the location of corpus callosum activation, activation was commonly observed in the callosal mid-body, isthmus/splenium, or both. Despite the variability, gray matter fMRI-guided tractography identified tracts that were co-localized with corpus callosum fMRI activation in all instances. The results confirmed that the activated regions of the corpus callosum were structurally connected to the functional network of gray matter regions involved in the

task. These findings are an important step towards establishing the functional significance of white matter fMRI activation, and provide a foundation for future research combining white matter fMRI and DTI tractography to study brain connectivity.

4.4. Introduction

White matter activation in functional magnetic resonance imaging (fMRI) is controversial. Traditionally, it was thought that fMRI is restricted to gray matter due to the relatively greater blood flow and volume in gray matter (Helenius et al., 2003; Preibisch and Haase, 2001; Rostrup et al., 2000; van der Zande et al., 2005; Wise et al., 2004). In addition, research has demonstrated that the primary source of fMRI signals are hemodynamic responses to post-synaptic potentials, which mainly occur in gray matter (e.g., Logothetis et al., 2001). Indeed, it has been stated that "a reasonable investigator may doubt the presence of a [blood oxygen level dependent] signal in white matter altogether" (Logothetis and Wandell, 2004, p. 755). Despite these issues, there is no direct evidence that precludes the possibility of detecting white matter fMRI activation. It has been suggested that the energy-dependent processes that take place in white matter may result in task-dependent changes, which could be measured with fMRI (Mazerolle et al., 2008; Tettamanti et al., 2002).

We have recently reported evidence for white matter fMRI activation at 4T using interhemispheric transfer tasks that specifically target the corpus callosum. Such tasks, in which functionally lateralized stimuli (words and faces) are presented to the right and left visual hemifields, have been used to study disconnection syndromes in split brain patients (e.g., Gazzaniga et al., 1965) and have been previously developed for fMRI (D'Arcy et al., 2006). Mazerolle and colleagues (2008) reported activation in the isthmus of the corpus callosum in 21% of individuals. Group level activation was also observed in this region, but at relaxed statistical thresholds ($p < 0.005$, uncorrected). Using a visuo-motor interhemispheric transfer task (lateralized light flashes; Poffenberger, 1912; Iacoboni and Zaidel, 2004), Gawryluk and colleagues (2009) reported white matter fMRI activation in 100% of individuals (using standard statistical thresholds) by improving sensitivity to white matter fMRI activation through increased T2 weighting of the functional images. In addition, other groups have reported white matter fMRI activation, providing further

evidence for the phenomenon (e.g., Mosier and Bereznaya, 2001; Omura et al., 2004; Tettamanti et al., 2002; Weber et al., 2005; Yarkoni et al., 2009).

With a growing number of reports of fMRI activation in white matter, it is important to determine how white matter fMRI activation is related to the functional gray matter network activated by a task. To do this, we employed diffusion tensor imaging (DTI) tractography to evaluate whether regions of white matter fMRI activation have structural connections to activated gray matter. Previous work has shown that fMRI-guided tractography can be successfully used in order to identify the structural connections within functional networks, including callosally-mediated networks (e.g., Lowe et al., 2006). Given this, it should be possible to use DTI tractography to determine whether the corpus callosum activation elicited during an interhemispheric transfer task is structurally connected to the functionally activated networks in gray matter.

In the current study, corpus callosum activation and corresponding tractography analyses were examined at the individual level. The objective was to determine whether the corpus callosum activation was co-localized with tracts seeded from activated clusters in gray matter. To test this hypothesis, a deterministic tractography algorithm was employed using the whole brain as a seed. Subsequently, regions-of-interest (ROIs) were defined within both the white matter activation of the corpus callosum (CC), as well as the cortical gray matter (GM) activation. The ROIs were used to identify whether a subset of fibres existed that tracked through both GM and CC activation.

4.5. Methods

4.5.1. Participants

Ten healthy participants (five females) took part in the study. The mean age of participants was 25.8 ± 6.0 years (range 19-40). The mean laterality quotient (measured using the Edinburgh Handedness Inventory; Oldfield, 1971) was 87.5 ± 15.6 (range 55-100), indicating that the participants were right-handed. The study was approved by local research ethics boards. Each participant provided written informed consent prior to participation and received compensation for participating.

4.5.2. Experimental Design

The participants performed an established interhemispheric transfer task (Mazerolle et al., 2008). Stimuli consisted of faces (right hemisphere stimuli) and words (left hemisphere stimuli) that were presented to the left and right visual fields (i.e., either directly to the relatively specialized hemisphere, or to the opposite hemisphere) in order to elicit interhemispheric transfer. Stimuli were either real (i.e., intact faces or words) or scrambled (i.e., faces with the features rearranged or pseudowords). On each trial, participants were asked to evaluate whether the stimulus presented was real or scrambled by pressing a button on an MR compatible response box (four button forced choice). Response hand was crossed for all trials (i.e., left hand for words and right hand for faces). All stimuli were presented laterally (> 2.3 degrees from fixation) and rapidly (150ms) in order to initially stimulate one hemisphere and avoid saccades. A '+' was displayed at the centre of the screen for the duration of the experiment; participants were asked to continually fixate on this point. E-Prime (Psychology Software Tools, Inc.) was used to present stimuli, which were displayed using back-projection to a screen mounted inside the bore, and viewed through a mirror mounted on the head coil. Prior to the experiment, each participant performed a short practice task (with feedback) to ensure compliance.

4.5.3. MRI Acquisition

Data were acquired from a 4 T Varian INOVA whole body MRI system. Gradients were provided by a body coil (Tesla Engineering Ltd.) operating at a maximum of 35.5 mT/m at 120 T/m/s, and driven by 950 V amplifiers (PCI). A TEM head coil (Bioengineering Inc.) was employed.

4.5.3.1. Functional MRI Acquisition. Functional MRI was conducted using an asymmetric spin echo (ASE) spiral sequence (Brewer et al., 2009). The ASE spiral sequence collects three images per slice per volume, one prior and two after a radiofrequency refocusing pulse. The T2' weighting[1] of these images is determined by the TE* parameter (see below) and is constant across the three images. The T2 weighting of these images, however, increases across the three images (determined by TE). Seventeen

[1] $1/T2^* = 1/T2 + 1/T2'$

axial slices (4 mm thick, no gap) were prescribed to cover the corpus callosum, as well as the region extending superiorly. Other parameters for functional imaging were: 64 x 64 matrix (220 x 220 mm^2), 1 shot, 170 volumes, TR/TE/TE* = 2000/68/27 ms (TE and TE* are the spin-echo centre and asymmetric echo times, respectively; Brewer et al., 2009).

4.5.3.2. DTI Acquisition. DTI data were acquired using a single shot spin echo spiral sequence. Twenty-four axial slices (3 mm thick, no gap) were collected, prescribed such that they were centred over the functional slab. A 64 x 64 matrix (220 x 220 mm^2) was used, with TR/TE = 6000/100 ms and two averages. Diffusion weighting was distributed along 30 directions (maximum b-value = 1007 s/mm^2). After every 10 diffusion weighted images, an image with a b-value of zero were acquired (for a total of three b = 0 images). Using these parameters, DTI data were acquired in approximately eight minutes, which was necessary in order to ensure adequate time for the fMRI and structural image acquisitions.

4.5.3.3. Structural Image Acquisition. Following the fMRI and DTI scans, a 3D magnetization prepared fast low angle shot (MPFLASH) whole brain high resolution T1-weighted anatomical image was collected (72 2 mm axial slices, 256 x 256 matrix, 220 x 220 mm^2), with TR/TI/TE = 10/500/5 ms and an 11 degree flip angle.

4.5.4. Data Analyses

4.5.4.1. Functional MRI Analysis. In order to increase the overall T2 weighting of the combined image, the three ASE images were combined using an inverted signal weighted averaging algorithm (Gawryluk et al., 2009). Statistical analyses were performed using the general linear model with fMRI expert analysis tool (FEAT) version 5.3 in FMRIB Software Library (FSL; Smith et al., 2004). Pre-statistics processing included the following steps: motion correction using MCFLIRT[2] (Jenkinson et al., 2002), non-brain removal using BET (Smith, 2002), spatial smoothing using a Gaussian kernel (6 mm full width at half maximum), mean-based intensity normalisation, and highpass temporal filtering (Gaussian weighted least-squares straight line fitting, with σ = 50 s). Time series statistical analyses were carried out using FILM with local autocorrelation correction (Woolrich et al., 2001). Motion parameters (output from the

[2] Summaries of the motion parameters are reported in Supplementary Table 4.1.

motion correction) were included in the model as regressors of no interest. *Z* (Guassianised *t*) statistic images were reported using a threshold for clusters determined by $z > 3.0$ and a (corrected) cluster significance threshold of $p < 0.05$ (Worsley et al., 1992). FLIRT was used to register the activation maps to structural space (seven degrees of freedom [DOF]).

4.5.4.2. DTI and Tractography Analysis. First, DTI data were resampled to a resolution of 1.7 x 1.7 x 2 mm^3. These data were then corrected for motion using a six parameter registration[3] (Jenkinson and Smith, 2001), which was followed by combining the two averages. A binary mask differentiating brain and non-brain matter was calculated with BET (Smith, 2002) from a volume with no diffusion weighting. This mask was applied to the entire DTI dataset. Deterministic tractography was then performed (using all voxels as seeds) in MedINRIA's DTI Track (Filliard et al., 2006). A fractional anisotropy threshold of 0.2 was applied. The anatomical image was registered to a volume with no diffusion weighting using seven DOF in FLIRT (Jenkinson et al., 2002; Jenkinson and Smith, 2001).

4.5.4.3. Functional MRI-Guided Tractography Analysis. The tractography analysis was guided by two functionally defined regions: 1) an ROI of CC activation, and 2) an ROI of cortical GM activation. First, activation maps were transformed into diffusion space. For the GM activation ROI, partial volume maps for gray matter, white matter, and cerebrospinal fluid (CSF) were created from the structural image automatically using FAST (Zhang et al., 2001). As has been previously noted, intensity-based segmentations can result in voxels at the interface of white matter and ventricles being misclassified as gray matter (Ashburner and Friston, 2000). In order to reduce this problem, the gray matter partial volume maps were thresholded such that a voxel was only considered gray matter if the probability that it was gray matter was higher than white matter and CSF. The mask was then transformed into the diffusion-registered structural space. The resulting mask was applied to the activation maps for each participant in order to create GM activation ROIs. Any remaining subcortical voxels (i.e.,

[3] We used a six DOF registration for correcting motion in the diffusion data as opposed to the standard 12 DOF for correcting for eddy currents. Six DOF was appropriate because our acquisition employed a spiral k-space trajectory, which manifests eddy current artifacts as image blurring as opposed to stretching (as is typical for EPI acquisitions).

voxels at the white matter-CSF interface that survived the threshold procedure or activation in subcortical gray matter voxels) were manually removed. Due to the isotropic diffusion and subsequent tractography difficulties in gray matter, the GM activation ROI was dilated using a 6mm spherical kernel in order to ensure that GM activation ROI on the gray matter-white matter borders extended into white matter. For each participant, the GM activation ROI was also divided into the right and left hemispheres in order to evaluate whether tracts reached bilateral gray matter activation.

The CC activation ROIs were manually defined. First, the activation maps were overlaid on the diffusion-registered structural space. To be included in the CC activation ROI, voxels had to appear to be on the CC in the axial, sagittal, and coronal views. In addition, the clusters had to have a local maximum on the CC. By ensuring the clusters had a local maximum on the CC as opposed to neighbouring gray matter, the potential contributions of partial volume effects were reduced. Figure 4.1 shows the fMRI activation and resulting CC and GM activation ROIs used for the fMRI-guided tractography analysis in a representative participant.

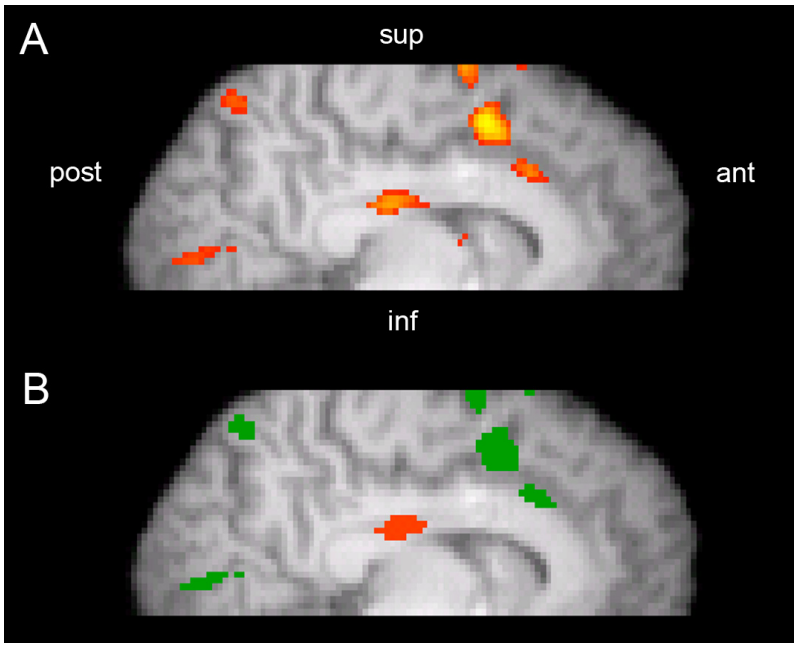

Figure 4.1. (A) A single participant's fMRI activation ($Z > 3$), and (B) the corresponding ROIs for fMRI-guided tractography (green: gray matter activation ROI; red: corpus callosum activation ROI; post: posterior; ant: anterior; sup: superior; inf: inferior).

For each participant, the CC and GM activation ROIs were imported into MedINRIA's DTI Track to identify whether any fibres existed that passed through both regions. Fibres were identified using the criterion that they had to overlap with voxels in both the CC and GM activation ROIs. Because the data were not transformed to standard space, brain regions were identified via visual inspection.

The results were further evaluated in two ways. First, percent signal change was calculated in order to allow comparisons between gray matter and white matter activation intensity. The CC and GM activation ROIs from the fMRI-guided tractography analysis were used as masks to calculate percent signal change based on the parameter estimates of the activation model using FSL's featquery. Second, the selectivity of the tractography analysis was assessed by determining the number of activated gray matter voxels with tracts to contralateral gray matter activation (i.e., candidate voxels for having tracts to the CC activation ROI). The percentage of these voxels that were also associated with tracts passing through the CC activation ROI was then calculated. In addition, we calculated the percentage of midsagittal CC voxels that contained tracts connecting bilateral GM activation.

4.6. Results

4.6.1. Overview of Corpus Callosum Activation

Group level fMRI activation results are reported elsewhere (Gawryluk et al., 2011a). Of the 10 participants, eight[4] had corpus callosum activation as defined in the Methods. Among these eight participants, the location of the CC activation varied. Four participants had both posterior and anterior CC activation (either one or two clusters in the splenium/isthmus and the mid-body of the corpus callosum). Two participants had activation restricted to posterior CC regions. One participant had both mid-body and genu activation, and the remaining participant had activation in the genu only.

[4] A ninth participant had an activation maximum on the border of the corpus callosum and lateral ventricle. However, we could not be confident that this activation originated from the corpus callosum because of potential peri-ventricle motion artifacts; therefore, this participant was excluded from the fMRI-guided tractography analysis.

4.6.2. Functional MRI-Guided Tractography Results

Of the eight participants with CC activation, fMRI-guided tractography demonstrated that seven had fibres connecting regions of CC activation to bilateral GM activation. All seven participants had tracts extending to premotor regions, parietal regions, or both. A representative participant with this pattern of results is presented in Figure 4.2. Two other participants had tracts to both premotor and parietal regions, with additional tracts to temporal regions (Supplementary Figures 4.1 and 4.2). One participant had tracts to premotor regions only, despite a small posterior CC activation in addition to activation in the mid-body (Supplementary Figure 4.3). One participant had a tract to prefrontal regions in addition to premotor regions (Supplementary Figure 4.4). Two participants did not have tracts to premotor regions; one had tracts extending to superior occipital/inferior parietal regions only (Supplementary Figure 4.5), whereas the other had both parietal and medial temporal tractography targets (Supplementary Figure 4.6).

The eighth participant with CC activation had tracts to prefrontal regions, but these tracts reached activation in the right hemisphere only (i.e., did not meet the criterion of tracking to bilateral gray matter activation targets). This participant is presented in Supplementary Figure 4.7.

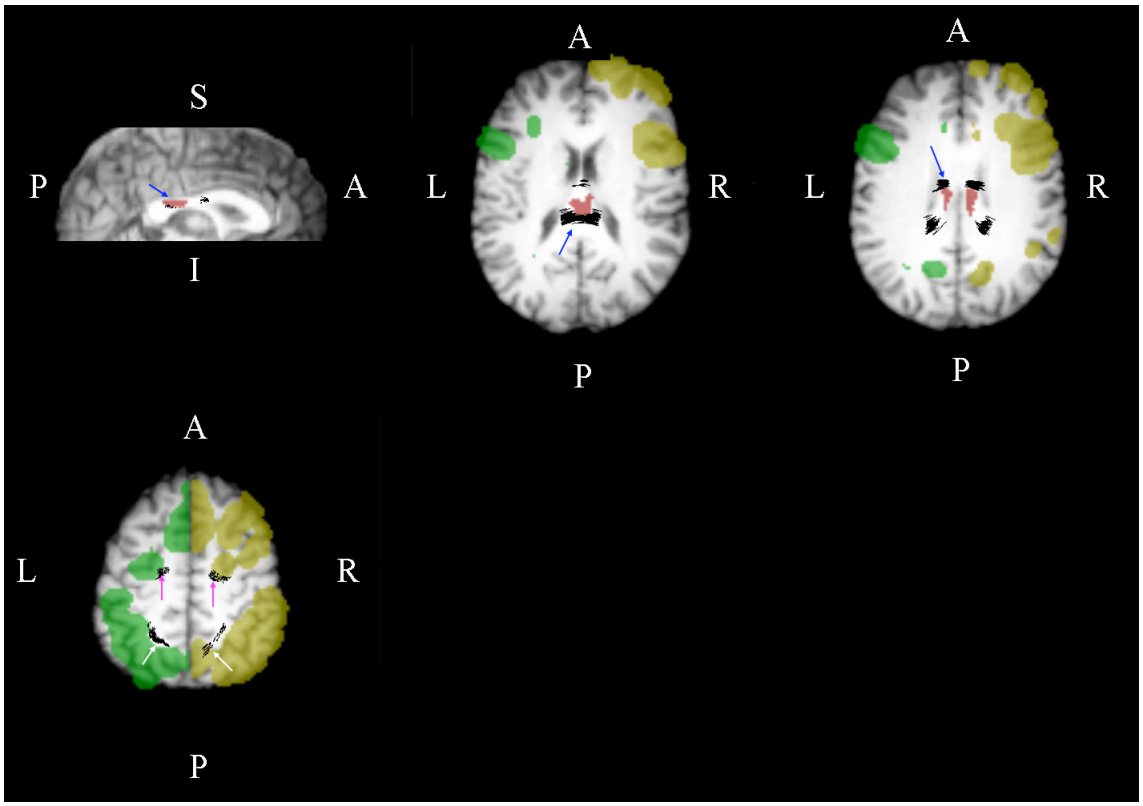

Figure 4.2. Functional MRI-guided tractography results for a representative participant (participant 1; green: left hemisphere gray matter activation ROI; yellow: right hemisphere gray matter activation ROI; red: corpus callosum activation ROI; black: tracts passing through all three ROIs; P: posterior; A: anterior; S: superior; I: inferior; R: right; L: left). The top images show fibres passing through corpus callosum activation in the sagittal view (left) and axial views (centre: isthmus activation; right: mid-body activation; blue arrows). The bottom image shows an axial view of tracts reaching targets in premotor cortex (magenta arrows) and parietal cortex (white arrows).

4.6.3. Percent Signal Change Analysis

The percent signal change values (90th percentile and maximum) for the CC and GM activation ROIs can be found in Table 4.1. Note that the maximum percent signal change values were, on average, about 4.5 times larger in the gray matter than the corpus callosum.

Table 4.1. Percent signal change across CC and GM activation ROIs.

	CC activation ROI		GM activation ROI	
Participant	90th percentile	Max	90th percentile	Max
1	1.3	1.4	1.3	5.7
2	0.6	0.6	1.1	4.2
3	0.6	1.2	1.6	5.3
4	0.8	1.1	1.4	4.0
5	0.9	1.0	1.1	4.5
6	0.3	0.3	0.8	2.1
7	0.4	0.7	1.0	3.3
8*	0.7	1.0	1.4	6.1
9	-	-	1.0	2.6
10	-	-	1.3	4.5
Mean	**0.70**	**0.91**	**1.20**	**4.23**

*The callosal activation did not track to bilateral gray matter targets for participant 8 (i.e., the tract reached right hemisphere gray matter activation only).

4.6.4. Evaluating the Selectivity of the Functional MRI-Guided Tractography Analysis

Given the distributed network of activated gray matter regions (see Figure 4.2 and Supplementary Figures 4.1-4.7), it was important to quantitatively evaluate the relationship between the activation in GM and CC regions. Table 4.2 shows that, on average, about 5% of activated GM voxels had connections to contralateral GM activation. Of these candidate GM activation voxels, approximately 13% were structurally connected to the CC activation ROI. The mean percentage of midsagittal CC voxels with tracts connecting bilateral GM activation was 49 ± 11%.

Table 4.2. Analysis of the selectivity of the fMRI-guided tractography analysis[#].

Participant	# of voxels in GM activation ROI	Subset with connections to contralateral GM activation*	%	Subset with connections to CC activation**	%
1	53123	4949	9.32	429	8.67
2	102263	6660	6.51	2859	42.93
3	81934	4380	5.35	517	11.80
4	65452	2539	3.88	16	0.63
5	77025	4721	6.13	371	7.86
6	64367	2505	3.89	371	14.81
7	86198	3586	4.16	276	7.70
8	87299	4380	5.02	-	-
9	51299	1577	3.07	-	-
10	64890	3384	5.21	-	-
Mean	73385	3868	**5.25**	691	**13.49**

[#] See text for more details.

* I.e., the number of voxels in the GM activation ROI with connections to contralateral GM activation (candidate GM targets).

**I.e., the number of voxels in the GM activation ROI with connections to contralateral GM activation and the CC activation ROI.

4.7. Discussion

Using fMRI-guided tractography, we confirmed that the white matter fMRI activation in the corpus callosum was structurally connected to the functional network in gray matter activated during the interhemispheric transfer task. This result occurred for eight out of 10 participants, with seven participants meeting the additional criterion of tracking to bilateral gray matter activation.

The analyses presented here were performed at the individual level, allowing an examination of the differences in terms of CC activation across individuals. The majority of participants (six) had activation in posterior CC regions (isthmus or splenium), consistent with previous results (Mazerolle et al., 2008). However, four of these participants also had anterior CC activation. Two additional participants had CC activation that was restricted to more anterior regions (mid-body or genu). The variability in terms of the location of CC activation was also reflected in the fMRI-guided

tractography analysis. In general, the CC activation described above was associated with tracts to GM activation in regions that are consistent with what is known about the anatomy of the CC (e.g., connections between the isthmus and parietal cortex; Zarei et al., 2006).

The increased variability in the location of CC activation relative to previous results might be explained by differences in white matter fMRI sensitivity between the two studies. The previous study employed a more typical T2* weighted fMRI acquisition and reported a considerably lower percentage of individuals with CC activation (21% versus the 80% reported here; Mazerolle et al., 2008). It is possible that the increased sensitivity provided by ASE spiral fMRI acquisition and increased T2 weighting (Brewer et al., 2009; Gawryluk et al., 2009) allowed detection of white matter activation not only in more participants, but also across a larger region of the corpus callosum. Given what is known about inter-individual functional anatomy differences in gray matter (e.g., Brett, 2002), such variability in white matter fMRI activation is not surprising. However, the functional significance of this regional variability within the corpus callosum, as well as how this variability relates to the activated networks of gray matter regions, remains to be determined. Future work with a larger sample size is necessary to better evaluate the inter-individual variability and identify the white matter fMRI activation and tractography patterns that are common within the population.

The analysis of percent signal change in gray and white matter supports previous claims that white matter fMRI activation is weaker than that of gray matter (Gawryluk et al., 2009; Mazerolle et al., 2008; Tetttamanti et al., 2002; Yarkoni et al., 2009). Sensitivity remains a major hurdle to potential applications of white matter fMRI. Previous work has demonstrated improved sensitivity to white matter fMRI activation through increased T2 weighting of fMRI pulse sequences (Gawryluk et al., 2009). Ongoing work investigating the mechanisms of the effect of T2 weighting may provide additional insight that can be applied to further optimize sensitivity to white matter fMRI activation.

Given the distributed nature of the gray matter fMRI activation elicited by our task, it was important to evaluate the selectivity of the fMRI-guided tractography analysis. In order to ensure adequate sensitivity to white matter fMRI activation, which is

relatively weak (Table 4.1), we designed the task to elicit strong activation across a number of interhemispheric brain networks (e.g., both face and word processing). However, this approach also resulted in extensive gray matter activation. Some measure of confidence in the results can be obtained by noting that the tracts we identified were consistent with what is already known about the organization of the corpus callosum (e.g., Zarei et al., 2006). In general, fMRI-guided tractography studies do not provide an indication of the false positive rate (i.e., the likelihood that a structural connection between two activated regions was identified by chance). We quantified the relationship between the GM and CC activation by determining the number of activated GM voxels with structural connections to contralateral GM activation. Then, we found the percentage of those voxels that also had tracts passing through the CC activation ROI (13%; Table 4.2). We also attempted to evaluate the specificity of the fMRI-guided tractography analysis by calculating the percentage of midsagittal CC voxels that contained tracts connecting bilateral GM activation. We found that 49% of midsagittal CC voxels had structural connections to bilateral GM activation. Ideally, the gray matter fMRI activation would be more specific, that is, most or all of the activated gray matter would be structurally connected to the CC activation. Ongoing work is aimed at improving the experimental task such that smaller networks of gray matter activation are elicited.

There are at least three caveats to consider when interpreting the relationship between the cortical gray matter and corpus callosum activation. First, due to relative insensitivity of the white matter fMRI technique (Table 4.1), it is possible that not all activated channels of the CC are detected. That is, there may be activity in regions of the CC that is not observable using current acquisition and analysis techniques. Second, it is possible that some of the structural connections between bilateral gray matter activation are not functionally activated by the current task (i.e., true negatives). This issue highlights the fact that white matter fMRI may provide functional information about brain networks that is not available using conventional measures of structural and functional brain connectivity (see below). Third, it is possible that some tracts are involved in inhibitory processes that result in CC activation without downstream activation in gray matter. This would prevent tracking to bilateral gray matter targets. Future work is needed

to understand the physiological basis of white matter fMRI signals in order to evaluate this possibility.

The combination of white matter fMRI and DTI tractography is a novel multimodal approach to studying functional brain connectivity. Currently, studies of functional brain connectivity make inferences about brain connections using inter-regional correlations or causal modelling approaches (e.g., dynamic causal modelling; Friston et al., 2003). Previous studies employing fMRI-guided tractography have focused on identifying the structural connections associated with regions of gray matter fMRI activation (e.g., Lowe et al., 2006) or evaluating the relationships between functional and structural measures of connectivity (e.g., Lowe et al., 2008; Skudlarski et al., 2008; Greicius et al., 2009). In contrast to these previous applications, our approach provides a more direct measure of the functional status of the structural connections involved in a particular task. While improved methods for evaluating the specificity of fMRI-guided tractography need to be developed, future studies may employ white matter fMRI to both identify the white matter region involved in a given task, as well as evaluate the region's functional dynamics by measuring experimentally induced changes in the activation patterns within the white matter tissue itself.

By confirming white matter fMRI activation using fMRI-guided tractography, this work represents a significant advance for white matter fMRI, the existence of which has previously been doubted (e.g., Logothetis and Wandell, 2004). The co-localization of white matter fMRI activation with tracts connected to regions of gray matter fMRI activation provides strong evidence that the white matter fMRI activation is not only functionally significant (e.g., Gawryluk et al., 2009; Mazerolle et al., 2008; Tettamanti et al., 2002; Yarkoni et al., 2009), but also structurally connected to the activated gray matter network. White matter accounts for 40-45% of brain parenchyma (e.g., Black, 2007) and it is known that connections play a critical role in brain function. Furthermore, dysfunctions in brain connections have been implicated in numerous neurological and psychiatric diseases (e.g., Bassett & Bullmore, 2009; Guye et al., 2008). Given this, white matter fMRI has the potential to be applied to answer highly relevant basic neuroscience questions (i.e., studying brain connectivity). In addition, fMRI activation in white matter may have future clinical applications. Indeed, fMRI investigations of neuropsychological

tests for evaluating white matter diseases have shown (but not reported) group level activation in white matter (Genova et al., 2009; Lazeron et al., 2003). Given the variability observed in the current study, future work is needed to determine whether this concept can be meaningfully applied at the individual patient level.

4.8. Acknowledgments

The authors gratefully acknowledge the contributions of K. Dillen, C. Liu, and J. Marshall, who facilitated data collection. Thanks are also extended to Dr. T. Rolheiser for help with DTI acquisition, and three anonymous reviewers for providing helpful feedback on an earlier version of this manuscript. This work was funded by the Natural Sciences and Engineering Research Council of Canada, the National Research Council, the Killam Trusts, L'Oréal/UNESCO, Dalhousie University, the Scottish Rite Charitable Foundation, and the Nova Scotia Health Research Fund.

Supplementary Table 4.1. Mean and max motion parameters output from the motion correction procedure (FSL's MCFLIRT) for each participant.

		Rotation (radians)			Translation (millimetres)		
Participant		X	Y	Z	X	Y	Z
1	Mean	0.0017	0.0012	0.0017	0.0697	0.0246	0.0720
	Max	0.0053	0.0029	0.0070	0.3262	0.1095	0.3221
2	Mean	0.0006	0.0004	0.0004	0.0121	0.0282	0.1135
	Max	0.0015	0.0017	0.0012	0.0480	0.0762	0.2155
3	Mean	0.0011	0.0007	0.0004	0.0345	0.0461	0.0271
	Max	0.0035	0.0021	0.0013	0.1245	0.1467	0.1235
4	Mean	0.0009	0.0005	0.0015	0.0681	0.0348	0.0505
	Max	0.0025	0.0012	0.0042	0.1766	0.0893	0.1175
5	Mean	0.0014	0.0003	0.0015	0.0190	0.0689	0.0697
	Max	0.0053	0.0010	0.0048	0.0590	0.2111	0.1648
6	Mean	0.0007	0.0002	0.0004	0.0139	0.0356	0.0577
	Max	0.0019	0.0009	0.0009	0.0461	0.0998	0.1661
7	Mean	0.0021	0.0012	0.0002	0.0184	0.0553	0.0300
	Max	0.0049	0.0036	0.0008	0.0666	0.1458	0.0932
8	Mean	0.0012	0.0003	0.0003	0.0147	0.0340	0.0446
	Max	0.0036	0.0010	0.0009	0.0468	0.1397	0.1517
9	Mean	0.0012	0.0008	0.0004	0.0501	0.0192	0.0638
	Max	0.0105	0.0020	0.0010	0.1636	0.1723	0.1855
10	Mean	0.0003	0.0002	0.0002	0.0139	0.0184	0.0498
	Max	0.0014	0.0007	0.0009	0.0480	0.0823	0.1587

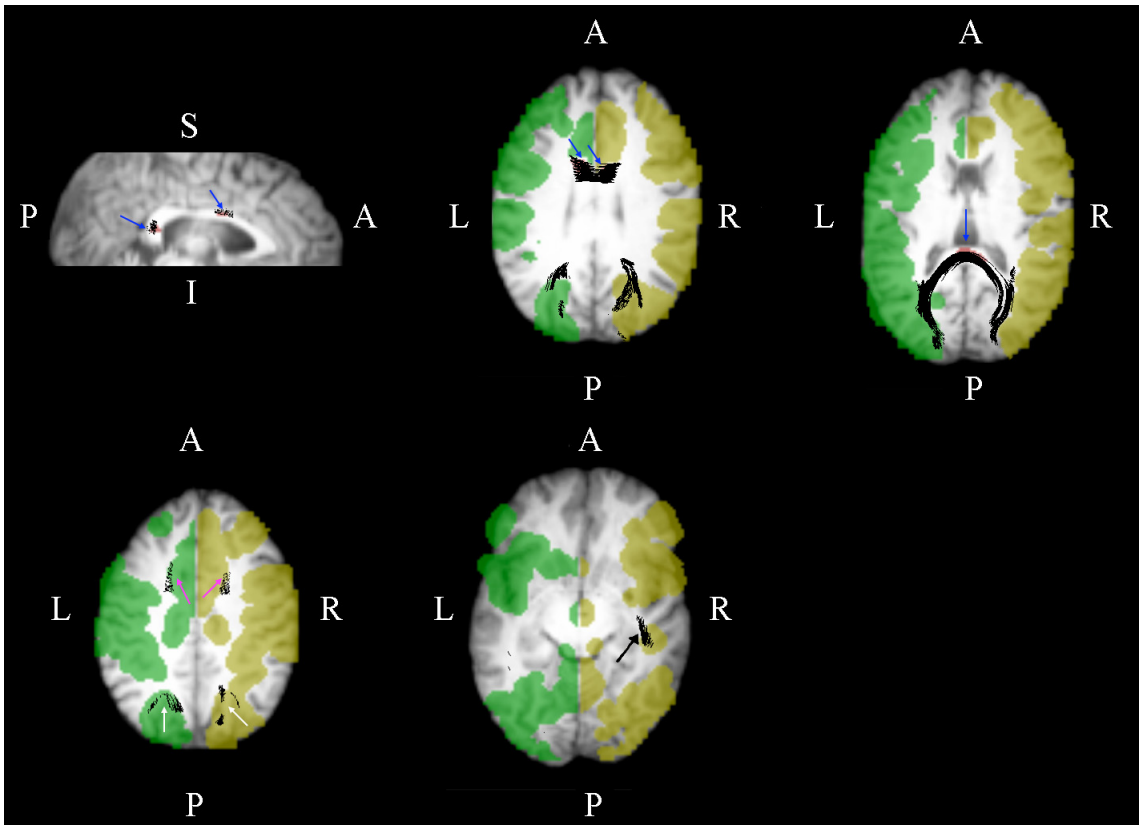

Supplementary Figure 4.1. Functional MRI-guided tractography results for participant 2 (green: left hemisphere gray matter activation ROI; yellow: right hemisphere gray matter activation ROI; red: corpus callosum activation ROI; black: tracts passing through all three ROIs; P: posterior; A: anterior; S: superior; I: inferior; R: right; L: left). The top images show fibres passing through corpus callosum activation in the sagittal view (left) and axial views (centre: mid-body activation; right: splenium activation; blue arrows). The bottom images show axial views of tracts reaching targets in premotor cortex (magenta arrows), parietal cortex (white arrows), and right inferior temporal cortex (black arrow).

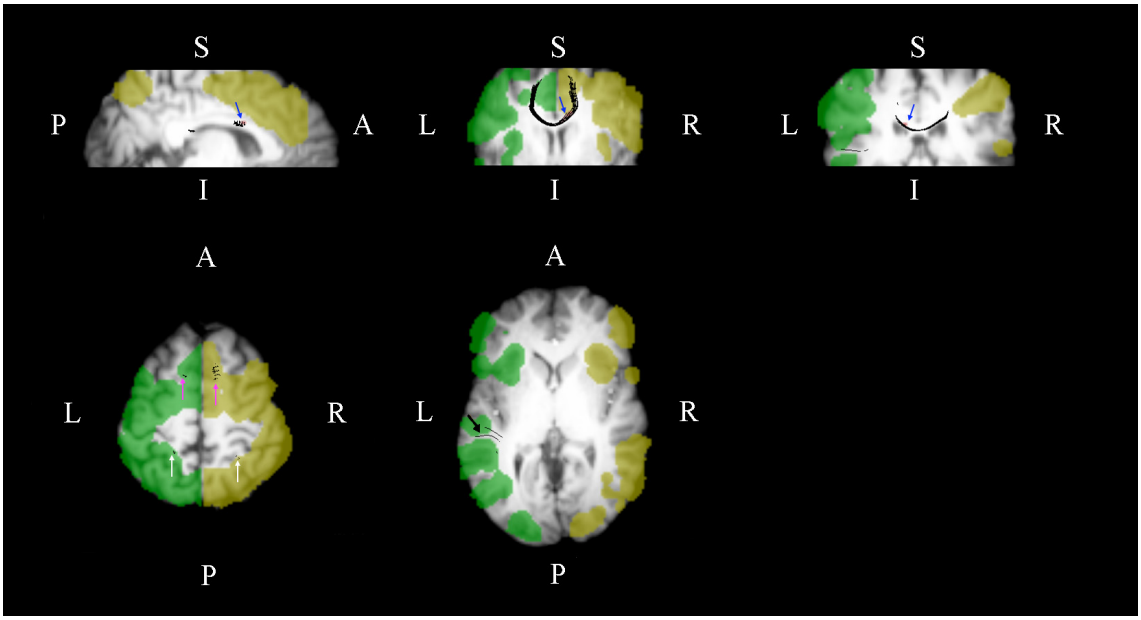

Supplementary Figure 4.2. Functional MRI-guided tractography results for participant 3. The top images show fibres passing through corpus callosum activation in the sagittal view (left) and coronal views (centre: mid-body activation; right: isthmus activation; blue arrows). The bottom images show axial views of tracts reaching targets in premotor cortex (magenta arrows), parietal cortex (white arrows), and left temporal cortex (black arrow). All other details as in Supplementary Figure 4.1.

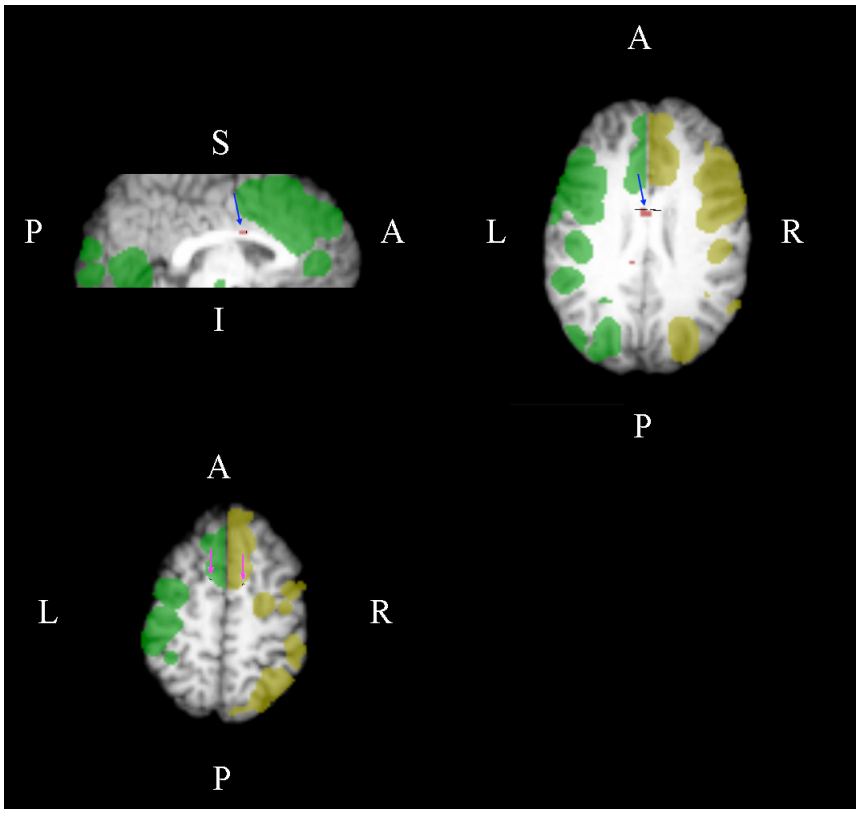

Supplementary Figure 4.3. Functional MRI-guided tractography results for participant 4. The top images show fbres passing through the corpus callosum activation in sagittal (left) and axial (right) views (blue arrows). The bottom image shows the tracts reaching targets in premotor cortex (axial view, magenta arrows). All other details as in Supplementary Figure 4.1.

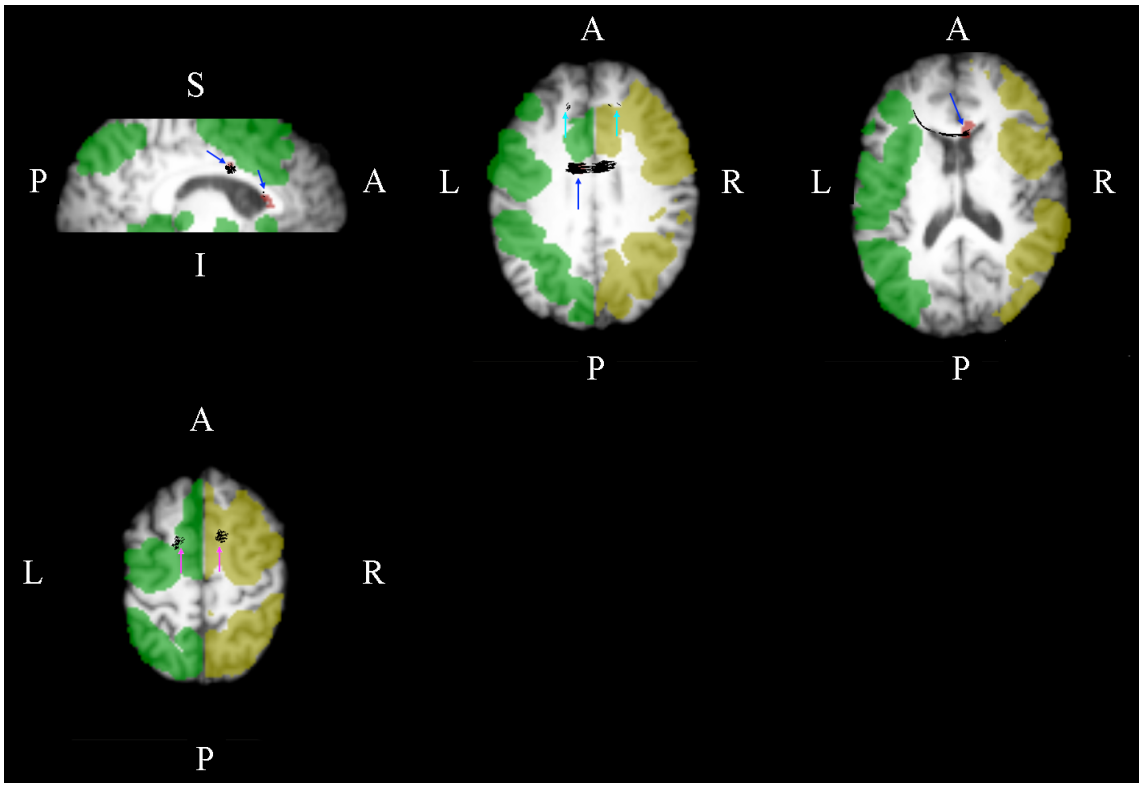

Supplementary Figure 4.4. Functional MRI-guided tractography results for participant 5. The top images show fibres passing through corpus callosum activation in the sagittal view (left) and axial views (centre: mid-body activation; right: genu activation; blue arrows). The bottom image shows tracts reaching targets in premotor cortex (axial view, magenta arrows). This participant also had tracts to prefrontal regions (top centre; cyan arrows). All other details as in Supplementary Figure 4.1.

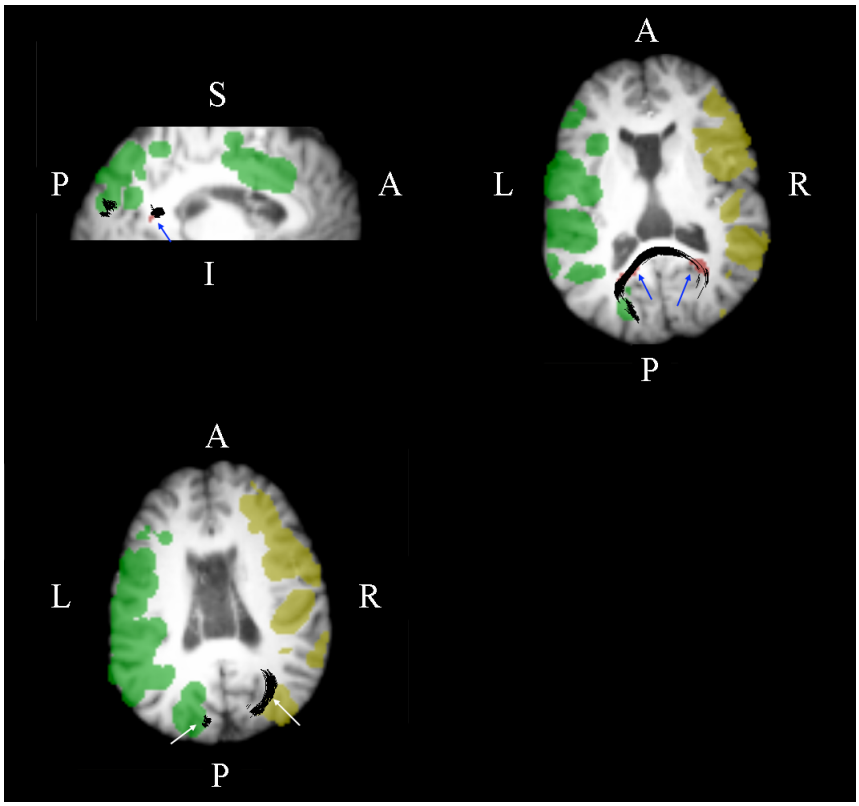

Supplementary Figure 4.5. Functional MRI-guided tractography results for participant 6. The top images show fibres passing through lateral, posterior corpus callosum activation in sagittal (left) and axial (right) views (blue arrows). The bottom images show axial views of tracts reaching targets in superior occipital/inferior parietal cortex (white arrows). All other details as in Supplementary Figure 4.1.

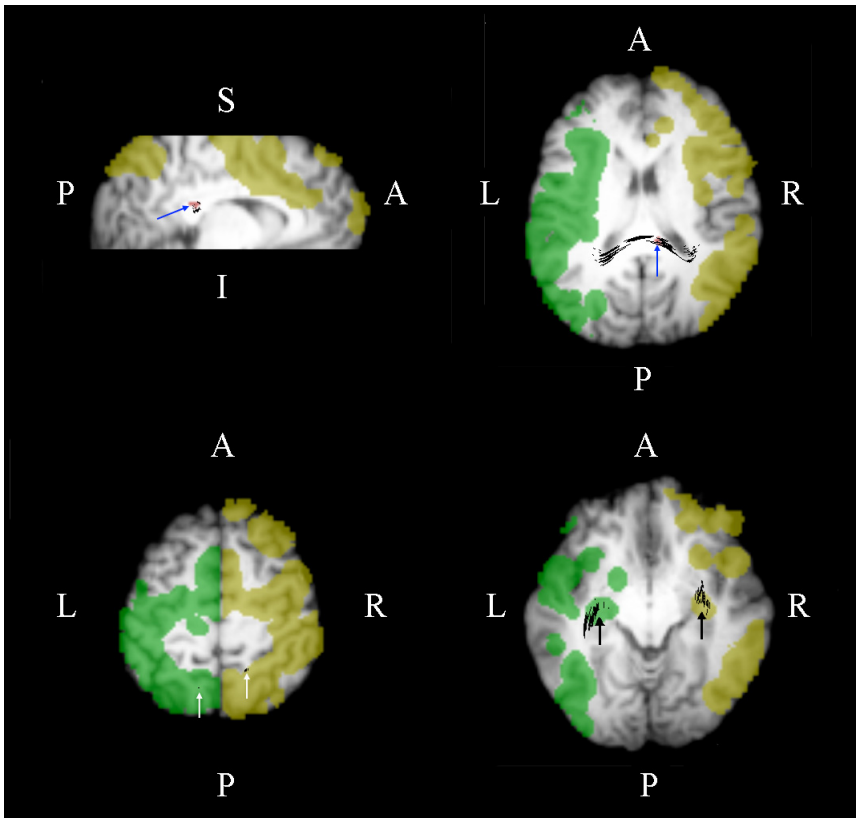

Supplementary Figure 4.6. Functional MRI-guided tractography results for participant 7. The top images show fibres passing through splenium activation in sagittal (left) and axial (right) views (blue arrows). The bottom images show axial views of tracts reaching targets in parietal cortex (white arrows) and medial temporal cortex (black arrows). All other details as in Supplementary Figure 4.1.

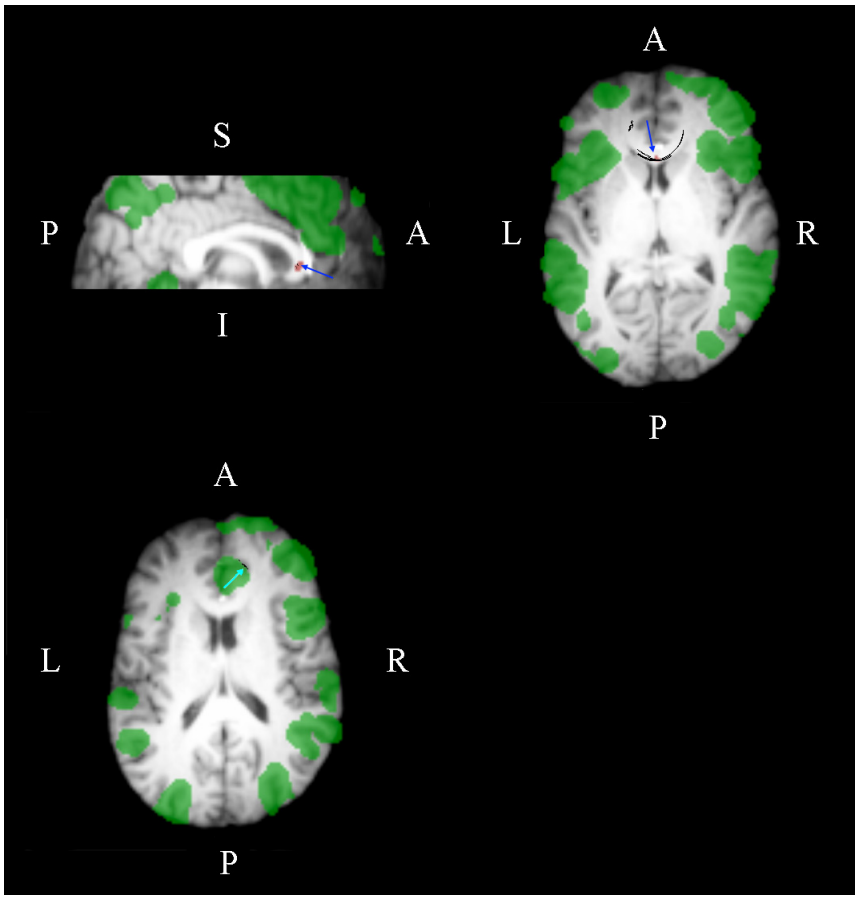

Supplementary Figure 4.7. Functional MRI-guided tractography results for participant 8. No tracts were identified that reach gray matter activation ROIs in both hemispheres for this participant; instead, the gray matter activation is represented by a single ROI (green). The top images show fibres passing through genu activation in sagittal (left) and axial (right) views (blue arrows). The bottom images show an axial view of tracts reaching targets in right prefrontal cortex (cyan arrow). All other details as in Supplementary Figure 4.1.

Chapter 5 Discussion

5.1. Overview

The discussion is divided into four sections. First, the results of Chapters 2, 3, and 4 are briefly summarized (Section 5.2). Second, further refinements to the understanding of white matter fMRI activation are proposed (Section 5.3). These refinements build upon the work presented in this thesis, and include: evaluating regional differences in sensitivity to white matter fMRI activation (Section 5.3.1); investigating white matter fMRI activation with improved spatial resolution (Section 5.3.2); characterizing the reliability of white matter fMRI activation (Section 5.3.3); and uncovering the neurophysiologic underpinnings of white matter fMRI activation (5.3.4). Potential sources of experimenter bias against white matter fMRI activation are discussed in Section 5.4, including recommendations to reduce bias in future studies. To conclude, the significance of this thesis is highlighted (Section 5.5).

5.2. Summary of Results

The research described in this thesis has expanded upon the current understanding of fMRI activation in white matter. The results of Chapter 2 demonstrated that hemodynamic changes could be detected in white matter in the absence of partial volume effects. This result confirmed that white matter fMRI activation clusters could be hemodynamic in origin. Importantly, Chapter 2 contradicted the notion that white matter CBF and CBV are insufficient for a detectable hemodynamic response, which is one of the main sources of controversy surrounding fMRI activation in white matter (Logothetis and Wandell, 2004; Weis et al., 2011).

In Chapter 3, the results confirmed that sensitivity to white matter fMRI activation is dependent on field strength. The results also showed that the field strength dependent sensitivity gains are larger in white matter than gray matter. Thus, it is possible that the scarcity of studies reporting white matter fMRI activation may be partially explained by the prevalence of 1.5 T MRI systems. If this were true, one would expect that as higher field systems become more widely available, reports of white matter fMRI activation would become more common. One question that remains is whether the sensitivity

conferred by 3 T MRI systems, which are significantly more widely available than 4 T systems, is sufficient to expect widespread reports of white matter fMRI activation.

Chapter 4 demonstrated that regions of white matter fMRI activation are structurally connected to activated gray matter regions, providing evidence that white matter fMRI activation is functionally relevant. In addition, this study is the first to employ both white matter fMRI and DTI to examine brain connectivity, providing a methodological foundation for future studies. Such a combined approach has the potential to elucidate brain connectivity beyond what could be obtained from current structural and functional connectivity techniques. For example, whether a particular white matter tract was involved in a given task could be evaluated directly by querying the functional dynamics of the tract itself, rather than inferring its involvement based on structural or functional connectivity results.

5.3. Further Refinements to the Understanding of White Matter Functional MRI Activation

The studies presented in Chapters 2, 3, and 4 provided key insight into white matter fMRI activation, and will allow for improved understanding and interpretation of future white matter fMRI activation results. However, more research should be done towards answering crucial questions about white matter fMRI activation that are still outstanding.

5.3.1. Regional Differences in Sensitivity

It is possible that regional differences exist in terms of sensitivity to white matter fMRI activation. This possibility stems from the fact that not all voxels were activated in the white matter ROIs described in Chapters 2 and 3. In Chapter 3, this could be due to the existence of functional sub-regions in the PLIC ROIs (i.e., parts of the PLIC that were not activated were not engaged by the finger tapping task). However, in Chapter 2, the breath-holding task was expected to elicit global (i.e., whole brain) hemodynamic changes, yet some voxels did not exhibit significant activation. This notion also arises from many reports of callosal activation (including Chapter 4; Mazerolle et al., 2008, 2010; Gawryluk et al., 2009, 2011a), which tend to be localized near the mid-sagittal

section, rather than along the entire length of the pathway. In fact, almost all reports of white matter fMRI activation are limited to the corpus callosum and/or the internal capsule (excluding Yarkoni et al., 2009; Weis et al., 2011). While this may be a feature of the experimental design of the particular studies (i.e., many of the studies were designed specifically to elicit interhemispheric transfer across the corpus callosum; D'Arcy et al., 2006; Gawryluk et al., 2009, 2011a; Mazerolle et al., 2008, 2010; Omura et al., 2004; Tettamanti et al., 2002; Weber et al., 2005), this reasoning does not explain the observation of voxels that were not activated by the breath-holding task in Chapter 2.

It is possible that fundamental physiological differences among white matter regions could affect the ability to detect activation in particular regions. Previous speculations on the source of regional differences in sensitivity to white matter fMRI activation have focused on two possible explanations. First, it is possible that hemodynamic differences among white matter regions results in regional sensitivity differences (Mazerolle et al., 2008). In gray matter, for example, there is evidence that vascularization differences among regions affects regional sensitivity to fMRI activation (e.g., the visual cortex is more highly vascularized than other regions; Lierse, 1963, as cited by Kastrup et al., 1999). In white matter, it has been shown that the corpus callosum and the optic nerve are differentially sensitivity to anoxia and aglycemia (Baltan, 2006). This suggests that metabolic differences between white matter regions exist, which, given the tight metabolic-hemodynamic coupling in the brain (Lecrux and Hamel, 2011), might correspond to hemodynamic differences. Thus, vascularization differences among regions could contribute to regional variability in sensitivity to white matter fMRI activation. By combining functional studies with measures of vessels (e.g., venograms, vessel size index imaging), it may be possible to begin to understand the source of regional sensitivity differences and, by doing so, begin to establish the practical limits of white matter fMRI studies.

Second, it has also been speculated that the density of fibres and/or action potentials contributes to regional sensitivity differences of white matter fMRI activation (Mazerolle et al., 2008). This notion stems from the relatively frequent observations of white matter fMRI activation in the medial corpus callosum (e.g., Mazerolle et al., 2008; Gawryluk et al., 2009, 2011a), where fibres are densely packed (relative to more lateral

callosal regions) and organized topographically according to the anterior-posterior position of the cortical regions that the fibres connect (Zarei et al., 2006). Thus, when a particular interhemispheric pathway is activated, it is likely that there is a high density of action potentials in the relevant callosal region. The spatial pattern of internal capsule fMRI activation may have an analogous explanation, as activation has been reported in more inferior regions as opposed to superior regions where the tract fans out to cortical targets (Gawryluk et al., 2011b). The relationship between fibre density and fMRI activation in white matter could be explored by using advanced diffusion MRI techniques such as AxCaliber, which provides a measure of axon diameter distribution, albeit with prohibitively long scan times for *in vivo* human applications (1.5 hours; Barazany et al., 2009; Assaf and Cohen, 2009). Characterizing the relationship between action potential density and white matter fMRI activation will likely rely on invasive electrophysiological recordings in animals.

In addition, it is also possible that regional differences in white matter sensitivity are due to differences in the shape of the hemodynamic response function (HRF). In gray matter, there is evidence that the shape of the HRF varies between regions, although whether this is due to differences in neural activity, neurovascular coupling, or vascularization is unknown. Analysis techniques that model activation using regionally optimized HRFs are thought to improve fMRI sensitivity (e.g., Handwerker et al., 2004; Miezin et al., 2000), although this approach is not routinely applied (i.e., most studies employ a canonical HRF to model activation in all voxels). While there is evidence that the shape of the HRF in white matter is the same as the canonical HRF (Fraser et al., submitted), other work has demonstrated slower responses in white matter compared to gray matter (Yarkoni et al., 2009). If differences between the gray matter and white matter HRF exist, the use of the gray matter canonical HRF for modeling activation would result in systematic underestimation of white matter activation, More research is needed to evaluate differences in the shape of the hemodynamic response function between gray matter and white matter, as well as among different white matter regions. Then, the potential benefits of regionally specific HRFs for detecting white matter fMRI activation could be evaluated.

5.3.2. Spatial Resolution

A refinement that directly relates to the work presented in this thesis is to determine whether fMRI activation in white matter can be detected using acquisitions with improved spatial resolution. Smaller voxels would reduce the potential contribution of partial volume effects and allow conservatively defined ROIs to encompass a larger volume of white matter. Higher spatial resolution is also important for confirming reports of fMRI activation in small white matter structures such as the internal capsule (discussed in Chapter 3). However, the SNR is proportional to voxel volume, which may limit the feasibility of detecting white matter fMRI activation using high spatial resolution acquisitions. Driver and colleagues (2010) were able to detect white matter signal changes associated with hypercapnia at high resolution (2 x 2 x 3 mm^3), suggests that, at least with high field MRI (3 T and 7 T), SNR of high resolution fMRI is not prohibitively low for detecting hemodynamic changes in white matter. Furthermore, preliminary work suggests that task-related white matter fMRI activation can indeed be detected at higher spatial resolution with 4 T MRI (3.1 x 3.1 x 2.9 mm^3; Gunde et al., unpublished observations) but more work is needed to verify this finding.

5.3.3. Reliability

Another factor that would strengthen interpretations of white matter fMRI activation results is an understanding of the reliability of the technique. Reliability is an active area of fMRI research. Varying degrees of reliability have been reported, depending on the analysis technique, reliability metric, test-retest interval, as well as the particular tasks and regions of interest (reviewed in Bennett and Miller, 2010). In general, greater reliability is observed for motor and sensory tasks relative to cognitive tasks (Bennett and Miller, 2010). Regional differences in reliability may be explained in part by the local microvasculature. For example, McGonigle and colleagues (2000) speculated that variability in visual cortex may be partially due to the high concentration of venules in the region, allowing a wider range of responses to visual stimulation. Thus, it is important to evaluate reliability specifically for white matter fMRI activation, particularly given the known differences in vasculature in white matter relative to gray matter (Duvernoy et al., 1981) and the lower blood flow and volume in white matter compared

to gray matter (Helenius et al., 2003; Preibisch and Hasse, 2001; Rostrup et al., 2000; van der Zande et al., 2005).

While reliable white matter fMRI activation has been observed anecdotally (D'Arcy et al., unpublished observations), experimentally evaluating the reliability of white matter fMRI activation will be a crucial step towards demonstrating its utility for basic and clinical neuroscience research. Proposed methods for evaluating reliability of white matter fMRI activation can be found in Appendix 2.

5.3.4. Neurophysiologic Basis

More generally, it is important to determine the neurophysiologic basis of fMRI signals in white matter. While there is indirect evidence that neural activity in white matter might be expected to result in measureable BOLD signal changes (discussed in Section 1.3.2.2), this has not been verified experimentally. A direct investigation of activity-dependent hemodynamic changes in white matter, for example, by electrically stimulating white matter in an animal model while simultaneously acquiring fMRI data, will provide significant insight into the neurophysiologic signals underpinning BOLD signal changes measured in white matter. While primate models are advantageous in terms of their phylogenetic relationship to humans, they are expensive and not always accessible. Rat models, which are inexpensive and widely available, have been extensively used to study neurovascular coupling (e.g., Smith et al., 2002; Angenstein et al., 2007; Goloshevsky et al., 2008; Huttunen et al., 2008; Maandag et al., 2007); however, before a rat model can be used to investigate the neurophysiology of white matter fMRI, it must first be verified that rat white matter is capable of supporting detectable hemodynamic changes.

A hypercapnic challenge could be used to elicit whole brain hemodynamic changes in the rat. Similar to the breath-holding task employed in Chapter 2, hypercapnia induces vasodilation, which elevates global CBF and CBV (e.g., Grubb et al., 1974) and is commonly used to measure the capacity of vessels to react to a stimulus (e.g., Cohen et al., 2004; Driver et al., 2010). Previous work has demonstrated hemodynamic changes in both gray and white matter associated with hypercapnia in humans (Cohen et al., 2004; Macey et al., 2003; Rostrup et al., 2000; van der Zande et al., 2005), but only gray matter

signal changes have been examined in rats (Kannurpatti et al., 2003; Lu et al., 2009; Sicard et al., 2003; Weneger and Wong, 2008; Wu et al., 2002). Therefore, the ability to measure hypercapnia-induced hemodynamic changes in rat white matter must first be established, before a rodent model can be used to further investigate the neurophysiologic basis of white matter fMRI activation. Proposed methods for a study of the cerebrovascular reactivity of rat white matter are outlined in Appendix 3.

5.4. Experimenter Bias against White Matter Functional MRI Activation

Despite the growing number of reports of white matter fMRI activation (Aramaki et al., 2006; D'Arcy et al., 2006; Fabri et al., 2011; Gawryluk et al., 2009, 2011a,b; Mazerolle et al., 2008, 2010; Mosier and Bereznaya, 2001; Newman et al., 2010; Omura et al., 2004; Tettamanti et al., 2002; Weber et al., 2005; Weis et al., 2011; Yarkoni et al., 2009) and the possible neurophysiologic explanations for fMRI signals in white matter (described in Section 1.3.2.2), the technique remains controversial. In this section, it is proposed that the reluctance to accept fMRI activation in white matter is partially the result of a systematic bias in the field of functional brain imaging.

The notion of experimenter bias in fMRI research is of fundamental importance. This is because fMRI is an indirect measure of functional brain activation, the validity of which is regularly evaluated based on what is already known about the functional organization of the brain. That is, because there is rarely a gold standard available for fMRI results to be compared against, experimenter expectations tend to play a major role in evaluating data quality and the validity of results. This sentiment is described well by Poline and colleagues (2006) in the introduction to their paper describing a contest in which a diverse group of fMRI researchers applied different techniques to the analysis of the same fMRI dataset:

> The most obvious goal was to determine which [analysis] techniques would yield the 'best' results. This is a legitimate question from neuroscientists or clinicians who typically assess the results in relation to their prior expectations, although this biases fMRI studies away from making new and unexpected discoveries. (p. 352)

The following sections consider potential sources of bias against reporting white matter fMRI activation, and provide recommendations to help reduce bias in future fMRI studies.

5.4.1. White Matter Functional MRI Signals as Noise

In some fMRI studies, the signal from white matter is used as a nuisance regressor in the analysis model (e.g., Leber, 2010). This approach has been recommended as best practice for resting state functional connectivity analyses (Van Dijk et al., 2010). White matter signals have also been used to estimate physiological noise in fMRI data (Behzadi et al., 2007). In addition, white matter signals have been used to set thresholds such that, for activation to be considered significant, its intensity must exceed that of white matter (Soltanian-Zadeh et al., 2004). Decreases in white matter fMRI activation have also been cited as evidence that a novel denoising procedure was successful (Tohka et al., 2008). Such steps not only preclude the detection of white matter fMRI activation in these particular studies, but also perpetuate the notion that activation observed in white matter is artifactual.

5.4.2. Selective Reporting of Activation Clusters

5.4.2.1. Examples. As noted in Chapter 4, the body of fMRI literature includes reports in which activation in white matter can be observed in figures but is not reported in text. While it is impossible to compile a complete list of such reports, some examples of studies in which white matter fMRI activation is pictured in figures but otherwise ignored include Genova and colleagues (2009; Figures 3 and 4), Bestmann and colleagues (2010; Figure 3), Dumontheil and colleagues (2011; Figures 5, 8, and 9), Lazeron and colleagues (2003; Figure 1), Mestres-Missé and colleagues (2010; Figures 1 and 2), and Wey and colleagues (2011; Figure 4). The bias against reporting functional activation in white matter may also extend beyond fMRI researchers; for example, a [^{14}C]deoxyglucose autoradiography study of the rat brain shows an increase in white matter glucose uptake, but it is not reported in text (Figure 3, Panel D2; Brown and Sharp, 1995).

5.4.2.2. Possible Explanations. In some cases, it is possible that the researchers reporting these studies may have failed to notice activation in white matter. However, inattention to white matter regions cannot explain the failure to report such clusters in all cases. A striking example is the study reported by Takahashi and colleagues (2009). While no white matter fMRI activation is visible on the main figures in their peer-reviewed article in *Science*, internal capsule activation is visible (but not reported) in Supplementary Figure 4 of their report. Furthermore, online coverage about the work in the popular media includes a version of the figure in which the internal capsule activation has been circled for emphasis (see Appendix 1).

It is possible that fMRI researchers are not comfortable reporting activation clusters in white matter due to the lack of information available about the potential neurophysiological source of white matter fMRI activation. However, this explanation is not consistent with the common practice of reporting activation in subcortical gray matter regions (e.g., Cabeza and Nyberg, 2000; Peyron et al., 2000; Dang-Vu et al., 2010), for which there have been few studies of neurovascular coupling until recently (but see Sloan et al., 2010, for an example). In fact, functional brain mapping applications of fMRI have continued to gain popularity despite the incomplete understanding of the neural events that are represented by fMRI signals (Logothetis, 2007; Raichle and Mintun, 2006). This suggests that, in general, fMRI researchers do not require all of the neurophysiological details to be understood before the value of such a technique can be appreciated.

Another possibility is that white matter is more prone to artifacts than gray matter, such that researchers might selectively exclude white matter activation from the interpretation of their results. This concept is expressed by Weis et al. (2011): "standard EPI sequences as used [by Weis and colleagues, 2011] are not optimal for detecting white matter activations and the risk of artifacts is augmented" (p. 388). This statement raises the question: what could cause an increase in artifactual activations in a manner specific to white matter, such that selectively discounting white matter fMRI activation would be a valid approach?

A common cause of artifactual activation is task-related motion. When participant motion is task-correlated, artifactual activations can occur, particularly at tissue boundaries (Johnstone et al., 2006). Thus, voxels near the boundaries between gray matter

and white matter, and between brain parenchyma and CSF, will be most sensitive to motion-induced artifactual activations. White matter voxels *per se* are unlikely to be more susceptible to false activations due to motion than other voxels; regions of deep white matter, which can be centimetres away from tissue boundaries, may be particularly insensitivity to such artifacts. Furthermore, the studies presented in this thesis, as well as some of the studies reporting white matter fMRI activation (Mazerolle et al., 2008; Gawryluk et al., 2011a,b), mitigated the risk of motion-related activations by including the estimated motion parameters (output by the motion correction) as regressors of no interest in the analysis model. Even with this approach, it is possible that nonlinear spin history effects caused by motion are not corrected (Yancey et al., 2011). However, spin history effects are likely to be most severe near regions of large magnetic gradients (i.e., susceptibility induced field gradients near the sinuses) and would not be expected to result in tissue-specific effects.

Another potential source of artifactual activation is physiological noise. When task-correlated, respiratory and cardiac artifacts can result in artifactual activation. Task-correlated respiratory and/or cardiac rate changes have been observed for tasks that require attention, are cognitively challenging, or are emotional (Birn et al., 2009). However, Birn and colleagues (2006) demonstrated that respiratory related artifacts tend to be most problematic in gray matter or near large vessels. Furthermore, as noted in Chapter 3, white matter has higher tSNR and less physiological noise than gray matter. Thus, it is unlikely that white matter is particularly prone to artifactual activation caused by physiological noise.

5.4.3. Recommendations for Future Functional MRI Studies

The practice of using white matter signal as a nuisance regressor should be avoided to prevent artifactually decreased sensitivity to white matter fMRI activation. Furthermore, in the absence of any specific examples of artifacts that could cause false activations in a tissue-specific manner, white matter fMRI activations should not be selectively ignored. Instead, all significantly activated clusters should be routinely reported in text or tables. This practice would help eliminate any existing systematic bias against detecting fMRI activation in white matter. In addition, estimated motion

parameters (output from motion correction algorithms) could be routinely reported in order to communicate the degree to which motion might have been a problem in a given study. Finally, physiological noise corrections such as retrospective image correction (RETROICOR; Glover et al., 2000) should be routinely applied in order to reduce the potential risk for physiological artifacts confounding fMRI activation results. While physiological artifacts are unlikely to impact white matter to a greater extent than gray matter, the application of such a rigorous approach could provide further evidence for white matter fMRI activation and help alleviate concerns regarding the potential impact of artifacts.

5.5. Conclusions and Significance

The studies presented in this thesis have refined the current understanding of fMRI activation in white matter, in terms of its probable hemodynamic basis (Chapter 2), its relationship with field strength (Chapter 3), and its relationship to the activated network of gray matter regions (Chapter 4). These findings, along with the discussion of the possible neurophysiological bases for white matter fMRI activation (Section 1.3.2.2), build upon the existing foundation of studies reporting white matter fMRI activation by providing more information about what white matter fMRI activation represents. As white matter fMRI activation becomes better understood (Section 5.3) and more accepted (Section 5.4), this technique could be applied to provide novel insights into brain connectivity. More specifically, the ability to detect activation in the brain's connections will open new research avenues into how the regions of a given brain network interact to support complex cognitive functions. For example, feedforward versus feedback connections might be distinguished on the basis of the tract's fMRI timecourse relative to timecourses of the gray matter nodes of the network; transient versus reentrant connections might be distinguished based on the duration of the fMRI response in the tract. Furthermore, white matter fMRI may provide key insight into white matter diseases such as multiple sclerosis, as well as diseases such as schizophrenia in which abnormal brain connectivity has been implicated.

Appendix 1 Popular Media Coverage of Takahashi and Colleagues (2009)

Source: http://www.dailymail.co.uk/sciencetech/article-1147525/The-green-eyed-monster-lives-brain-Scientists-discover-jealousy-lobe.html#ixzz1mTnlT88x

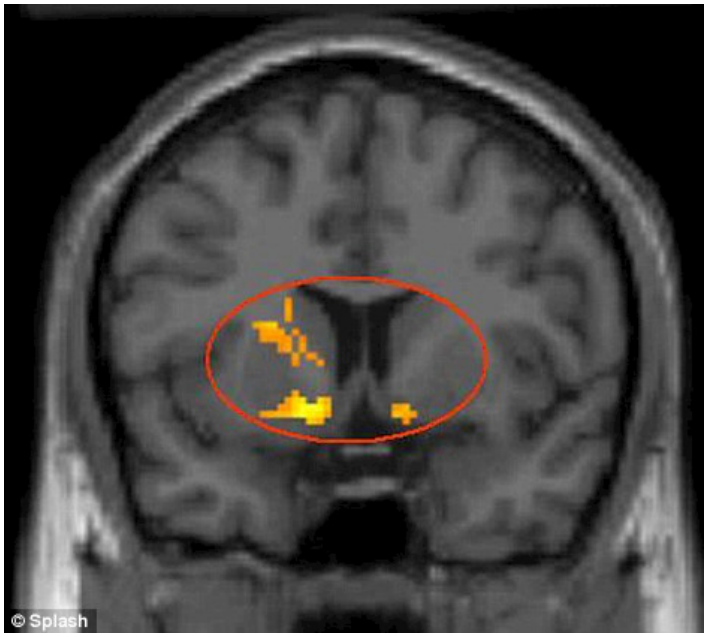

Schadenfreude: This is the region of the brain that controls taking delight in other people's misfortune

Appendix 2 Proposed Methods: Reliability of White Matter Functional MRI Activation

A2.1. Introduction

Recent research has demonstrated that detection of activation in white matter may be possible with functional magnetic resonance imaging (fMRI; Aramaki et al., 2006; D'Arcy et al., 2006; Fabri et al., 2011; Gawryluk et al., 2009, 2011a,b; Mazerolle et al., 2008, 2010; Newman et al., 2010; Omura et al., 2004; Tettamanti et al., 2002; Weber et al., 2005; Weis et al., 2011; Yarkoni et al., 2009). By providing a metric of the functional status of the brain's connections, white matter fMRI has potential to provide insight into the functional dynamics of brain connectivity. This is in contrast to current techniques for studying brain connectivity, which have mainly used diffusion tensor imaging tractography and functional connectivity analyses to map structural and functional connections, respectively. Neither tractography nor functional connectivity techniques can directly measure activation in white matter pathways. Studying activation in white matter pathways is crucial for understanding interactions among different nodes in a brain network, as well as evaluating whether structural white matter changes are associated with functional changes. This approach may also clarify whether observed correlations between gray matter regions (a typical approach to studying functional connectivity using fMRI) result from direct connections, or indirect connections mediated by other gray matter areas. Before this potential can be meaningfully applied, an understanding of the reliability of white matter fMRI activation results is necessary.

Reliability is an active area of fMRI research. Varying degrees of reliability have been reported, depending on the analysis technique, reliability metric, test-retest interval, as well as the particular tasks and regions of interest (reviewed in Bennett and Miller, 2010). In general, greater reliability is observed for motor and sensory tasks relative to cognitive tasks (Bennett and Miller, 2010). Regional differences in reliability may be explained in part by the local microvasculature. For example, McGonigle and colleagues (2000) speculated that variability in visual cortex may be partially due to the high concentration of venules in the region, allowing a larger range of responses to visual stimulation. Thus, it is important to evaluate reliability specifically for white matter

activation, particularly given the known differences in vasculature in white matter relative to gray matter (Duvernoy et al., 1981) and the lower blood flow and volume in white matter compared to gray matter (Helenius et al., 2003; Preibisch and Hasse, 2001; Rostrup et al., 2000; van der Zande et al., 2005).

We propose to evaluate fMRI reliability for a cognitive task that has been previously shown to elicit activation in white matter (D'Arcy et al., 2006; Gawryluk et al., 2011a; Mazerolle et al., 2008, 2010). We hypothesize that reliability of white matter fMRI activation will be comparable to that of gray matter regions activated by the same task.

A2.2. Methods

A2.2.1. Participants

At least ten healthy participants will be recruited for the study.

A2.2.2. Experimental Design

Each participant will complete three scanning sessions. All participants will be experienced with previous MRI research studies to reduce effects of novelty and/or anxiety. For each participant, scanning sessions will take place at approximately the same time of day, on consecutive days. Within each session, three runs of the task will be performed. At each session, the participant will receive the same instructions (read from a script by the same investigator). The same technician will operate the MRI for each scan in this study. Care will be taken to position the participants in the head coil/MRI in approximately the same position for each session. Participants will be asked to make sure that their sleep patterns and their intake of caffeine, nicotine, alcohol, and medications are approximately equivalent each day for the day preceding the first session and the three days on which the sessions are acquired.

A2.2.3. Task

An interhemispheric transfer task which has previously been shown to elicit activation in the corpus callosum will be used (D'Arcy et al., 2006; Gawryluk et al., 2011a; Mazerolle et al., 2008, 2010). Stimuli consist of faces (Troje and Bulthoff, 1996;

i.e., right hemisphere stimuli) and words (Coltheart, 1981; Wilson, 1988; i.e., left hemisphere stimuli) that are presented to the left and right visual fields (i.e., either directly to the relatively specialized hemisphere, or to the opposite hemisphere) to elicit interhemispheric transfer. Half the stimuli are real words and faces; the other half are scrambled, that is, pseudowords and faces with the features rearranged within the face outline. The participants will be asked to respond (via a four button forced choice) to indicate whether each stimulus is a real word, real face, scrambled word, or scrambled face. Participants will always use their left hand to respond to word stimuli and their right hand to respond to face stimuli, with their index fingers assigned to real stimuli and their middle fingers assigned to scrambled stimuli. In each run, eight blocks of eight stimuli per block (22 s duration) will be alternated with 18 s rest blocks. The blocks are equally divided between two conditions: no visual cross (noVC) and visual cross (VC). In the noVC blocks, stimuli are presented to the relatively specialized hemisphere (i.e., word stimuli to the right visual field/left hemisphere; face stimuli to the left visual field/right hemisphere). In the VC blocks, stimuli are presented to the opposite hemisphere. The block design was selected to maximize reliability (Bennett and Miller, 2010). The total duration of each run is 338 s. To mitigate habituation, different word and face stimuli are presented in each run. All stimuli will be presented laterally (>2.3 degrees of visual angle from fixation) and rapidly (150 ms) in order to initially stimulate one hemisphere and avoid saccades. Participants will be asked to fixate on a central point throughout the experiment. At the beginning of each session, participants will perform a short practice task (with feedback) to ensure compliance. The practice task will be repeated until the participant obtains an accuracy of greater than or equal to 50%. E-Prime (Psychology Software Tools, Inc.) will be used to present stimuli, which will be displayed using back-projection to a screen mounted inside the magnet bore, and viewed through a mirror mounted on the head coil. Responses will be collected using a Lumina fibre optic response system (Cedrus).

A2.2.4. MRI Acquisition

Data will be acquired using a 4 T Oxford Magnet with an DirectDrive console (Agilent Technologies Inc.). Magnetic field gradients are provided by a body coil (Tesla

Engineering Ltd.) operating at a maximum of 35.5 mT/m at 120 T/m/s, and driven by 950 V amplifiers (PCI). A TEM head coil (Bioengineering Inc.) is used for transmit/receive. Foam padding will be used to restrict head motion.

A2.2.4.1. Functional MRI Acquisition. Functional MRI will be conducted using an optimized sequence (to be decided).

A2.2.4.2. Structural Image Acquisition. Following the functional MRI scans, a 3D magnetization prepared fast low angle shot (MPFLASH) T1-weighted whole brain anatomical image will be acquired with the following parameters: TR/TI/TE=10/700/3.5 ms, 256 x 160 x 110 data acquisition matrix, 220 x 220 x 165 mm FOV, 4 segments, 300 ms segment delay, 11 degree flip angle.

A2.2.5. Data Analyses

A2.2.5.1. Behavioural Data Analysis. Reaction time and accuracy data will be input to a repeated-measures analysis of variance (ANOVA) with the following factors: session, run, noVC/VC, real/scrambled. Statistical significance will be evaluated using $p < 0.05$.

A2.2.5.2. Functional MRI Analysis. Pre-processing and statistical analyses will be performed with the fMRI expert analysis tool (FEAT) version 5.98 in FMRIB Software Library (FSL; Smith et al., 2004; www.fmrib.ox.ac.uk/fsl). Pre-statistics processing includes the following steps: motion correction using MCFLIRT (Jenkinson et al., 2002), non-brain removal using BET (Smith, 2002), spatial smoothing using a Gaussian kernel of FWHM 6 mm, mean-based intensity normalisation, and highpass temporal filtering (Gaussian weighted least-squares straight line fitting, with sigma = 50 s).

For the first-level analyses, time-series statistical analyses will be carried out using FMRIB's Improved Linear Model (FILM) with local autocorrelation correction (Woolrich et al., 2001). Motion parameters (output from the motion correction) will be included in the model as regressors of no interest. *Z* (Gaussianised *t*) statistic images will be reported using a threshold for clusters determined by $z > 2.3$ and a (corrected) cluster significance threshold of $p < 0.05$ (Worsley et al., 1992). *T*-contrasts will be calculated to evaluate activation for task > baseline, VC > noVC, and noVC > VC. FLIRT will be used

to register the activation maps to the anatomic images (seven degrees of freedom; Jenkinson and Smith, 2001; Jenkinson et al., 2002). At the second level, the three runs within each scanning session will be combined for each subject using a fixed effects analysis.

A2.2.5.3. Reliability Analysis. Reliability will be evaluated for all three *t*-contrasts calculated (task > baseline, VC > noVC, and noVC > VC). Reliability of gray matter and white matter activation will be considered separately. Gray and white matter regions of interest (ROIs) will be created for each subject as follows: First, the anatomic images from each scanning session are registered to one another using FLIRT and averaged together. This average anatomic image is input to FMRIB's Automated Segmentation Tool (FAST; Zhang et al., 2001) to create gray and white matter tissue segmentations. *A priori* tissue probability maps are used for segmentation initialization. The fMRI data are then registered to the average anatomic image such that the gray and white matter ROIs can be applied to the fMRI results.

For each subject, reliability between pairs of scanning sessions will be evaluated in two ways: 1) by calculating difference images of the thresholded activation maps; and 2) by calculating *t*-contrasts to statistically compare the scanning sessions in a third level analysis of fixed effects.

Appendix 3 Proposed Methods: Can Functional MRI Detect Hemodynamic Changes in Rat White Matter?

A3.1. Introduction

Until recently, functional magnetic resonance imaging (fMRI) activation was generally thought to be restricted to gray matter (GM; e.g., Logothetis and Wandell, 2004). However, there is a growing body of evidence supporting the notion that it is possible to detect fMRI activation in white matter (WM; D'Arcy et al., 2006; Fabri et al., 2011; Gawryluk et al., 2009, 2011a,b; Mazerolle et al., 2008, 2010; Mosier and Bereznaya, 2001; Newman et al., 2010; Omura et al., 2004; Tettamanti et al., 2002; Weber et al., 2005; Weis et al., 2011; Yarkoni et al., 2009). The ability to detect fMRI activation in WM has the potential to greatly expand the breadth of functional neuroimaging research. For example, WM fMRI can be applied to the study of brain connectivity by measuring activation patterns in the WM pathways themselves. This is in contrast to current approaches for studying brain connectivity, which can only infer the functional involvement of connections on the basis of functional connectivity analyses and/or structural connectivity approaches such as tractography (e.g., Guye et al., 2008). WM fMRI activation also has potential clinical applications, such as improving the diagnosis and assessment of WM disorders. For example, current clinical MRI measures for multiple sclerosis (MS) often do not correlate well with the functional deficits experienced by patients (i.e., the clinico-radiological paradox; e.g., Pelletier et al., 2009). By evaluating the functional status of WM regions, WM fMRI activation may provide a metric that is more closely linked to the patient's functional deficits.

Evidence for WM fMRI activation comes mainly from human studies using interhemispheric transfer tasks that target the corpus callosum (e.g., Gawryluk et al., 2009, 2011a; Mazerolle et al., 2008, 2010; Omura et al., 2004; Tettamanti et al., 2002; Weber et al., 2005). In addition, fMRI activation has been elicited across functionally distinct regions of the corpus callosum by using various sensory and motor tasks (Fabri et al., 2011). Corpus callosum activation has also been reported in fMRI studies of swallowing (Mosier and Bereznaya, 2001) and inflectional morphology processing

(Newman et al., 2010). There is also evidence for WM fMRI signal changes in the internal capsule during motor tasks (Gawryluk et al., 2011b). In addition to studies reporting task-related fMRI activation, fMRI signal changes correlated with reaction time have been observed in the genu of the corpus callosum and the corona radiata (Yarkoni et al., 2009).

Despite these reports, the neurophysiologic bases of fMRI activation in WM are not understood, which limits interpretation and application of WM fMRI activation. In GM, BOLD fMRI signal changes have been linked to post-synaptic potentials (e.g., Logothetis et al., 2001), but neural activity in WM is dominated by action potentials. Our group and others have previously speculated that action potentials might cause activity-dependent metabolic increases that result in a corresponding hemodynamic response (Mazerolle et al., 2008; Tettamanti et al., 2002). Consistent with this notion, there is evidence from [^{18}F]fluorodeoxyglucose autoradiography that electrical stimulation of rat corpus callosum is associated with increased glucose metabolism (Weber et al., 2002). In addition, cerebral blood flow (CBF) increases associated with heroin administration have been observed in rat internal capsule using [^{14}C]iodoantipyrine autoradiography (Trusk and Stein, 1987). However, neural activity-dependent hemodynamic responses in WM have not been conclusively demonstrated with fMRI.

The first step toward investigating the neural and hemodynamic events that underlie WM activation is to confirm that hemodynamic changes can be detected in the WM of an animal model using fMRI. To do this, we will use a hypercapnic challenge to elicit whole brain hemodynamic changes in the rat. Hypercapnia induces vasodilation, which elevates global CBF and cerebral blood volume (CBV; e.g., Grubb et al., 1974). While there is some evidence that hypercapnia elicits changes in metabolic and neural activity (Martin et al., 2006), hypercapnia is commonly used to measure the capacity of vessels to react to a stimulus (e.g., Cohen et al., 2004; Driver et al., 2010). Previous work has demonstrated hemodynamic changes in both GM and WM associated with hypercapnia in humans (Cohen et al., 2004; Macey et al., 2003; Rostrup et al., 2000; van der Zande et al., 2005), but to our knowledge, only GM activation has been examined in rats (Kannurpatti et al., 2003; Lu et al., 2009; Sicard et al., 2003; Weneger and Wong,

2008; Wu et al., 2002). Therefore, we propose to evaluate hypercapnia-induced hemodynamic changes in rat GM and WM.

In addition to blood oxygen level dependent (BOLD) fMRI, which is non-invasive and typically acquired in human studies, we will also acquire cerebral blood volume (CBV) fMRI using an exogenous blood pool contrast agent. A previous study of GM suggested that CBV fMRI is more uniformly sensitive across brain regions than BOLD fMRI, in which regional sensitivity increases monotonically with resting blood volume (Mandeville and Marota, 1999). Given that WM has lower blood volume relative to GM (e.g., Göbel et al., 1990; Klein et al., 1986; Sicard et al., 2003; Vaucher et al., 1995), we predict that CBV fMRI would be more sensitive than BOLD fMRI to signal changes in WM.

A3.2. Methods

A3.2.1. Acquisition

Anatomic images with 200 μm isotropic voxels will be acquired using 3D balanced steady state free precession (b-SSFP; TR = 10 ms, TE = 5 ms, 50˚ flip angle, 160 × 160 × 160 matrix, 32 mm field of view [FOV], 8 averages, maximum intensity projection (MIP) processing of two phase cycle frequencies, 68 min acquisition time). Pilot testing confirmed that these parameters provide sufficient tissue contrast for satisfactory GM/WM segmentation (see Section A.2.2.2.2). High resolution fMRI data (i.e., 250 x 250 x 1000 μm voxels) will be collected, with slices prescribed to image the region centered between the cerebellum and olfactory bulb. Given the small size of WM structures (e.g., the superior-inferior dimension of the rat corpus callosum is approximately 1mm at its largest point; Paxinos and Watson, 2004), high spatial resolution is required to reduce partial volume effects. CBV fMRI data will be acquired after intravenous administration of a blood pool contrast agent that has a blood half life of several hours (e.g., 30 nm Molday ION superparamagnetic iron oxide [SPIO], BioPAL, Worcester, MA).

Six adult male Long-Evans rats will be anesthetized via an intraperitoneal injection of urethane (1.6 g/kg). Urethane does not have a significant effect on neurotransmission, neuronal firing, or neurovascular coupling (e.g., Huttunen et al.,

2008). Rats will be immobilized using a head holder with ear bars and a nose cone, which will be used for administering gases. The hypercapnic challenge will be preceded by a 2 min baseline (medical air), followed by 6 min of 5% CO_2 (balance air) alternated with 6 min of medical air, repeated thrice. Throughout the experiment, respiration rate and temperature will be monitored.

A3.2.2. Analysis

A3.2.2.1. Functional MRI. Motion correction will be performed on the fMRI data in Statistical Parametric Mapping (SPM; Worsley and Friston, 1995). After temporal filtering (highpass: Gaussian-weighted least-squares straight line fitting, with sigma = 360 s; lowpass: 2.8 s half width at half maximum Gaussian kernel) and spatial smoothing (375 μm full width at half maximum Gaussian kernel), fMRI statistical analysis will be performed in FMRIB Software Library (FSL; Smith et al., 2004) using the general linear model in FEAT. Activation will be modeled as a boxcar function representing the hypercapnia paradigm, convolved with a sine basis function (120 s window). Before statistical thresholding, an intensity-based brain mask will be applied. This mask will also be registered and applied to the CBV fMRI analysis. *T*-contrasts will be calculated comparing hypercapnic and baseline states. Statistical significance will be determined using a cluster-level correction for multiple comparisons ($z > 2.3$, $p < 0.05$).

A3.2.2.2. Region of Interest (ROI). The anatomic images will be segmented in SPM using the SPMMouse toolbox (Sawiak et al., 2009) to create GM and WM probability maps. See Figure A3.1 for an example of the segmentation output. These probability maps will be used to create GM and WM masks (80% probability threshold[1]). ROIs of GM regions (cortical GM, hippocampus, striatum, and thalamus) and WM regions (corpus callosum and internal capsule) will be manually created from the GM and WM masks, respectively, using a rat brain atlas as a guide (Paxinos and Watson, 2004). Figure A3.2 depicts an example of the ROIs that can be created using these methods.

[1] Previous studies have used a wide range of probability thresholds to identify WM. For example, Macey and colleagues (2003) used 50%, whereas Driver and colleagues (2010) used 99%. We selected 80% because this threshold produced conservative WM masks (i.e., no voxels appeared to be in GM when the WM masks were overlaid on the anatomic images).

FLIRT will be used to register the anatomic b-SSFP image to the functional images, which will allow the ROIs to be registered to functional space. Mean percent signal change for the ROIs will be calculated for significantly activated voxels using FSL's Featquery based on the contrasts of parameter estimates. One-way repeated-measures analyses of variance (ANOVAs) will be performed to compare mean percent signal change across the ROIs for both BOLD and CBV fMRI data. We will also compared BOLD and CBV fMRI results in terms of extent of activation (i.e., the percentage of activated voxels for a given ROI).

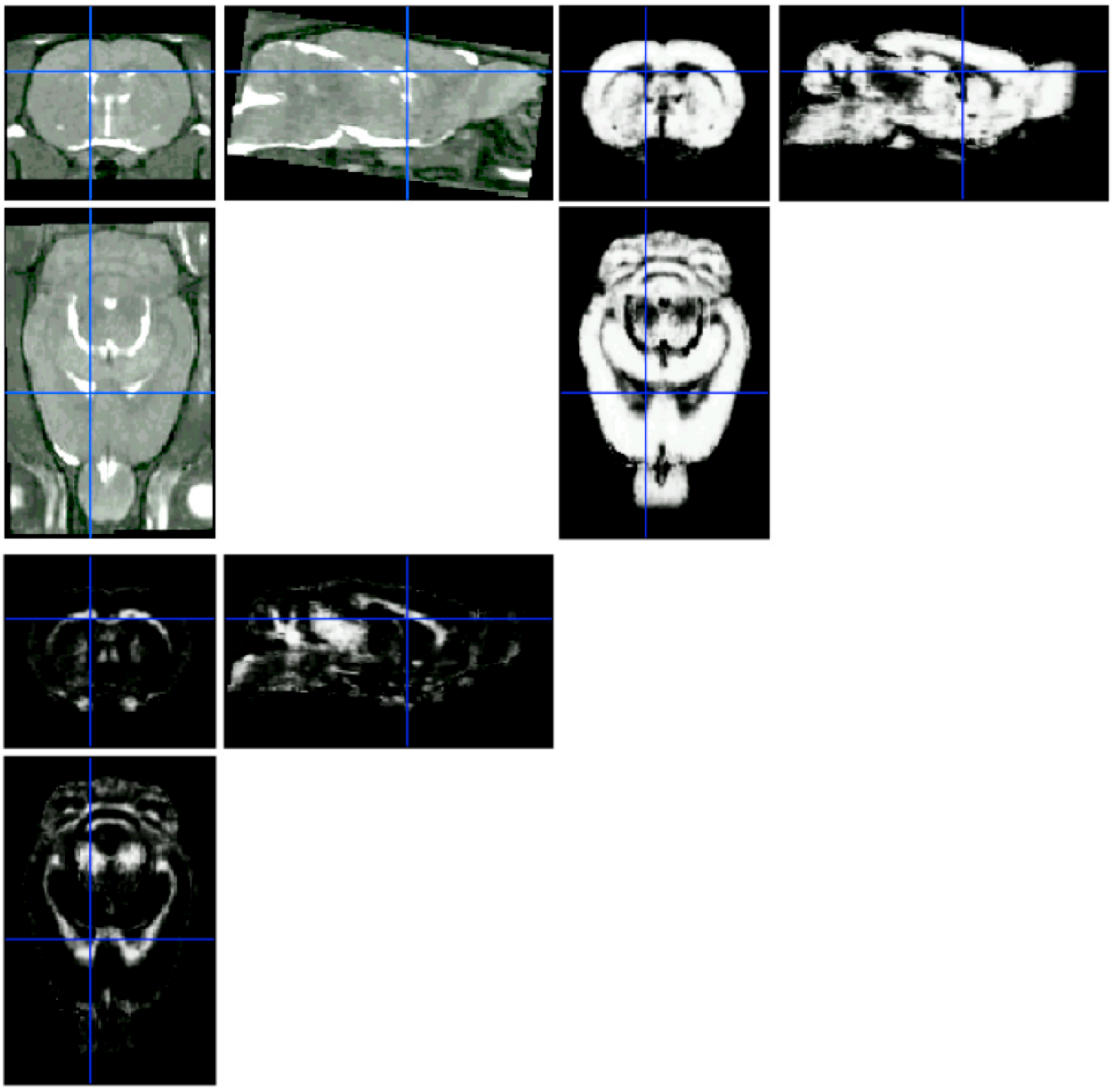

Figure A2.1. An example of the GM/WM tissue segmentation output by SPM. Top left: anatomic image; top right: GM map; bottom left: WM map.

A3.2.2.3. Partial Volume Effects. Even with high spatial resolution, the small size of WM structures in the rat might result in partial volume effects, such that non-WM fMRI signal changes might be erroneously assigned to WM structures. We will estimate the potential contribution of partial volume effects on our findings by transforming the corpus callosum and internal capsule masks from functional space (used to calculate percent signal change) back to anatomic space (200 μm isotropic resolution) using nearest neighbour interpolation. The resulting masks, called the resampled ROIs, can be compared to the original corpus callosum and internal capsule masks, which are assumed to represent true WM voxels (i.e., true positives). This assumption is reasonable because the original masks were created with an 80% probability threshold. The rate of voxels that are falsely characterized as WM (i.e., false positive rate) will be evaluated by comparing the true positive ROIs to the resampled ROIs. Figure A3.3 depicts true positive and false positive voxels for a corpus callosum ROI from a pilot animal.

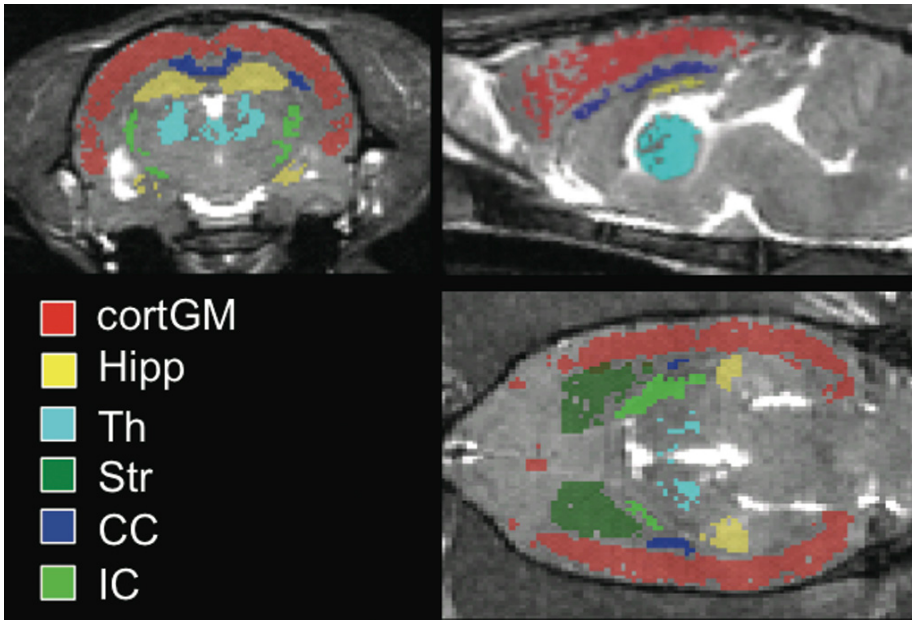

Figure A3.2. The six ROIs overlaid on a representative animal's anatomic brain image, with coronal (top left), sagittal (top right), and horizontal (bottom right) views shown (cortGM: cortical gray matter; Hipp: hippocampus; Th: thalamus; Str: striatum; CC: corpus callosum; IC: internal capsule).

After determining the proportion of false positives in the WM ROIs, we can test whether the signal changes measured in WM could be attributed to partial volume effects.

If one adopts the null hypothesis that there are no signal changes in WM, then the measured signal changes must be due to partial volume effects entirely. In this case, the proportion of false positives in the WM ROIs can be multiplied by the mean percent signal change in neighbouring GM ROIs to obtain an estimate of the mean percent signal change that can be attributed to partial volume effects. For the corpus callosum ROI, the cortical GM and hippocampus ROIs will be used to estimate neighbouring GM percent signal change. For the internal capsule ROI, the cortical GM and thalamus ROIs will be used to estimate neighbouring GM percent signal change. One-tailed paired *t*-tests will be performed to determine if the measured percent signal change in the WM ROIs is significantly greater than the estimate from partial volume effects.

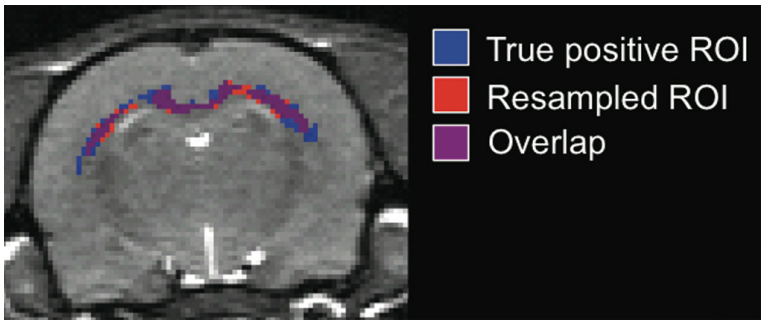

Figure A3.3. The corpus callosum ROIs for the partial volume effects analysis (representative animal, coronal view). The true positive ROI (blue) is overlaid with the resampled ROI (red). The purple voxels represent the overlapping region. Areas of the resampled ROI that do not overlap with the true positive ROI are considered false positives.

References

Aiello GL, Bach-y-Rita P (2000) The cost of an action potential. J Neurosci Methods 103:145–149.

Andersson JLR, Jenkinson M, Smith SM (2007a) Non-linear optimization. FMRIB technical report TR07JA1.

Andersson JLR, Jenkinson M, Smith SM (2007b) Non-linear registration, aka spatial normalisation. FMRIB technical report TR07JA2.

Angenstein F, Kammerer E, Niessen HG, Frey JU, Scheich H, Frey S (2007) Frequency-dependent activation pattern in the rat hippocampus, a simultaneous electrophysiological and fMRI study. NeuroImage 38:150-163.

Arai K, Lo EG (2009) Oligovascular signalling in white matter stroke. Biol Pharm Bull 32:1639-1644.

Aramaki U, Honda M, Okada T, Sadato N (2006) Neural correlates of the spontaneous phase transition during bimanual coordination. Cereb Cortex 16:1338-1348.

Ashburner J, Friston KJ (2000) Voxel-based morphometry—the methods. NeuroImage 11:805–821.

Assaf Y, Cohen Y (2009) Inferring microstructural information of white matter from diffusion MRI. In: Diffusion MRI: From Quantitative Measurement to In Vivo Neuroanatomy (Johansen-Berg H, Behrens TEJ, eds.), pp3-10. Elsevier: Amsterdam.

Attwell D, Iadecola C (2002) The neural basis of functional brain imaging signals. Trends Neurosci 25:621-625.

Attwell D, Laughlin SB (2001) An energy budget for signalling in the grey matter of the brain. J Cereb Blood Flow Metab 21:1133-1145.

Baltan S (2006) Surviving anoxia: a tale of two white matter tracts. Crit Rev Neurobiol 18:95-103.

Barazany D, Basser PJ, Assaf Y (2009) *In vivo* measurement of axon diameter distribution in the corpus callosum of rat brain. Brain 132:1210-1220.

Basser PJ, Özarslan E (2009) Introduction to diffusion MR. In: Diffusion MRI: From Quantitative Measurement to In Vivo Neuroanatomy (Johansen-Berg H, Behrens TEJ, eds.), pp3-10. Elsevier: Amsterdam.

Bassett DS, Bullmore ET (2009) Human brain networks in health and disease. Curr Opin Neurol 22:340–347.

Beckmann C, Jenkinson M, Smith SM (2003) General multi-level linear modeling for group analysis in FMRI. NeuroImage 20:1052-1063.

Behzadi Y, Restom K, Liau J, Liu TT (2007) A component based noise correction method (CompCor) for BOLD and perfusion based fMRI. NeuroImage 37:90-101.

Bennett CM, Miller MB (2010) How reliable are the results from functional magnetic resonance imaging? Ann NY Acad Sci 1191:133-155.

Bestmann S, Swayne O, Blankenburg F, Ruff CC, Teo J, Weiskopf N, Driver J, Rothwell JC, Ward NS (2010) The role of contralesional dorsal premotor cortex after stroke as studied with concurrent TMS-fMRI. J Neurosci 20:11926-11937.

Birn RM, Diamond JB, Smith MA, Bandettini P (2006) Separating respiratory-variation-related fluctuations from neuronal-activity-related fluctuations in fMRI. NeuroImage 31:1536-1548.

Birn RM, Murphy K, Handwerker DA, Bandettini P (2009) fMRI in the presence of task-correlated breathing variations. NeuroImage 47:1092-1104.

Biswal B, DeYoe EA, Hyde JS (1996) Reduction of physiological fluctuations in fMRI using digital filters. Magn Reson Med 35:107-113.

Black SE (2007) Imaging white matter and the burden of small vessel disease. Brain Cogn 63:191-196.

Bodurka J, Ye F, Petridou N, Murphy K, Bandettini PA (2007) Mapping the MRI voxel volume in which thermal noise matches physiological noise–implications for fMRI. NeuroImage 34:542-549.

Brandt T, Stephan T, Bense S, Yousry TA, Dieterich M (2000) Hemifield visual motion stimulation: an example of interhemispheric crosstalk. NeuroReport 11:2803-2809.

Brett M (2002) The problem of functional localization in the human brain. Nat Rev Neurosci 3:243–249.

Brewer KD, Rioux JA, D'Arcy RCN, Bowen CV, Beyea SD (2009) Asymmetric spin-echo (ASE) spiral improves BOLD fMRI in inhomogeneous regions. NMR Biomed 22:654-662.

Brown AM, Tekkök SB, Ransom BR (2004) Energy transfer from astrocytes to axons: the role of CNS glycogen. Neurochem Int 45:529–536.

Brown LL, Sharp FR (1995) Metabolic mapping of rat striatum: somatotopic organization of sensorimotor activity. Brain Res 686:207-222.

Cabeza R, Nyberg L (2000) Imaging cognition II: an empirical review of 275 PET and fMRI studies. J Cogn Neurosci 12:1-47.

Calabrese M, Rinaldi F, Grossi1 P, Gallo P (2011) Cortical pathology and cognitive impairment in multiple sclerosis. Expert Rev Neurother 11:425–432.

Carmignoto G, Gómez-Gonzalo M (2010) The contribution of astrocyte signalling to neurovascular coupling. Brain Res Rev 63:138-148.

Catani M, ffytche DH (2005) The rises and falls of disconnection syndromes. Brain 128:2224-2239.

Cauli B, Tong X-K, Rancillac A, Serluca N, Lambolez B, Rossier J, Hamel E (2004) Cortical GABA interneurons in neurovascular coupling: relays for subcortical vasoactive pathways. J Neurosci 24:8940-8949.

Charil A, Filippi M, Falini A (2006) High-field strength MRI (3.0 T or more) in white matter diseases. In: High Field Brain MRI (Salvolini U, Scarabino T, eds.), pp. 186-193. Springer: Berlin.

Chiu M-J, Lin C-C, Chuang K-H, Chen J-H, Huang K-M (2001) Tissue segmentation-assisted analysis of fMRI for human motor response: an approach combining artificial neural network and fuzzy C means. J Digit Imaging 14:38-47.

Cohen ER, Rostrup E, Sidaros K, Lund TE, Paulson OB, Uğurbil K, Kim S-G (2004) Hypercapnic normalization of BOLD fMRI: comparison across field strength and pulse sequences. NeuroImage 23:613-624.

Collins DL, Holmes CJ, Peters TM, Evans AC (1995) Automatic 3-D model-based neuroanatomical segmentation Hum Brain Mapp 3:190-208.

Coltheart M (1981) The MRC Psycholinguistic Database. Quarterly J Exp Psych 33A:497-505.

Dagli MS, Ingeholm JE, Haxby JV (1999) Localization of cardiac-induced signal change in fMRI. NeuroImage 9:407-415.

D'Arcy RCN, Hamilton A, Jarmasz M, Sullivan S, Stroink G (2006) Exploratory data analysis reveals visuo-visual interhemispheric transfer in fMRI. Magn Reson Med 55:952-958.

Dang-Vu TT, Schabus M, Desseilles M, Sterpenich V, Bonjean M, Maquet P (2010) Functional neuroimaging insights into the physiology of human sleep. Sleep 33:1589-1603.

Devonshire IM, Papadakis NG, Port M, Berick J, Kennerley AJ, Mayhew JEW, Overton PG (2012) Neurovascular coupling is brain region-dependent. NeuroImage 59:1997-2006.

Di Salle F, Esposito F, Elefante A, Scarabino T, Volpicelli A, Cirillo S, Elefante R, Seifritz E (2003) High field functional MRI. Eur J Radiol 48:138-145.

Drake CT, Iadecola C (2007) The role of neuronal signaling in controlling cerebral blood flow. Brain Lang 102:141–152

Driver I, Blockley N, Fisher J, Francis S, Gowland P (2010) The change in cerebrovascular reactivity between 3 T and 7 T measured using graded hypercapnia. NeuroImage 51:274-279.

Dumontheil I, Thompson R, Duncan J (2011) Assembly and use of new task rules in fronto-parietal cortex. J Cogn Neurosci 23:168-82.

Duong TQ, Yacoub E, Adriany G, Hu , Uğurbil K, Kim S-G (2003) Microvascular BOLD contribution at 4 and 7 T in the human brain: gradient-echo and spin-echo fMRI with suppression of blood effects. Magn Reson Med 49:1019-1027.

Duvernoy HM, Delon S, Vannson JL (1981) Cortical blood vessels of the human brain. Brain Res Bull 7:519-579.

Erecińska M, Dagani F (1990) Relationships between the neuronal sodium/potassium pump and energy metabolism. Effects of K+, Na+, and adenosine triphosphate in isolated brain synaptosomes. J Gen Physiol 95:591-616.

Fabri M, Polonara G, Mascioli G, Salvolini U, Mazoni T (2011) Topographical organization of human corpus callosum: an fMRI mapping study. Brain Res 1370:99-111.

Fera F, Yongbi MN, van Gelderen P, Frank JA, Mattay VS, Duyn JH (2004) EPI- BOLD fMRI of human motor cortex at 1.5 T and 3.0 T: sensitivity dependence on echo time and acquisition bandwidth. J Magn Reson Imaging 19:19-26.

Filliard P, Toussaint N, Pennec X (2006) MedINRIA: DT-MRI processing and visualization software. Similar NoE Tensor Workshop, Las Palmas.

Friston KJ, Harrison L, Penny W (2003) Dynamic causal modelling. NeuroImage 19:1273-1302.

Gati JS, Menon RS, Rutt BK (2000) Field strength dependence of functional MRI signals. In: Functional MRI (Moonen CTW, Bandettini PA, eds), pp277-282. Berlin: Springer.

Gati JS, Menon RS, Uğurbil K, Rutt BK (1997) Experimental determination of the bold field strength dependence in vessels and tissue. Magn Reson Med 38:296-302.

Gawryluk JR, Brewer KD, Beyea SD, D'Arcy RCN (2009) Optimizing the detection of fMRI activation in white matter using asymmetric spin echo spiral. NeuroImage 45:83-88.

Gawryluk JR, D'Arcy RC, Mazerolle EL, Brewer KD, Beyea SD (2011a) Functional mapping in the corpus callous: a 4T fMRI study of white matter. NeuroImage 54:10-15.

Gawryluk JR, Mazerolle EL, Brewer KD, Beyea SD, D'Arcy RCN (2011b) Investigation of fMRI activation in the internal capsule. BMC Neurosci 12:56.

Gazzaniga MS, Bogen JE, Sperry RW (1965) Observations on visual perception after disconnexion of the cerebral hemispheres in man. Brain 88:221-236.

Genova HM, Hillary FG, Wylie G, Rypma B, DeLuca J (2009) Examination of processing speed deficits in multiple sclerosis using functional magnetic resonance imaging. J Int Neuropsychol Soc 15:383-393.

Gjedde A (2002) Brain energy metabolism and the physiological basis of the haemodynamic response. In: Functional MRI an introduction to methods (Jezzard P, Matthews PM, Smith SM, eds), pp37-66. Oxford: Oxford UP.

Glover GH, Li T-Q, Ress D (2000) Image-based method for retrospective correction of physiological motion effects in fMRI: RETROICOR. Magn Reson Med 44:162-167.

Goloshevsky AG, Silva AC, Dodd SJ, Koretsky AP (2008) BOLD fMRI and somatosensory evoked potentials are well correlated over a broad range of frequency content of somatosensory stimulation of the rat forepaw. Brain Res 1195:67-76.

Gonzalez-Castillo J, Roopchansingh V, Bandettini PA, Bodurka J (2011) Physiological noise effects on the flip angle selection in BOLD fMRI. NeuroImage 54:2764-2778.

Greicius MD, Supekar K, Menon V, Dougherty RF (2009) Resting-state functional connectivity reflects structural connectivity in the default mode network. Cereb Cortex 19:72-78.

Greve DN, Mueller BA, Liu T, Turner JA, Vovodic J, Yetter E, Diaz M, McCarthy G, Wallace S, Roach BJ, Ford JM, Mathalon DH, Calhoun VD, Wible CG, Brown GG, Potkin SG, Glover G (2011) A novel method for quantifying scanner instability in fMRI. Magn Reson Med 65:1053-1061.

Grubb RL, Raichle ME, Eichling JO, Terpogos MM (1974) Effects of changes in $PaCO_2$ on cerebral blood volume, blood flow, and vascular mean transit time. Stroke 5:630-639.

Guye M, Bartolomei F, Ranjeva JP (2008) Imaging structural and functional connectivity: towards a unified definition of human brain organization? Curr Opin Neurol 21:393-403.

Guye M, Parker GJ, Symms M, Boulby P, Wheeler-Kingshott CA, Salek-Haddadi A, Barker GJ, Duncan JS (2003) Combined functional MRI and tractography to demonstrate the connectivity of the human primary motor cortex in vivo. NeuroImage 19:1349-1360.

Hamilton NB, Attwell D, Hall CN (2010) Pericyte-mediated regulation of capillary diameter: a component of neurovascular coupling in health and disease. Front Neuroenerg 2:5.

Handwerker DA, Ollinger JM, D'Esposito M (2004) Variation of BOLD hemodynamic responses across subjects and brain regions and their effects on statistical analysis. NeuroImage 21:1639-1651.

Harris JJ, Attwell D (2012) The energetics of CNS white matter. J Neurosci 32:356-371.

Helenius J, Perkio J, Soinne L, Ostergaard L, Carano RA, Salonen O, Savolainen S, Kaste M, Aronen HJ, Tatlisumak T (2003) Cerebral hemodynamics in a healthy population measured by dynamic susceptibility contrast MR imaging. Acta Radiol 44:538-546.

Hoenig K, Kuhl CK, Scheef L (2005) Functional 3.0-T MR assessment of higher cognitive function: are there advantages over 1.5T-imaging? Neuroradiology 234:860-868.

Hu X, Norris DG (2004) Advances in high-field magnetic resonance imaging. Annu Rev Biomed Eng 6:157-184.

Huppert TJ, Jones PB, Devor A, Dunn AK, Teng IC, Dale AM, Boas DA (2009) Sensitivity of neural-hemodynamic coupling to alterations in cerebral blood flow during hypercapnia. J Biomed Opt 14:044038.

Huttunen JK, Gröhn O, Penttonen M (2008) Coupling between simultaneously recorded BOLD response and neuronal activity in the rat somatosensory cortex. NeuroImage 39:775-785.

Iacoboni M, Zaidel E (2004) Interhemispheric visuo-motor integration in humans: the role of the superior parietal cortex. Neuropsychologia 42:419-425.

Iliff JJ, D'Ambrosio R, Ngai AC, Winn HR (2003) Adenosine receptors mediate glutamate-evoked arteriolar dilation in the rat cerebral cortex. Am J Physiol Heart Circ Physiol 284:H1631-H1637.

Jenkinson M, Smith SM (2001) A global optimisation method for robust affine registration of brain images. Med Image Anal 5:143-156.

Jenkinson M, Bannister P, Brady M, Smith S (2002) Improved optimisation for the robust and accurate linear registration and motion correction of brain images. NeuroImage 17:825-841.

Jezzard P, Clare S (2002) Principles of nuclear magnetic resonance and MRI. In: Functional MRI an introduction to methods (Jezzard P, Matthews PM, Smith SM, eds), pp67-92. Oxford: Oxford UP.

Jochimsen TH, Ivanov D, Ott DVM, Heinke W, Turner R, Möller HE, Richenbach JR (2010) Whole-brain mapping of venous vessel size in humans using the hypercapnia-induced BOLD effect. NeuroImage 51:765-774.

Johnstone T, Ores Walsh KS, Greischar LL, Alexander AL, Fox AS, Davidson RJ, Oakes TR (2006) Motion correction and the use of motion covariates in multiple-subject fMRI analysis. Hum Brain Mapp 27:779-788.

Jones DK, Simmons A, Williams SCR, Horsfield MA (1999) Non-invasive assessment of axonal fiber connectivity in the human brain via diffusion tensor MRI. Magn Reson Med 42:37-41.

Kalsi AS, Greenwood K, Wilkin G, Butt AM (2004) Kir4.1 expression by astrocytes and oligodendrocytes in CNS white matter: a developmental study in the rat optic nerve. J Anat 204:475-485.

Kannurpatti SS, Biswal BB, Hudetz AG (2003) Regional dynamics of the fMRI-BOLD signal response to hypoxia-hypercapnia in the rat brain. J Magn Reson Imaging 17:641-647.

Kastrup A, Krüger G, Glover GH, Neumann-Haefelin T, Moseley ME (1999) Regional variability of cerebral blood oxygenation response to hypercapnia. NeuroImage 10:675-681.

Kida I, Hyder F (2005) Physiology of functional magnetic resonance imaging. In: Magnetic Resonance Imaging: Methods and Biologic Applications. (Prasad PV, ed), pp175-195. Totowa NJ: Humana Press.

Klein B, Kuschinskey W, Schröck H, Vetterlein F (1986) Interdependency of local capillary density, blood flow, and metabolism in rat brains. Am J Physiol 251:1333-1340.

Kleinfeld D, Blinder P, Drew PJ, Driscoll JD, Muller A, Tsai PS, Shih AY (2011) A guide to delineate the logic of neurovascular signaling in the brain. Front Neuroenerg 3:1.

Kocharyan A, Fernandes P, Tong X-K, Vaucher E, Hamel E (2008) Specific subtypes of cortical GABA interneurons contribute to the neurovascular coupling response to basal forebrain stimulation. J Cereb Blood Flow Metab 28: 221-231.

Koehler RC, Roman RJ, Harder DR (2008) Astrocytes and the regulation of cerebral blood flow. Trends Neurosci 32:160-169.

Krasnow B, Tamm L, Greicius MD, Yang TT, Glover GH, Reiss AL, Menon V (2003) Comparison of fMRI activation at 3T and 1.5T during perceptual, cognitive, and affective processing. NeuroImage 18:813-826.

Krüger G, Kastrup A, Glover GH (2001) Neuroimaging at 1.5 T and 3.0 T: comparison of oxygenation-sensitive magnetic resonance imaging. Magn Reson Med 45:595-604.

Lancaster JL, Tordesillas-Gutiérrez D, Martinez M, Salinas F, Evans A, Zilles K, Mazziotta JC, Fox PT (2007) Bias between MNI and Talairach coordinates analyzed using the ICBM-152 brain template. Hum Brain Mapp 28:1194-1205.

Lancaster JL, Woldorff MG, Parsons LM, Liotti M, Freitas CS, Rainey L, Kochunov PV, Nickerson D, Mikiten SA, Fox PT (2000) Automated Talairach atlas labels for functional brain mapping. Hum Brain Mapp 10:120-131.

Lauritzen M (2005) Reading vascular changes in brain imaging: is dendritic calcium the key? Nat Rev Neurosci 6:77-85.

Lauritzen M, Gold L (2003) Brain function and neurophysiological correlates of signals used in functional neuroimaging. J Neurosci 23:3972-3980.

Lazeron RHC, Rombouts SARB, de Sonnevilee L, Barkhof F, Scheltens P (2003) A paced visual serial addition test for fMRI. J Neurol Sci 213:29-34.

Leber AB (2010) Neural predictors of within-subject fluctuations in attentional control. J Neurosci 30:11458-11465.

Lecrux C, Hamel E (2011) The neurovascular unit in brain function and disease. Acta Physiol (Oxf) 203:47-59.

Lierse W (1963) Die Kapillardichte im Wirbeltiergehirn. Acta Anat 54:1–31.

Logothetis NK (2003) The underpinnings of the BOLD functional magnetic resonance imaging signal. J Neurosci 23:3963-3971.

Logothetis NK (2007) The ins and outs of fMRI signals. Nat Neurosci 10:1230-1232.

Logothetis NK, Pauls J, Augath M, Trinath T, Oeltermann A (2001) Neurophysiological investigation of the basis of the fMRI signal. Nature 412:150-157.

Logothetis NK, Wandell BA (2004) Interpreting the BOLD Signal. Annu Rev Physiol 66:735-769.

Lowe MJ, Beall EB, Sakaie KE, Koenig KA, Stone L, Marrie RA, Phillips MD (2008) Resting state sensorimotor functional connectivity in multiple sclerosis inversely correlates with transcallosal motor pathways transverse diffusivity. Hum Brain Mapp 29:818-827.

Lowe MJ, Horenstein C, Hirsch JG, Marrie RA, Stone L, Bhattacharyya PK, Gass A, Phillips MD (2006) Functional pathway-defined MRI diffusion measures reveal increased transverse diffusivity of water in multiple sclerosis. NeuroImage 32:1127-1133.

Lu J, Dai G, Egi Y, Huang S, Kwon SJ, Lo EH, Kim YR (2009) Characterization of cerebrovascular responses to hyperoxia and hypercapnia using MRI in rat. NeuroImage 45:1126-1134.

Maandag NJG, Coman D, Sanganahalli BG, Herman P, Smith AJ, Blumenfeld H, Shulman RG, Hyder F (2007) Energetics of neuronal signaling and fMRI activity. Proc Natl Acad Sci USA 104:20546-20551.

Macey PM, Alger JR, Kumar R, Macey KE, Woo MA, Harper RM (2003) Global BOLD MRI changes to ventilatory challenges in congenital central hypoventilation syndrome. Respir Physiol Neurobiol 139: 41-50.

Mandell DM, Han JS, Poublanc J, Crawley AP, Kassner A, Fisher JA, Mikulis DJ, (2008) Selective reduction of blood flow to white matter during hypercapnia corresponds with leukoaraiosis. Stroke 39:1993-1998.

Mandeville JB, Marota JJA (1999) Vascular filters of functional MRI: spatial localization using BOLD and CBV contrast. Magn Reson Med 42:591-598.

Martin C, Jones M, Martindale J, Mayhew J (2006) Haemodynamic and neural responses to hypercapnia in the awake rat. Eur J Neurosci 24:2601-2610.

Matthews PM (2002) An introduction to functional magnetic resonance imaging of the brain. In: Functional MRI an introduction to methods (Jezzard P, Matthews PM, Smith SM, eds), pp3-34. Oxford: Oxford UP.

Mazerolle EL, D'Arcy RC, Beyea SD (2008) Detecting fMRI activation in white matter: interhemispheric transfer across the corpus callosum. BMC Neurosci 9:84.

Mazerolle EL, Beyea SD, Gawryluk JR, Brewer KD, Bowen CV D'Arcy RCN (2010) Confirming white matter fMRI activation in the corpus callosum: co-localization with DTI tractography. NeuroImage 50:616-621.

Mazziotta J, Toga A, Evans A, Fox P, Lancaster J, Zilles K, Woods R, Paus T, Simpson G, Pike B, Holmes C, Collins L, Thompson P, MacDonald D, Iacoboni M, Schormann T, Amunts K, Palomero-Gallagher N, Geyer S, Parsons L, Narr K, Kabani N, Le Goualher G, Boomsma D, Cannon T, Kawashima R, Mazoyer B (2001) A probabilistic atlas and reference system for the human brain: International Consortium for Brain Mapping (ICBM). Phil Trans Royal Soc B Biol Sci 356:1293-1322.

McGonigle DJ, Howseman AM, Athwal BS, Friston KJ, Frackowiak RSJ, Holmes AP (2000) Variability in fMRI: an examination of intersession differences. NeuroImage 11:708-734.

Meindl T, Born C, Britsch S, Reiser M, Schoenberg S (2008) Functional BOLD MRI: comparison of different field strengths in a motor task. Eur Radiol 18:1102-1113.

Mestres-Missé A, Rodriguez-Fornells A, Münte TF (2010) Neural differences in the mapping of verb and noun concepts onto novel words. NeuroImage 49:2826-2835.

Miezin FM, Maccotta L, Ollinger JM, Petersen SE, Buckner RL (2000) Characterizing the hemodynamic response: effects of presentation rate, sampling procedure, and the possibility of ordering brain activity based on relative timing. NeuroImage 11:735-759.

Mosier K, Bereznaya I (2001) Parallel cortical networks for volitional control of swallowing in humans. Exp Brain Res 140:280-289.

Mosier K, Liu W-C, Maldjian JA, Shah R, Modi B (1999a) Lateralization of cortical function in swallowing: a functional MR imaging study. Am J Neuroradiol 20:1520-1526.

Mosier K, Patel R, Liu W-C, Kalnin A, Maldjian J, Baredes S (1999b) Cortical representation of swallowing in normal adults: functional implications. Laryngoscope 109:1417-1423.

Mukherjee P, Berman JI, Chung SW, Hess CP, Henry RG (2008) Diffusion tensor MR imaging and fibre tractography: theoretic underpinnings. Am J Neuroradiol 29: 632-641.

Newman AJ, Supalla T, Hauser P, Newport EL, Bavelier D (2010) Dissociating neural subsystems for grammar by contrasting word order and inflection. PNAS 107:7539–7544.

Nucifora PGP, Verma P, Lee S-K, Melhem ER (2007) Diffusion-tensor MR imaging and tractography: exploring brain microstructure and connectivity. Radiology 245:367-384.

Oishi K, Faira AV, van Zigl PCM, Mori S (2005) MRI Atlas of Human White Matter. Elsevier: Amsterdam.

Oldfield RC (1971) The assessment and analysis of handedness: The Edinburgh inventory. Neuropsychologia 9:97-113.

Omura K, Tsukamoto T, Kotani Y, Ohgami Y, Minami M, Inoue Y (2004) Different mechanisms involved in interhemispheric transfer of visuomotor information. NeuroReport 15:2707-2711.

Paxinos G, Watson C (2004) The Rat Brain in Stereotaxic Coordinates, 5th edn. Boston: Academic Press.

Pelletier J, Audoin B, Reuter F, Ranjeva JP (2009) Plasticity in MS: from functional imaging to rehabilitation. Int MS J 16:26-31.

Petzold GC, Murthy VN (2011) Role of astrocytes in neurovascular coupling. Neuron 71:782-797.

Peyron R, Laurent B, García-Larrea L (2000) Functional imaging of brain responses to pain. A review and meta-analysis. Neurophysiol Clin 30:263-288.

Poffenberger AT (1912) Reaction time to retinal stimulation with special reference to the time lost in conduction through nervous centers. Arch Psychol 23:1-73.

Poline J-B, Strother SC, Dehaene-Lambertz G, Egan GF, Lancaster JL (2006) Motivation and synthesis of the FIAC experiment: reproducibility of fMRI results across expert analyses. Hum Brain Mapp 27:351-359.

Preibisch C, Haase A (2001) Perfusion imaging using spin-labeling methods: contrast-to-noise comparison in functional MRI applications. Magn Reson Med 46:172-182.

Raichle ME, Mintun MA (2006) Brain work and brain imaging. Ann Rev Neurosci 29:449-476.

Rash JE (2010) Molecular disruptions of the panglial syncytium block potassium siphoning and axonal saltatory conduction: pertinence to neuromyelitis optica and other demyelinating diseases of the central nervous system. Neuroscience 168:982-1008.

Rauch A, Rainer G, Augath M, Oeltermann A, Logothetis NK (2008) Pharmacological MRI combined with electrophysiology in non-human primates: effects of lidocaine on primary visual cortex. NeuroImage 40: 590-600.

Robson MD, Gore JC, Constable T (1997) Measurement of the point spread function in MRI using constant time imaging. Magn Reson Med 38:733-740.

Rostrup E, Law I, Blinkenburg M, Larsson HBW, Born AP, Holm S, Paulson OB (2000) Regional differences in the CBF and BOLD response to hypercapnia: a combined PET and fMRI study. NeuroImage 11:87-97.

Sawiak SJ, Wood NI, Williams GB, Morton AJ, Carpenter TA (2009) SPMMouse: a new toolbox for SPM in the animal brain. In: Proceedings of the 17th Annual Meeting of the International Society for Magnetic Resonance in Medicine.

Sicard K, Shen Q, Brevard ME, Sullivan R, Ferris CF, King JA, Duong TQ (2003) Regional cerebral blood flow and BOLD responses in conscious and anesthetized rats under basal and hypercapnic conditions: implications for functional MRI studies. J Cereb Blood Flow Metab 23:472-481.

Sirotin YB, Das A (2009) Anticipatory haemodynamic signals in sensory cortex not predicted by local neuronal activity. Nature 457: 475-480.

Skudlarski P, Jagannathan K, Calhoun VD, Hampson M, Skudlarska BA, Pearlson G (2008) Measuring brain connectivity: diffusion tensor imaging validates resting state temporal correlations. NeuroImage 15:554-561.

Sloan HL, Austin VC, Blamire AM, Schnupp JWH, Lowe AS, Allers KA, Matthews PM, Sibson NR (2010) Regional differences in neurovascular coupling in rat brain as determined by fMRI and electrophysiology. NeuroImage 53:399-411.

Smith AJ, Blumenfeld H, Behar KL, Rothman DL, Shulman RG, Hyder F (2002) Cerebral energetics and spiking frequency: the neurophysiological basis of fMRI. Proc Natl Acad Sci USA 99:10765-10770.

Smith S (2002) Fast robust automated brain extraction. Hum Brain Mapp 17:143-155.

Smith S, Jenkinson M, Woolrich M, Beckmann C, Behrens T, Johansen-Berg H, Bannister P, De Luca M, Drobnjak I, Flitney D, Niazy R, Saunders J, Vickers J, Zhang Y, De Stefano N, Brady J, Matthews P (2004) Advances in functional and structural MR image analysis and implementation as FSL. NeuroImage 23(S1):208-219.

Soltanian-Zadeh H, Peck DJ, Hearshen DO, Lajiness-O'Neill RR (2004) Model-independent method for fMRI analysis. IEEE Trans Med Imaging 23:285-296.

Takahashi H, Kato M, Matsuura M, Mobbs D, Suhara T, Okubo Y (2009) When your gain is my pain and your pain is my gain: neural correlates of envy and schadenfreude. Science 323:937-939.

Talairach J, Tournoux P (1988) Co-Planar Stereotaxic Atlas of the Human Brain. Thieme: New York.

Tettamanti M, Paulesu E, Scifo P, Maravita A, Fazio F, Perani D, Marzi CA (2002) Interhemispheric transfer of visuomotor information in humans: fMRI evidence. J Neurophysiol 88:1051-1058.

Tohka J, Foerde K, Aron AR, Tom SM, Toga AW, Poldrack RA (2008) Automatic independent component labeling for artifact removal in fMRI. NeuroImage 39:1227-1245.

Triantafyllou C, Wald LL, Hoge RD (2005) Echo-time and field strength dependence of BOLD reactivity in veins and parenchyma using flow-normalized hypercapnic manipulation. PLoS One 6:e24519.

Troje N, Bulthoff HH (1996) Face recognition under varying poses: the role of texture and shape. Vision Res 36:1761-1771.

Trusk TC, Stein EA (1987) Effect of intravenous heroin and naloxone on regional cerebral blood flow in the conscious rat. Brain Res 406:238-245.

Turner R, Jezzard P, Wen H, Kwong KK, LeBihan D, Zeffiro T, Balaban RS (1993) Functional mapping of the human visual cortex at 4 and 1.5 Tesla using deoxygenation contrast EPI. Magn Reson Med 29:277-279.

Uğurbil K, Chen W, Hu X, Kim S-G, Zhu X-H, Ogawa S (2007) Functional MRI at high fields: practice and utility. Encyclopedia of Magnetic Resonance.

Uğurbil K, Garwood M, Hendrich K, Hinke R, Hu X, Menon RS, Merkle H, Ogawa S, Salmi R (1993) Imaging at high magnetic fields: initial experiences at 4 Tesla. Magn Reson Q 9:259–277.

Uğurbil K, Hu X, Chen W, Zhu XH, Kim SG, Georgopoulos A (1999) Functional mapping in the human brain using high magnetic fields. Philos Trans R Soc Lond B Biol Sci 13:915-921.

Van der Zande FHR, Hofman PAM, Backes WH (2005) Mapping hypercapnia-induced cerebrovascular reactivity using BOLD fMRI. Neuroradiology 47:114-120.

Van der Zwaag W, Francis S, Head K, Peters A, Gowland P, Morris P, Bowtell R (2009) fMRI at 1.5, 3 and 7 T: characterising BOLD signal changes. NeuroImage 47:1425-1434.

Van Dijk KRA, Hedden T, Vekataraman A, Evans KC, Lazar SW, Buckner RL (2010) Intrinsic functional connectivity as a tool for human connectomics: theory, properties, and optimization. J Neurophysiol 103:297-321.

Vaucher E, Borredon J, Seylaz J, Lacombe P (1995) Autoradiographic distribution of cerebral blood flow increases elicited by stimulation of the nucleus basalis magnocellularis in the unanesthetized rat. Brain Res 691:57-68.

Vaucher E, Tong X-K, Cholet N, Lantin S, Hamel E (2000) GABA neurons provide a rich input to microvessels but not nitric oxide neurons in the rat cerebral cortex: a means for direct regulation of local cerebral blood flow. J Comp Neurol 421:161-171.

Vaughan JT, Garwood M, Collins CM, Liu W, DelaBarre L, Adriany G, Andersen P, Merkle H, Goebel R, Smith MB, Uğurbil K (2001) 7T vs. 4T: RF power, homogeneity, and signal-to-noise comparison in head images. Magn Reson Med 46:24-30.

Waxman SG, Ritchie JM (1993) Molecular dissection of the myelinated axon. Ann Neurol 33:121-136.

Weber B, Fouad K, Burger C, Buck A (2002) White matter glucose metabolism during intracortical electrostimulation: a quantitative [18F]fluorodeoxyglucose autoradiography study in the rat. NeuroImage 16:993-998.

Weber B, Treyer V, Oberholzer N, Jaermann T, Boesiger P, Brugger P, Regard M, Buck A, Savazzi S, Marzi CA (2005) Attention and interhemispheric transfer: a behavioural and fMRI study. J Cogn Neurosci 17:113-123.

Wegener S, Wong E (2008) Longitudinal MRI studies of the isoflurane-anesthetized rat: long-term effects of a short hypoxic episode on regulation of cerebral blood flow as assessed by pulsed arterial spin labeling. NMR Biomed 21:696-703.

Weis S, Leube D, Erb M, Heun R, Grodd W, Kircher T (2011) Functional neuroanatomy of sustained memory encoding performance in healthy aging and in Alzheimer's disease. Int J Neurosci 121:384-392.

Wey H-Y, Wang DJ, Duong TQ (2011) Baseline CBF, and BOLD, CBF, and $CMRO_2$ fMRI of visual and vibrotactile stimulations in baboons. J Cereb Blood Flow Metab 31:715-724.

White T, Nelson M, Lim KO (2008) Diffusion tensor imaging in psychiatric disorders. Top Magn Reson Imaging 97-109.

Wilson MD (1998) The MRC psycholinguistic database: machine readable dictionary, version 2. Behav Res Methods Instrum Comput 20:6-11.

Wise RG, Ide K, Poulin MJ, Tracey I (2004) Resting fluctuations in arterial carbon dioxide induce significant low frequency variations in BOLD signal. NeuroImage 21:1652-1664.

Woolrich MW (2008) Robust group analysis using outlier inference. NeuroImage 41:286-301.

Woolrich MW, Behrens TEJ, Beckmann CF, Jenkinson M, Smith SM (2004) Multi-level linear modeling for FMRI group analysis using Bayesian inference. NeuroImage 21:1732-1747.

Woolrich MW, Ripley BD, Brady JM, Smith SM (2001) Temporal autocorrelation in univariate linear modelling of fMRI data. NeuroImage 14:1370-1386.

Worsley KJ, Evans AC, Marrett S, Neelin P (1992) A three-dimensional statistical analysis for CBF activation studies in human brain. J Cereb Blood Flow Metab 12:900-918.

Worsley KJ, Friston KJ (1995) Analysis of fMRI time-series revisited--again. NeuroImage 2:173-181.

Wu G, Luo F, Li Z, Zhao X, Li S-J (2002) Transient relationships among BOLD, CBV, and CBF changes in rat brain as detected by functional MRI. Magn Reson Med 48:987-993.

Yacoub E, Shmuel A, Pfeuffer J, Van De Moortele PF, Adriany G, Andersen P, Vaughan JT, Merkle H, Uğurbil K, Hu X (2001) Imaging brain function in humans at 7 Tesla. Magn Reson Med 45:588-594.

Yancey SE, Rotenberg DJ, Tam F, Chiew M, Ranieri S, Biswas L, Anderson KJ, Baker SN, Wright GA, Graham SJ (2011) Spin-history artifact during functional MRI: potential for adaptive correction. Med Phys 38:4634-4646.

Yang Y, Wen H, Mattay VS, Balaban RS, Frank JA, Duyn JH (1999) Comparison of 3D BOLD functional MRI with spiral acquisition at 1.5 and 4.0 T. NeuroImage 9:446-451

Yarkoni T, Barch DM, Gray JR, Conturo TE, Braver TS (2009) BOLD correlates of trial-by-trial reaction time variability in gray and white matter: a multi-study fMRI analysis. PLoS One 4:e4257.

Zarei M, Johansen-Berg H, Smith S, Ciccarelli O, Thompson AJ, Matthews PM (2006) Functional anatomy of interhemispheric cortical connections in the human brain. J Anat 209:311-320.

Zhang Y, Brady M, Smith S (2001) Segmentation of brain MR images through a hidden Markov random field model and the expectation maximization algorithm. IEEE Trans Med Imaging 20:45-57.